AFCRL-63-63

EFFICIENT FLUSHMOUNTED SURFACE WAVE LAUNCHER

By MATS E. VIGGH

Scientific Report Number 4
Contract Number AF19(604)-8057

AFCRL-63-63

EFFICIENT FLUSHMOUNTED SURFACE WAVE LAUNCHER

by

Mats E. Viggh

TRG, Incorporated
400 Border St.
East Boston 28, Massachusetts

Contract Number AF19(604)-8057
Project Number 151
Scientific Report Number 4

November 28, 1962

Project 4600
Task 460002

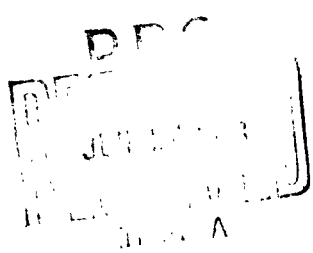

PREPARED FOR

ELECTRONICS RESEARCH DIRECTORATE
AIR FORCE CAMBRIDGE RESEARCH LABORATORIES
OFFICE OF AEROSPACE RESEARCH
UNITED STATES AIR FORCE
BEDFORD, MASSACHUSETTS

Requests for additional copies by Agencies of the Department of Defense, their contractors, and other Government agencies should be directed to the:

ARMED SERVICES TECHNICAL INFORMATION AGENCY
ARLINGTON HALL STATION
ARLINGTON 12, VIRGINIA

Department of Defense contractors must be established for ASTIA services or have their "need-to-know" certified by the cognizant military agency of their project or contract.

All other persons and organizations should apply to the:

U.S. DEPARTMENT OF COMMERCE
OFFICE OF TECHNICAL SERVICES
WASHINGTON 25, D. C.

TABLE OF CONTENTS

LIST OF FIGURES

LIST OF FIGURES (cont'd)

LIST OF FIGURES (cont'd)

ABSTRACT

Various methods for launching surface waves are reviewed, and the basic design principles are outlined for different kinds of launchers.

The case of a slot in a dielectric-clad groundplane is analyzed in detail, and experiments supporting the calculated results are reported. A way of combining several slots for good launching efficiency is derived and a five-slot launcher designed after this principle is described. Results from measurements of radiation patterns and efficiency are reported, as well as from measurements of radiation patterns from discontinuities on a surface waveguide excited by this launcher in combination with a cylindrical parabolic reflector.

In particular, a launching efficiency of over 80 percent was achieved with five slots, as compared to about 48 percent with one slot. Radiation patterns due to abrupt changes in dielectric thickness were measured, and compared with theoretical results for a corresponding change in surface reactance. The agreement was good at least within the main lobe.

I - INTRODUCTION

Theories about and techniques for surface wave launching have been treated by a great number of authors. [1, 2, 3]

The reasons for carrying out the work reported here were the following:

a) to develop a flush-mounted launcher, with small dimensions in terms of wavelengths and good efficiency.

A flushmounted launcher would have application as a feed for surface wave antennas in cases where good aerodynamic performance is imperative. Small size is also important in antennas of this kind, and high efficiency is desired for clean patterns and good noise performance.

b) to design an efficient launcher with low radiation in the direction at which the main surface wave is set up.

Such a launcher is very desirable for work involving measurement of radiation from inhomogeneities on surface waveguides, such as discontinuities or gradual variations of the reactance ("modulations") or other radiating structures coupled to the surface wave. Measuring the radiation patterns from such inhomogeneities in the presence of a relatively strong feed radiation is next to impossible, and this difficulty accounts to a large degree for the fact that very few successful experiments of this type have been reported.

The report begins with a brief account of basic properties of various classes of surface wave launchers, including a review of the basic problems involved in their design. Based on this discussion, a design principle is selected that appears promising with respect to the requirements stated above; detailed design formulas are worked out and results from tests of an experimental launcher

are presented.

II - DIFFERENT APPROACHES TO SURFACEWAVE LAUNCHING.

a) Coordinate System

Before entering into a discussion on surface wave launching arrangements, it is suitable to define the coordinate system which will be used throughout this report. We assume that the guiding surface is the plane z = 0, and use the coordinates shown in Figure 1. The plane z = 0, will also be referred to as "horizontal," and the z-axis as "vertical" in the following:

$R = z \cos \theta$

$r = z \sin \theta$

$x = r \cos \phi$

$y = r \sin \phi$

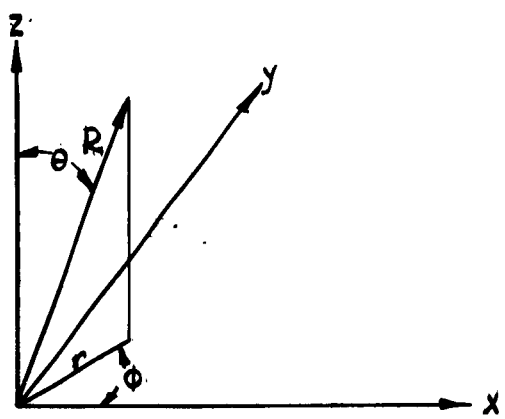

FIGURE 1 - COORDINATE SYSTEM

We also define the following propagation constants for the fields:

$\gamma_x = \alpha_x + j\beta_x$ propagation constant in the x direction

$\gamma_y = \alpha_y + j\beta_y$ propagation constant in the y direction

$\gamma_z = \alpha_z + j\beta_z$ propagation constant in the z direction

b) Characterization of Launchers

The accepted way of characterizing a surfacewave launcher is by the spectrum of plane waves that form its primary field, i.e., the field that would be emitted by the launcher if no guiding structure were present, and the launcher was radiating into free space. The primary spectrum can be derived from the free space radiation pattern of the launcher,[4] or from the fields on some plane surface that may be called the aperture plane.[3, 4, 5] In the latter case, the spectrum is obtained by carrying out a Fourier analysis of the aperture field. This yields the spectrum for all angles, real as well as complex.[3] The far field radiation pattern will only give information about real angles, but since the spectrum is an analytic function it can be continued for complex angles. (Readers not familiar with the concept of complex angles are referred to [3], [4] and following paragraphs).

c) Types of Guiding Surfaces to be Considered

The discussion will here be limited to flat, homogeneous guiding surfaces supporting TM-type surface waves, and presenting a positive reactance to a vertically incident field. Examples of such structures are corrugated surfaces,[6] metallic planes covered with a dielectric slab,[7] and "fakirs' beds."[8] For all these surfaces, a plane surface wave traveling in the x-direction (no variation in the y-direction) has three field components for $z > 0$: (Time factor $e^{j\omega t}$ is assumed).

$$H_y = H_0 e^{-\beta_0 X z - j\beta_0 x\sqrt{1+X^2}}$$

(1)
$$E_z = \frac{\beta_0\sqrt{1+X^2}}{\omega\epsilon_0} H_y$$

$$E_x = -j\sqrt{\frac{\mu_0}{\epsilon_0}}\, X H_y$$

where $\beta_0 = \frac{\omega}{c} = \frac{2\pi}{\lambda_0}$, λ_0 being the free space wavelength; and X is the reactance of the surface.

A surface wave of this kind can be interpreted as a plane wave propagating in a direction given by a complex angle.

For a plane wave in two dimensions, propagating in the direction $\theta = \theta_0$, we have the phase factor:

(2)
$$F = e^{-j\beta_0 R\cos(\theta-\theta_0) + j\omega t}.$$

With the substitution, $x = R\sin\theta$, $z = R\cos\theta$, (2) becomes

(3)
$$F = e^{-j\beta_0(z\cos\theta_0 + x\sin\theta_0) + j\omega t}.$$

If $\theta_0 = \frac{\pi}{2} - j\theta_1$, we get

$$\cos\theta_0 = j\sinh\theta_1, \text{ and } \sin\theta_0 = \cosh\theta_1 = \sqrt{1+\sinh^2\theta_1}.$$

With the notation $X = \sinh \theta_1$, the phase factors of (1) and (3) become the same, and the analogy is obvious.

III - DIFFERENT KINDS OF LAUNCHERS

There are four main classes of launchers that may be used for exciting waves of this kind:

1. horns or slots with their aperture in the plane x = 0
2. horns or slots with their aperture planes parallel to the plane z = 0
3. directional coupler feeds
4. short vertical monopoles or dipoles

A brief discussion of these classes of launchers will be given below. For the cases 1 and 2, we assume a structure of infinite width in the y-direction, thus restricting the problem to the dimensions x and z.

a) Apertures in the Plane x = 0

Call the H_y field in the aperture $H_0(z)$. The primary spectrum is then the Fourier transform of H_0, which can be written:

$$\tilde{H}_0(\beta_z) = \int_0^\infty e^{j\beta_z z} H_0(z)dz \quad . \tag{4}$$

It can be shown [4] that the primary field in the quadrant $z > 0$, $x > 0$ can be expressed as

$$H_y(x, z) = \frac{1}{2\pi} \int_{-\infty}^{+\infty} e^{-j(\beta_z z + \chi x)} \tilde{H}_0(\beta_z)d\beta_z \tag{5}$$

where

$$\beta_x = \sqrt{\beta_0^2 - \beta_z^2} \quad .$$

The presence of the surface gives rise to reflections, and the total field is:

$$(6) \qquad H_y(x,z) = \frac{1}{2\pi} \int_{-\infty}^{+\infty} e^{-j\beta_x x} (e^{-j\beta_z z} + Q \cdot e^{j\beta_z z}) \tilde{H}_0(\beta_z) d\beta_z$$

where Q is a "reflection coefficient," that is a function of β_z.

From (6) it is possible to calculate the radiation pattern and the surface wave amplitude. We first rewrite the integrand of (6):

$$(7) \qquad H_y(x,z) = \frac{1}{2\pi} \int_{-\infty}^{+\infty} [\tilde{H}_0(\beta_z) + Q(-\beta_z)\tilde{H}_0(-\beta_z)] e^{-j(\beta_x x + \beta_z z)} d\beta_z \quad .$$

The expression in the bracket is now the resulting spectrum, and is proportional to the radiation pattern, if $\beta_z = \beta_0 \cos\theta$ is inserted.

The surface wave appears as a residue term from a pole in Q, located as shown in Figure 2.

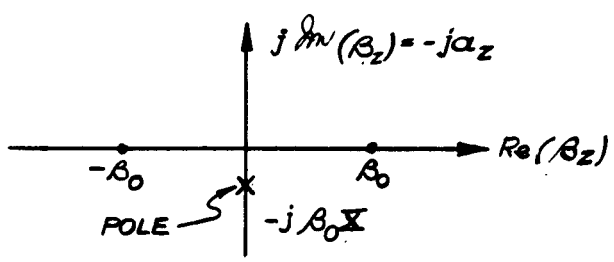

FIGURE 2 - LOCATION OF THE POLE IN Q OF EQ(6)

To illustrate the conditions for a typical case, let us assume a dielectric clad metallic plane (dielectric constant ϵ, thickness of dielectric = d), fed by a horn whose radiation pattern is symmetric around its peak at $\theta = \frac{\pi}{2}$. For this case we have on the real axis of Figure 2:

$$Q(-\beta_z) = \frac{\epsilon\beta_z - j\beta_z' \tan\beta_z' d}{\epsilon\beta_z + j\beta_z' \tan\beta_z' d} \tag{8}$$

where

$$\beta_z' = \sqrt{\beta_0^2(\epsilon - 1) + \beta_z^2} \quad . \tag{9}$$

On the imaginary axis of Figure 2 we have $\beta_z = -j\alpha_z$, and on this axis we have

$$Q(-\beta_z) = \frac{\epsilon\alpha_z + \beta_z' \tan\beta_z' d}{\epsilon\alpha_z - \beta_z' \tan\beta_z' d} \tag{10}$$

$$\beta_z' = \sqrt{\beta_0^2(\epsilon - 1) - \alpha_z^2} \tag{11}$$

Q has a pole for $\alpha_z = \beta_0 X$ (definition of X!).

In the real axis of Figure 2 we can obviously expand $\tilde{H}_0(\beta_z)$ in a Taylor series in the vicinity of $\beta_z = 0$, and because of the symmetry assumed we obtain

$$\tilde{H}_0(\beta_z) = \tilde{H}_0(0) - \tilde{H}_0''(0)\frac{\beta_z^2}{\beta_0^2} + \ldots. \tag{12}$$

In the imaginary axis, $\tilde{H}_0(\alpha_z)$ becomes

$$\tilde{H}_0(\alpha_z) = \tilde{H}_0(0) + \tilde{H}_0''(0)\frac{\alpha_z^2}{\beta_0^2} + \ldots. \tag{13}$$

The narrower the pattern of the horn is, the larger $\tilde{H}_0''(0)/\tilde{H}_0(0)$, but before we can draw any more definite conclusions, we have to evaluate the complete spectrum function around $\beta_z = 0$.

On the real axis of Figure 2 we get

$$S(\beta_z) \approx \frac{2\epsilon\beta_z}{\epsilon\beta_z + j\beta_z \tan\beta_z d}\left(\tilde{H}_0(0) - \tilde{H}_0''(0)\frac{\beta_z^2}{\beta_0^2}\right). \tag{14}$$

On the imaginary axis, we have

$$S(\alpha_z) \approx \frac{-2\epsilon\alpha_z}{\epsilon\alpha_z - \beta_z \tan\beta_z d}\left(\tilde{H}_0(0) + \tilde{H}_0''(0)\frac{\alpha_z^2}{\beta_z^2}\right). \tag{15}$$

Figure 3 shows the normalized radiation patterns, given by $S(\beta_z)\cdot \sin\theta$ for two cases. In both cases $d = \lambda_0/10$ and $\epsilon = 2.5$. The solid curve represents the case $\tilde{H}_0(0) >> \tilde{H}_0''(0)$, which corresponds to a small horn with a wide primary pattern, and the dotted curve is the pattern for $\tilde{H}_0(0) = 0.1\,\tilde{H}_0''(0)$ corresponding to a 3db beamwidth of about 30° in the primary pattern of the

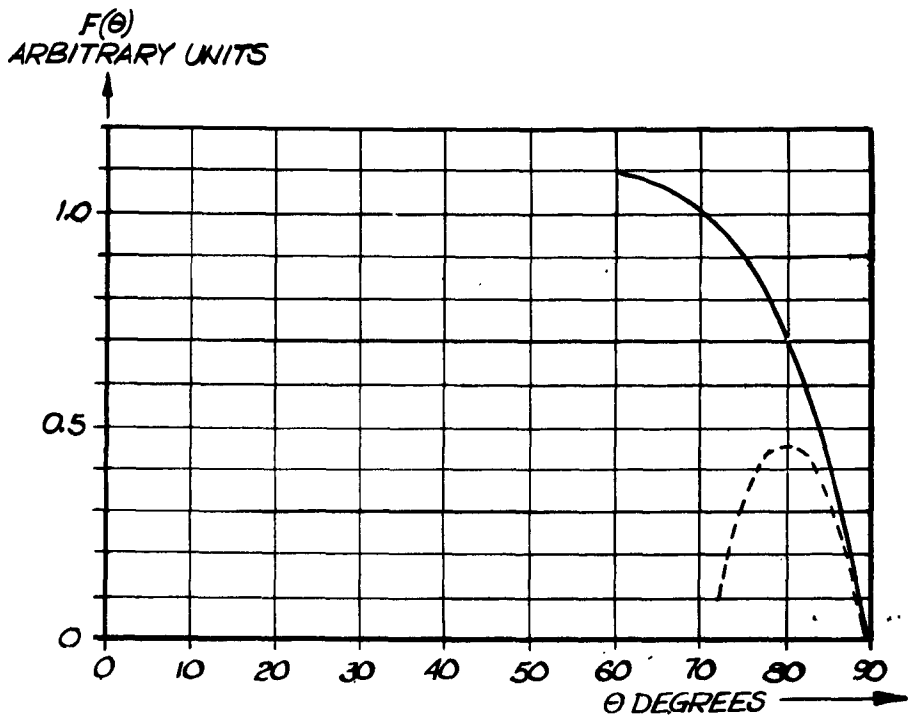

FIGURE 3 - RADIATION PATTERNS CLOSE TO ENDFIRE FOR TWO DIFFERENT HORNS FEEDING A SURFACE WAVEGUIDE

Horn Pattern: $F_0(\theta) = \tilde{H}_0 - \tilde{H}_0'' \cdot \cos^2 \theta$

Solid Curve: $\tilde{H}_0'' << \tilde{H}_0$

Broken Curve: $\tilde{H}_0'' = 10\,\tilde{H}_0$

$\epsilon = 2.5, \quad d = \lambda_0/10$

launcher.

For the assumed values of ϵ and d we have $X = 0.41$, and the residue at the pole is

$$\text{Res} = -\frac{2\epsilon\beta_0 X \cdot \tilde{H}_0(0)}{(\epsilon+1)(1+\frac{\epsilon X^2}{\epsilon-1-X^2})}\left(1+\frac{\tilde{H}_0''(0)}{\tilde{H}_0(0)}X^2\right). \tag{16}$$

The residue is 2.7 times larger when $\tilde{H}_0''(90) = 10 \cdot \tilde{H}_0(0)$ compared to the case $\tilde{H}_0''(0) << \tilde{H}_0(0)$; and the difference in radiation patterns (Figure 3) also tends to increase the launching efficiency. From this example, we can conclude that the more directive the primary pattern is, the better the efficiency for this type of launcher. However, it is also apparent that the main radiation from the feed is concentrated in a lobe close to the direction $\theta = \pi/2$. This makes the launcher less suitable for measurements of radiation patterns from discontinuities or other radiating structures located on the surface in front of the launcher. To achieve high efficiency for other applications, the aperture of the horn will have to be large, and this is undesirable when good aerodynamic properties are necessary.

It is theoretically possible to create an aperture distribution $H_0(z)$, that for good efficiency will give a low value of $\tilde{H}_0(\beta_z)$ in the region $-\beta_0 < \beta_z < \beta_0$, and a high value at the surface wave pole.

However, if we assume a spectrum function $\tilde{H}_0(\beta_z)$ and calculate $H_0(z)$ from the inversion of (4) we generally arrive at a $H_0(z)$ that is not zero for $z < 0$, which is required by the physical situation. In the case of

a dielectric slab over a ground plane, one also has to deal with sources within the dielectric. [9] The situation is thus very complicated, but this alone should of course not rule out further work in this direction. The main reason for abandoning the vertical apertures for practical applications is that for reasonably good aerodynamic properties, the aperture will have to be small, say in the order of one wavelength or less. What the synthesis procedure touched on above really means under such circumstances is to create an antenna with high supergain ratio and small dimensions. This always results in severe problems in realizing the desired aperture distribution, as well as poor bandwidth performance.

b) Apertures in the Plane z = 0

To illustrate this case, let us consider a ground plane at z = -d, covered by a dielectric slab of thickness d, and relative dielectric constant ϵ.

The **E** field in the aperture (located at z = -d) is assumed to have only an x component $\mathbf{E}_0(x)$ and we define:

$$\tilde{\mathbf{E}}_0(\beta_x) = \int_{-\infty}^{+\infty} e^{j\beta_x x}\, \mathbf{E}_0(x)dx. \tag{17}$$

Above the dielectric, the H_y-field turns out to be (for proof see following chapter).

$$H_y(x, z) = \frac{1}{2\pi} \int_{-\infty}^{+\infty} \tilde{\mathbf{E}}_0(\beta_x)\, Q(\beta_x) e^{-j(\beta_x x + \beta_z z)}\, d\beta_x \tag{18}$$

where

(19) $$Q = \frac{\beta_x \epsilon}{\epsilon \beta_z \cos \beta'_z d - j\beta'_z \sin \beta'_z d}$$

(20) $$\beta_z = \sqrt{\beta_0^2 - \beta_x^2}$$

and

(21) $$\beta_z' = \sqrt{\beta_0^2 \epsilon - \beta_x^2} = \sqrt{\beta_0^2 (\epsilon - 1) + \beta_z^2} \ .$$

Q has poles for $\beta_x = \pm \beta_0 \sqrt{1 + X^2}$ (Figure 4) giving surface waves in both positive and negative x-direction. The radiation pattern $F(\theta)$ can be written:

(22) $$F(\theta) = \cos \theta \, \tilde{E}_0(\beta_x = \beta_0 \sin \theta) \, Q(\beta_x = \beta_0 \sin \theta).$$

The endfire direction here corresponds to $\beta_x = \beta_0$, and for pure endfire radiators the relationship between primary pattern and efficiency is similar to that for the vertical aperture. The design of supergain structures is, however, simpler in this case, since one can work directly with the spectrum function $\tilde{E}_0(\beta_x)$.

Assuming some suitable shape for $\tilde{E}_0$ will, of course, lead to an infinite aperture also here but we are now free to include negative x and truncate the

aperture function on both sides of x= 0 in points where it has a low value. A few examples will be carried out to illustrate this.

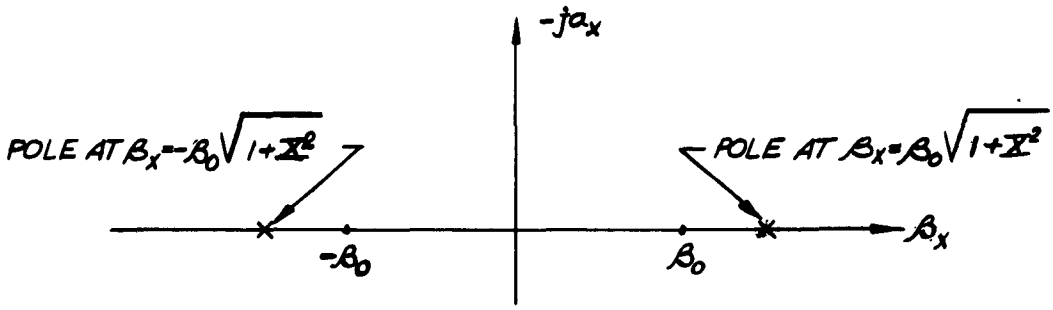

FIGURE 4 - LOCATION OF POLES IN Q OF EQ(19)

1. One suitable form for $\tilde{E}_0(\beta_x)$ would obviously be a narrow pulse-type spectrum with its peak at one of the poles, giving a surface wave in one direction only (Figure 5).

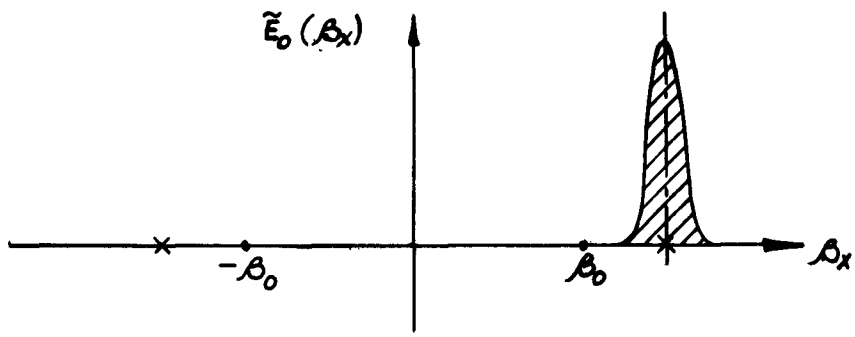

FIGURE 5 - PULSE-SHAPED SPECTRUM

Such a function could be approximated by:

$$\tilde{E}_0(\beta_x) = \frac{\sin A(\beta_x - \beta_0\sqrt{1+X^2})}{(\beta_x - \beta_0\sqrt{1+X^2})} \tag{23}$$

where A is a constant that can be varied to give the pulse the desired height and width. $E_0(x)$ is now given by the inverse of (17):

$$E_0(x) = \frac{1}{2\pi}\int_{-\infty}^{+\infty} \tilde{E}_0(\beta_x)\, e^{-j\beta_x x}\, d\beta_x \tag{24}$$

and one obtains:

$$E_0(x) = \frac{1}{2} e^{-j\beta_0 x\sqrt{1+X^2}} \qquad -A < x < A$$

$$E_0(x) = 0 \qquad |x| > A\ . \tag{25}$$

This means a traveling wave with the same phase-velocity as the surface-wave, and the length of the aperture is 2A.

The spectrum-function given by (23) is known to have a "main lobe" and "sidelobes."[10] To determine the order of magnitude of A for reasonably good efficiency, let us assume that the first null is located at $\beta_x = \beta_0$, so that only the "sidelobes" contribute to the radiation fields. This gives:

$$\frac{2A}{\lambda_0} = \frac{1}{\sqrt{1+X^2} - 1}\ . \tag{26}$$

Figure 6 shows aperture length versus X, derived from (26). For low X-values, the length of the aperture becomes very large, and there are some additional problems with this type of launcher that will be described in more detail in connection with directional coupler feeds.

Before taking another example, it should be pointed out that the result above can be obtained from well-known results in filter theory. The Fourier pair (17), (24) suggests such an analogy, and we can interpret $\tilde{E}_0(\beta_x)$ as a time function, and $E_0(x)$ as the transfer function of a filter. The reverse is also possible, but since our aperture functions are complex it is more convenient to interpret $E_0(x)$ as the transfer function. (23) is then clearly the pulse response from a filter with constant amplitude response in the passband, 2A and a linear phase characteristic.

2. In the previous example, we have really introduced rather severe limitations on $\tilde{E}_0(\beta_x)$. For $|\beta_x| > \beta_0\sqrt{1+X^2}$, the value of $\tilde{E}_0(\beta_x)$ is non-critical, and the spectrum shown in Figure 7 would also be acceptable.

If we assume that the step is located at $\beta_x = \beta_a$, such that $\beta_0 < \beta_a < \beta_0\sqrt{1+X^2}$, and that the shape for $\beta_x > \beta_a$ is that of an exponential function, we can write:

$$E_0(x) = \frac{1}{2\pi}\int_{\beta_a}^{+\infty} e^{-b(\beta_x-\beta_a)}\, e^{-j\beta_x x}\, \frac{d\beta_x}{\beta_a} \quad . \tag{27}$$

This assumption will lead to an infinitely large aperture, but as will be shown later, it is relatively easy to estimate the effect of a truncation of the aperture

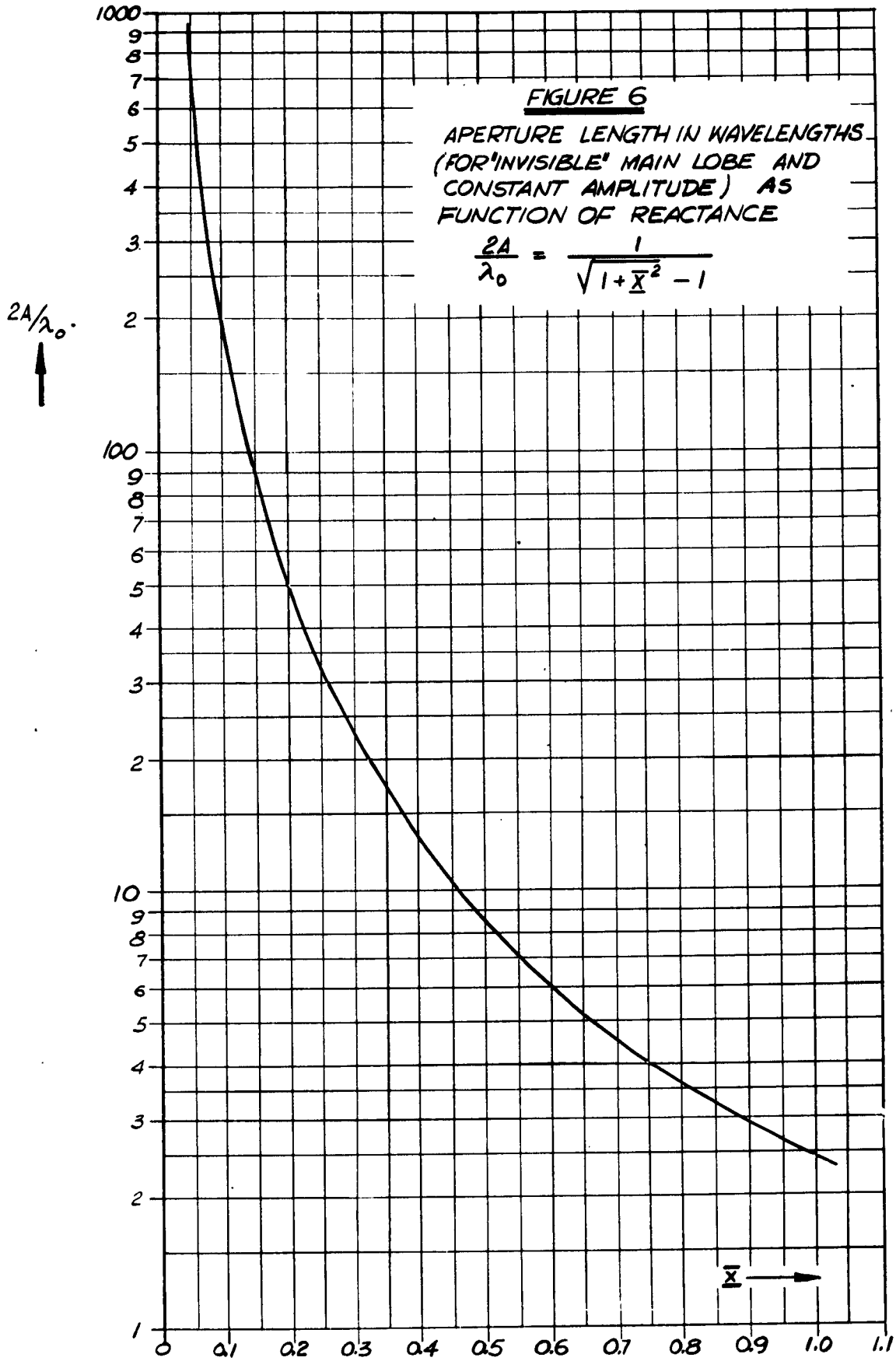
FIGURE 6
APERTURE LENGTH IN WAVELENGTHS (FOR "INVISIBLE" MAIN LOBE AND CONSTANT AMPLITUDE) AS FUNCTION OF REACTANCE
$\frac{2A}{\lambda_0} = \frac{1}{\sqrt{1+\bar{X}^2}-1}$
$2A/\lambda_0$
1000
100
10
1
0
0.1
0.2
0.3
0.4
0.5
0.6
0.7
0.8
0.9
1.0
1.1
$\bar{X}$

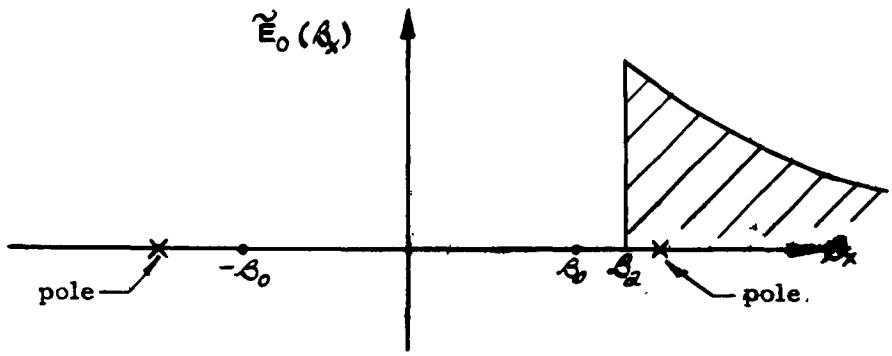

FIGURE 7 - STEP-SHAPED SPECTRUM

to a finite length. From (27) we obtain:

$$E_0(x) = \frac{1}{2\pi\beta_a b\sqrt{1 + x^2/b^2}}\, e^{-j(\beta_a x + \tan^{-1}(x/b))} \tag{28}$$

The aperture field is here basically a traveling wave with varying amplitude but has an extra phase retardation in the center (close to x = 0). Figure 8 shows magnitude and phase of $E_0(x)$ for the case $\beta_a b = 1$. The fact that the magnitude of $E_0(x)$ decreases for increasing $|x|$ indicates that some finite aperture with this distribution would give a good result. It may be reasonable to try a truncation at $x/b = \pm 10$, where the magnitude of $E_0(x)$ is about 20db down from the peak at $x = 0$. The choice of the parameter β_a will then determine the length of the aperture in terms of wavelengths. If the aperture length is 2A, we get:

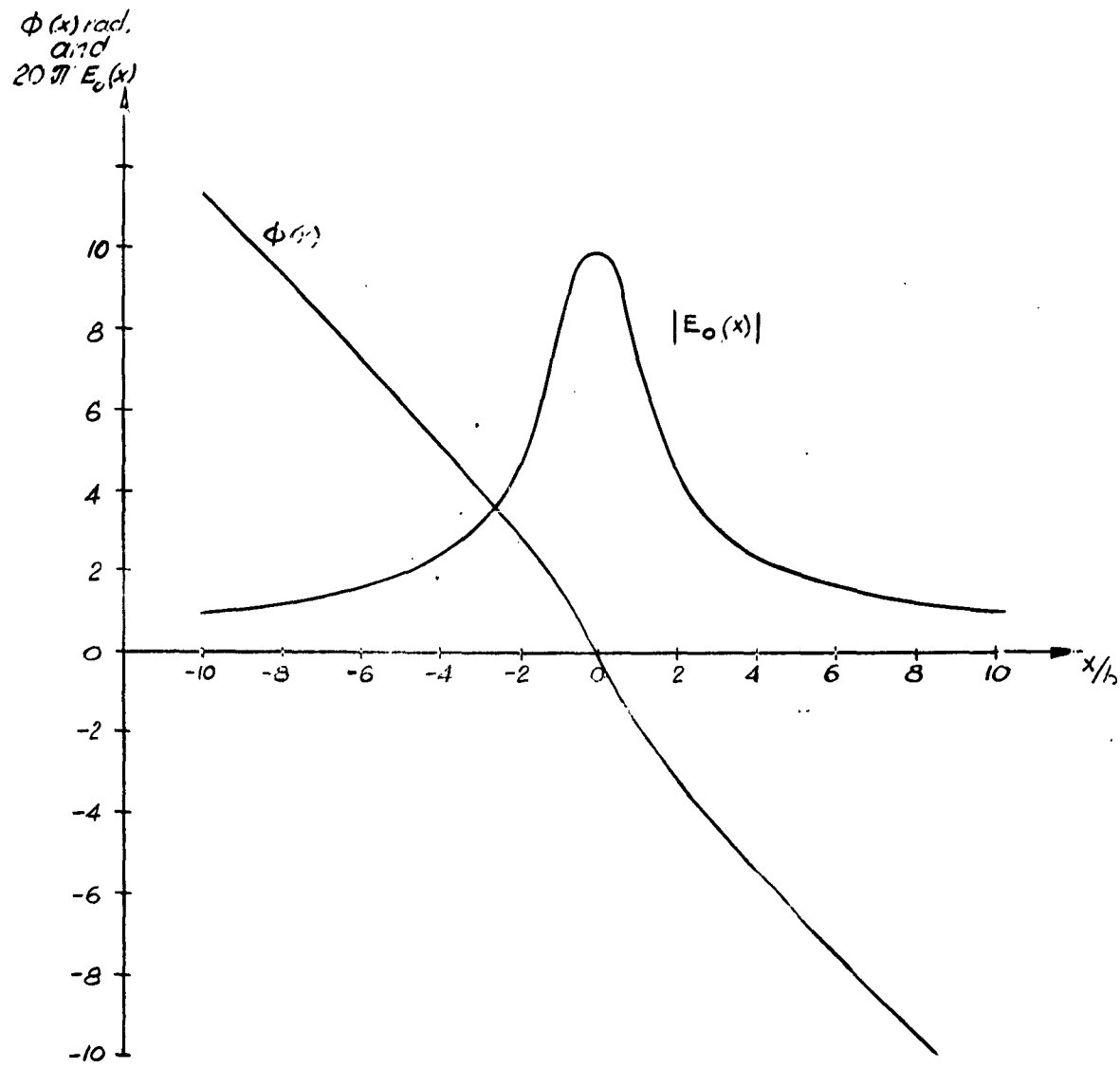

FIGURE 8 - AMPLITUDE AND PHASE OF APERTURE FIELD FOR OBTAINING THE SPECTRUM IN FIGURE 7

(29) $$\frac{2A}{\lambda_0} = \frac{10}{\pi} \beta_a b \frac{\beta_0}{\beta_a} < 3\beta_a b .$$

The aperture length is thus roughly proportional to $\beta_a b$, but when making this parameter small, one encounters another practical limitation. The propagation constant of the aperture field in the center is $\beta_a(1 + \frac{1}{\beta_a b})$ and for small $\beta_a b$ this means a very slow wave, and in addition a fast variation in phase velocity near $x = 0$. Some compromise has to be made between aperture length and the rate of phase velocity variation.

The effect of finite aperture size can be easily determined for $A/b \geq 10$. We get:

(30) $$\tilde{E}_0(\beta_x) = \int_{-A}^{+A} \frac{1}{2\pi\beta_a} \frac{e^{-j(\beta_a - \beta_x)x}}{b + jx} dx.$$

For $x > A$, we can write:

(31) $$E_0(x) \approx \frac{1}{2\pi\beta_a} \frac{e^{-j(\beta_a - \beta_x)x}}{jx} .$$

Using this approximation, the spectrum for $\beta_x < \beta_a$ (normalized to the value at the peak when $A \rightarrow \infty$) can be written:

(32) $$\tilde{E}_0(\beta_x < \beta_a)_{norm} = \frac{1}{2} - \frac{Si(A(\beta_a - \beta_x))}{\pi} .$$

This expression is independent of b,* as long as $A \geq 10b$. Figure 9 shows a plot of (32) and the effect of finite aperture size is exactly what one can expect from the filter analogy. The "rise time" is inversely proportional to the "bandwidth" and from this follows that for small X, β_a will have to be close to β_0. A large value on A will then be required to prevent the flank of the spectrum from falling within the region $\beta_x < \beta_0$.

Like in the previous example, the arrangement arrived at above suggests a "directional coupler" type launcher, but with varying "coupling" and changing phase velocity in the "driving" transmission line.

These aspects will be discussed in connection with directional coupler feeds; but it is already obvious that using continuous distributions with traveling wave characteristics may lead to problems with rapidly changing phase-velocities. If individually fed discrete sources were used, it would be somewhat easier to control phase and amplitude of the aperture function. Returning to the time-frequency analogy, this would correspond to passing a time-function through a filter with several narrow passbands some distance apart (frequency sampling). Such a process is known to result in a time-function at the output of the filter that closely approximates the input function in a time interval whose length is inversely proportional to the spacing of the passbands. Translating this into our "language" tells us that it should be possible to approximate the desired spectrum function $\tilde{E}_0(\beta_x)$ in the region $-\beta_0 < \beta_x < \beta_0$ using point sources along the aperture with a certain maximum spacing.

To be more specific, assume that we have arrived at a desirable continuous

* within the limits of the approximation (31)

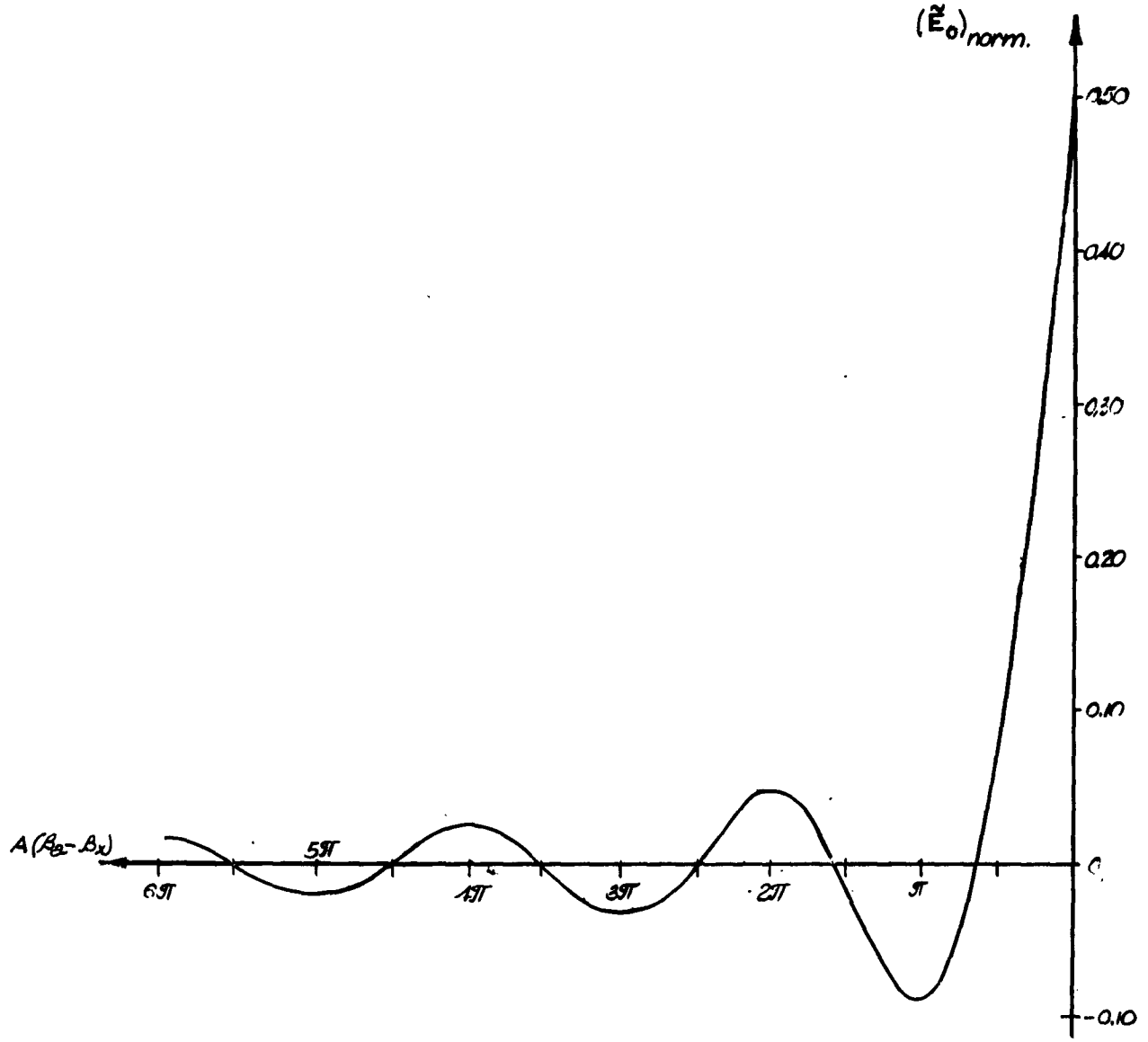

FIGURE 9 - SPECTRUM FOR $\beta_x < \beta_a$, WHEN THE APERTURE FUNCTION IN FIGURE 8 IS TRUNCATED AT $x = \pm 10b$

aperture field given by:

$$\mathbf{E}_0(x) = G(x)e^{j\phi(x)}. \tag{33}$$

Assume further that $G(-x) = G(x)$, and $\phi(-x) = -\phi(x)$; which is always true when $\tilde{\mathbf{E}}_0(\beta_x)$ is real for real β_x. The spectrum is then:

$$\tilde{\mathbf{E}}_0(\beta_x) = 2\int_0^\infty G(x)\cos(\beta_x x - \phi(x))dx. \tag{34}$$

If the aperture is made up of point sources at $x = 0, \pm x_1, \pm x_2, \ldots \pm x_N$, with voltages $V_n = G(x_n)e^{j\phi(x_n)}$, the spectrum becomes:

$$\tilde{\mathbf{E}}_0(\beta_x) = \sum_{n=0}^{N} G(x_n)\cos(\beta_x x_n - \phi(x_n)). \tag{35}$$

For $x_n = nd$, where d is a constant length, (35) has the form of a Fourier series, and provided $\phi(nd) = n\phi_0$, where ϕ_0 is a constant phase-angle, the series will have only cosine terms. This suggests that $\mathbf{E}_0(\beta_x)$ has a periodic behavior. If now a periodic spectrum-function is selected, and its Fourier series is calculated, the location of the slots, as well as the proper excitation voltages (both phase and magnitude) are immediately given.

This seems to be by far the simplest way of designing a launcher of this type, and is in essence the method used for the launcher to be described in this report.

c) Vertical Monopoles or Dipoles

A vertical dipole at some height above the guiding surface, or a monopole on the surface will launch a surface wave. [12] The situation is very similar to that of a vertical aperture, but cylindrical coordinates have to be used for describing the problem completely. The current distribution along the conductor will determine the spectrum, and very little can be done to shape the spectrum from one short dipole. In this respect a single dipole or monopole has the same drawbacks as a low-silhouette vertical aperture. On the other hand, if several elements are distributed over the surface, one has the same possibilities to design for suitable "group spectra" (c.f. "group pattern" in array theory) in the same way as can be done with the slots in the ground-plane treated in the previous paragraph.

d) Directional Coupler Type Launchers

The two examples of launchers with horizontal aperture described above both have aperture fields with traveling wave characteristics. This immediately suggests an open transmission line as the basic element in the launcher. The aperture is then in a sense the coupling region in a directional coupler, between the feeding line and the surface waveguide. This is at least a convenient way of treating the problem of setting up the desired aperture field.

The directional coupler approach has been used for launcher design [13], and for a detailed analysis, this report should be consulted. The analysis is based upon even and odd coupled modes in the coupling region, and several conditions have to be fulfilled simultaneously to allow 100 percent power transfer between

the two waveguides. The design problems may, in a practical case, be more or less severe, but the dual viewpoint of directional coupling and aperture field and spectrum is certainly the most convenient one to apply in the design of traveling wave type launchers.

From the previous discussion it can be deduced that a horizontal aperture made up of discrete sources should offer many advantages. In the following such a launcher will be described and analyzed, and results from tests of an experimental launcher will be presented. The design principles are in essence those already described, but the formulas have to be modified to include a third dimension and put into a form permitting numerical calculations.

First, formulas will be derived for radiation and surface-wave fields excited by a single slot in an infinite ground plane covered by a dielectric slab. The results will then be used to determine a suitable distribution of slots and their proper excitation for obtaining high launching efficiency.

IV. SINGLE SLOT IN A GROUND PLANE COVERED BY A DIELECTRIC SLAB

a) Solution of the Boundary Value Problem

The arrangement considered in this chapter is shown in Figure 10. In the slot ($z = -d$) we assume the **E**-field to be:

$$\mathbf{E}_x = \mathbf{E}_0 \cos \frac{\pi}{2\ell} y \tag{36}$$

$$\mathbf{E}_y = 0.$$

In all other parts of the plane $z = -d$, we have $\mathbf{E}_x = \mathbf{E}_y = 0$, and this plane can be considered as the aperture. Next the aperture field is transformed to a spectrum

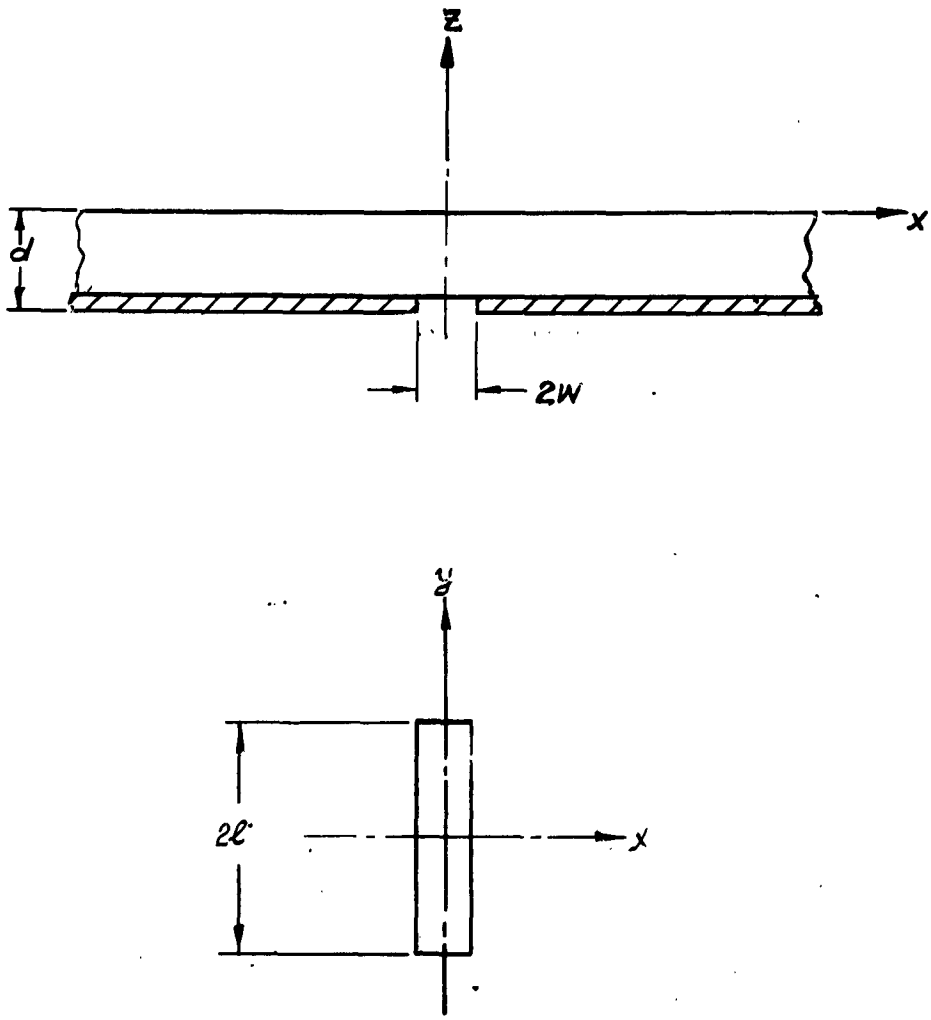

FIGURE 10 - SLOT GEOMETRY

function by means of a two-dimensional Fourier integral:

$$\tilde{\mathbf{E}}_{x0}(\beta_x, \beta_y) = \iint_{-\infty}^{+\infty} \mathbf{E}_x(x, y, -d) e^{j(\beta_x x + \beta_y y)}\, dx\, dy. \tag{37}$$

The spectrum function represents a set of plane waves, and for each pair β_x, β_y one has a wave in a direction represented by the angles ϕ and θ, given by

$$\begin{aligned} \beta_x &= \beta_0 \sin\theta \cos\phi \\ \beta_y &= \beta_0 \sin\theta \sin\phi \end{aligned} \tag{38}$$

We also define

$$p = \beta_0 \sin\theta = \sqrt{\beta_x^2 + \beta_y^2} \tag{39}$$

and

$$\beta_z = \sqrt{\beta_0^2 - p^2} = \beta_0 \cos\theta. \tag{40}$$

If the dielectric were not present, the $\mathbf{E}_x$ field for $z = -d$ would be given by[4]

$$\mathbf{E}_x(x, y, z) = \frac{1}{4\pi^2} \iint_{-\infty}^{+\infty} \tilde{\mathbf{E}}_{x0}(\beta_x, \beta_y) e^{-j(\beta_x x + \beta_y y + \beta_z z)}\, d\beta_x d\beta_y. \tag{41}$$

Now the dielectric is present, and a boundary value problem must be solved. This is done in the following three steps:

1. Each elementary wave (given by a pair β_x, β_y) is split up into one "TE wave" characterized by $E_z = 0$, and one "TM wave" with $H_z = 0$. Together these two waves represent the most general combination giving a certain E_x at $z = -d$, with $E_y = 0$. [4]
2. The boundary conditions in $z = 0$ are introduced for each such wave, and additional fields are introduced to fulfill these conditions.
3. The resulting elementary waves are summed up, using an integral similar to (41) which gives the total field.

During this process we will be working with "field components" that are really "spectrum" or "transform" functions. To stress this fact, the transform signs $\sim$ will be retained throughout the calculations.

The splitting into "TM" and "TE" waves is illustrated in Figures 11 and 12. The two waves are characterized by their "transverse" components $\tilde{E}_t$ and $\tilde{H}_t$, transverse in the sense that they are perpendicular to the direction of propagation. The direction of $\tilde{H}_t$ and $\tilde{E}_t$ is into the paper in Figures 11, 12. From the conditions in the plane $z = -d$, we get:

$$\tilde{E}_t(\beta_x, \beta_y) = \frac{-\beta_y}{p} \tilde{E}_{x0}(\beta_x, \beta_y)$$

(42)

$$Z_0 \tilde{H}_t(\beta_x, \beta_y) = \frac{\beta_x \beta_0}{p \beta_z} \tilde{E}_{x0}(\beta_x, \beta_y).$$

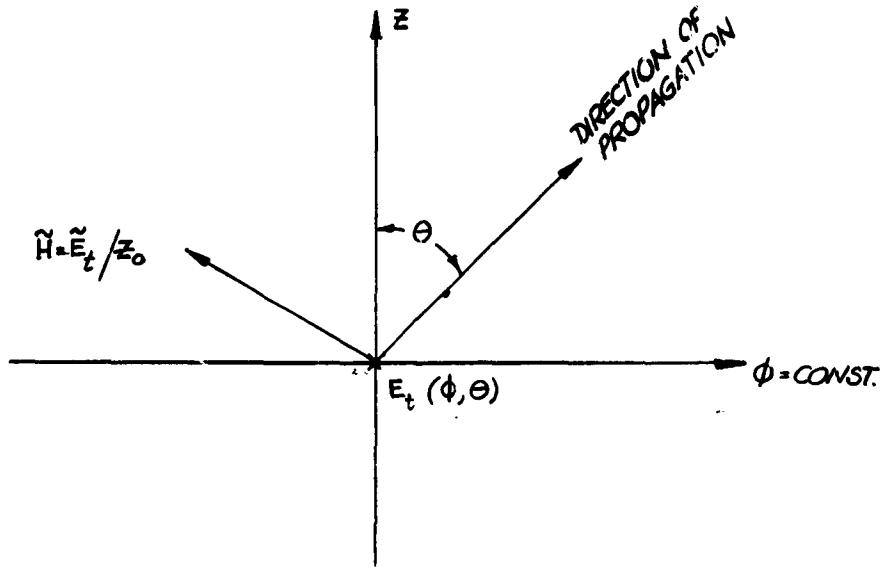

FIGURE 11 - FIELD CONFIGURATION OF THE TE WAVE

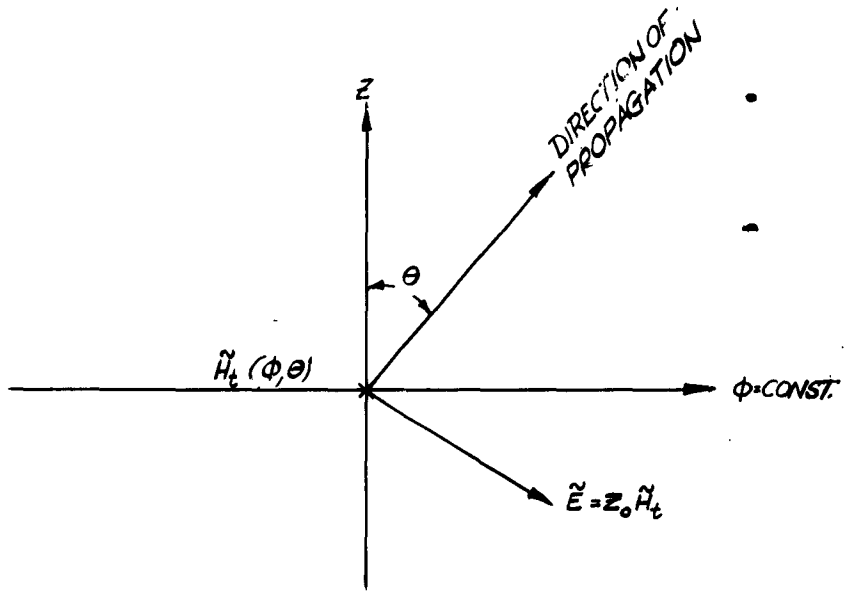

FIGURE 12 - FIELD CONFIGURATION OF THE TM WAVE

Since the surface is isotropic, we can solve the boundary value problems for $\tilde{H}_t$ and $\tilde{E}_t$ for any ϕ, and this can be done as follows:

For the TE waves we assume in the region $z > 0$:

$$\tilde{E}'_t = A_1 e^{-j(\beta_x x + \beta_y y + \beta_z z)} \tag{43}$$

and for $-d < z < 0$

$$E''_t = \left[A_2 e^{-j\beta'_z (z+d)} + A_3 \sin\beta'_z (z+d)\right] e^{-j(\beta_x x + \beta_y y)} \tag{44}$$

where

$$\beta'_z = \sqrt{\beta_0^2 \epsilon - \beta_x^2 - \beta_y^2}. \tag{45}$$

Comparing (44) and (42), we have:

$$A_2 = E'_t(z = -d) = -\frac{\beta_y}{p} \tilde{E}_{x0}(\beta_x, \beta_y). \tag{46}$$

At $z = 0$ the boundary conditions are that both $\tilde{E}_t$ and $\partial/\partial z(\tilde{E}_t)$ are continuous. This gives, after elimination of A_3:

$$A_1 = -\frac{\beta_y}{p} \tilde{E}_{x0} \frac{1}{\cos\beta'_z d + j(\beta_z/\beta'_z)\sin\beta'_z d}. \tag{47}$$

The second term of (44) represents reflections in the boundary between air and dielectric. Since this added field is zero at the ground plane, the boundary conditions there are satisfied.

For $\tilde{H}_t$, we do not know the total field at the groundplane, only the part associated with $\tilde{E}_{x0}$, as given by (42). By treating this part as a "driving" primary field, and adding a reflection term that gives no additional $\tilde{E}_x$ or $\tilde{E}_y$ at z = -d, we can arrive at the correct field.

For $z > 0$, we assume:

$$\tilde{H}'_t = M_1 e^{-j(\beta_x x + \beta_y y + \beta_z z)} \tag{48}$$

and for the region $0 > z > -d$ the assumption is

$$\tilde{H}''_t = \left[M_2 e^{-j\beta_z'(z+d)} + M_3 \cos \beta'_z d \right] e^{-j(\beta_x x + \beta_y y)} . \tag{49}$$

In the dielectric (42) has the form

$$M_2 = \tilde{H}_t(z = -d) = \frac{\beta_x}{p} \frac{\beta_0 \sqrt{\epsilon}}{\beta_z'} \frac{\sqrt{\epsilon}}{Z_0} \tilde{E}_{x0}(\beta_x, \beta_y). \tag{42a}$$

The boundary conditions at $z = 0$ are

$$\tilde{H}_t' = \tilde{H}_t'' ; \quad \frac{\partial}{\partial z} \tilde{H}_t' = \frac{1}{\epsilon} \frac{\partial}{\partial z} \tilde{H}_t'' .$$

After elimination of M_3 between (48) and (49), and introduction of (42a) one obtains

$$M_1 = \frac{\beta_x}{p}\frac{\beta_0}{\beta_z}\frac{\tilde{E}_{x0}}{Z_0}\frac{1}{\cos\beta'_z d + j(\beta'_z/\epsilon\beta_z)\sin\beta'_z d} \tag{50}$$

The fields for $z > 0$ are then given by

$$E_t(x, y, z) = \frac{1}{4\pi^2}\iint_{-\infty}^{+\infty} A_1(\beta_x, \beta_y)e^{-j(\beta_x x+\beta_y y+\beta_z z)}\,d\beta_x d\beta_y \tag{51}$$

$$H_t(x, y, z) = \frac{1}{4\pi^2}\iint_{-\infty}^{+\infty} M_1(\beta_x, \beta_y)e^{-j(\beta_x x+\beta_y y+\beta_z z)}\,d\beta_x d\beta_y . \tag{52}$$

b) Radiation Fields

The radiation fields can be obtained from (51) and (52) using saddle point integration. The result is

$$\begin{aligned} E_\phi &= \frac{j\beta_0}{2\pi}A_1(\phi, \theta)\cos\theta\frac{e^{-j\beta_0 R}}{R} \\ H_\theta &= \frac{E_\phi}{Z_0} \\ H_\phi &= \frac{j\beta_0}{2\pi}M_1(\phi, \theta)\cos\theta\frac{e^{-j\beta_0 R}}{R} \\ E_\theta &= Z_0 H_\phi \end{aligned} \tag{53}$$

The calculations leading from (51), (52) to (53) are collected in Appendix I.

For power calculations, we also need an expression for the Poynting vector in the far field. We have

$$S = \frac{1}{4\pi^2} \frac{\beta_0^2}{R^2} \cos^2\theta \left[\frac{A_1 A_1^*}{Z_0} + Z_0 M_1 M_1^* \right] \tag{54}$$

where * denotes complex conjugates.

c) Surface Wave Fields

As is described in Appendix I, the surface wave fields can be obtained from the residues in the poles of A_1 and M_1. In the general case, both these functions will have poles, but if $\beta_0 d\sqrt{\epsilon - 1} < \frac{\pi}{2}$, M_1 will have only one pole, and A_1 has none. [9] The p-value at the pole can be written $p = \beta_0\sqrt{1 + X^2}$, where X is obtained from equation (A18) in Appendix II. Using (50) and (A13), we can write the H_ϕ component of the surface wave field

$$H_{\phi s} = \frac{1 + j}{4\pi^2} 2\pi j \sqrt{\frac{\pi \beta_0 \sqrt{1 + X^2}}{r}} e^{-\beta_0 X z - j\beta_0 r\sqrt{1+X^2}} \tag{55}$$

$$\cdot \lim_{p \to \beta_0\sqrt{1+X^2}} \left[(p - \beta_0\sqrt{1 + X^2}) M_1(p, \phi) \right] .$$

The expression (55) can now be compared with (A15) of Appendix II, to establish the correct value of K. The "power density" in the surface wave (i.e. the power contained in an angular interval $\Delta\phi$ of unit measure) is then

obtained from (A16). By integrating the surface wave power and the radiated power as obtained from (54), the efficiency of one slot is readily determined. In next section, the efficiency will be calculated for a specific case, as well as the distribution of radiation fields and surface wave.

V. RADIATION AND SURFACE WAVE FIELDS FROM ONE SLOT

a) Radiation Fields

The following numerical values on the various parameters will be used:

(56)

$$\lambda_0 = 1.20 \text{ inch} \qquad 2\ell = 0.54 \text{ inch}$$
$$\omega = 2\pi \cdot 9.83 \cdot 10^9 \text{ rad/sec.} \qquad 2w = 1/16 \text{ inch}$$
$$\epsilon = 2.30 \qquad d = 1/8 \text{ inch}$$

First, the radiation pattern will be computed, using the formulas derived in Appendix I.

We observe, that for $|p| < 2\beta_0$, $pw < 0.1$, so that the factor $\sin(pw \cos\phi)/(pw \cos\phi)$ in (A3) is ≈ 1 for all p-values of interest. With this approximation, A_1 and M_1 become:

$$(57) \quad A_1 = -\frac{16E_0 w\ell}{\pi} \frac{\cos\left[\frac{\pi}{2}\frac{4\ell}{\lambda_0}\sin\theta\sin\phi\right]}{\left[1-\left(\frac{4\ell}{\lambda_0}\right)^2\sin^2\theta\sin^2\phi\right]} \frac{\sin\phi}{\left[\cos\tau + \frac{j\cos\theta}{\sqrt{\epsilon-\sin^2\theta}}\sin\tau\right]}$$

$$(58) \quad M_1 = \frac{16E_0 w\ell}{\pi} \frac{\cos\left[\frac{\pi}{2}\frac{4\ell}{\lambda_0}\sin\theta\sin\phi\right]}{\left[1-\left(\frac{4\ell}{\lambda_0}\right)^2\sin^2\theta\sin^2\phi\right]} \frac{\cos\phi}{\left[\cos\tau\cos\theta + j\left(\sqrt{\epsilon-\sin^2\theta}/\epsilon\right)\sin\tau\right]}$$

where:

$$\tau = \beta_0 d\sqrt{\epsilon - \sin^2\theta} \quad .$$

The power pattern can now be obtained from (54).

For convenience in later computations, we normalize the pattern so that the variable part is unity for $\theta = 0$. This gives:

$$S = \frac{S_0}{R^2} \frac{\cos^2\left[\frac{\pi}{2}\frac{4\ell}{\lambda_0}\sin\theta \cdot \sin\phi\right]}{\left[1 - (\frac{4\ell}{\lambda_0})^2 \sin^2\theta \cdot \sin^2\phi\right]^2} \left[\frac{\cos^2\theta \cdot \sin^2\phi(1 - \frac{\epsilon-1}{\epsilon}\sin^2\tau_0)}{1 - \frac{\epsilon - 1}{\epsilon - \sin^2\theta}\sin^2\tau}\right.$$

(59)

$$\left. + \frac{\cos^2\phi(1 - \frac{\epsilon-1}{\epsilon}\sin^2\tau_0)}{1 - \frac{\epsilon-1}{\epsilon^2}\frac{\epsilon\cos^2\theta - \sin^2\theta}{\cos^2\theta}\sin^2\tau}\right]$$

where $\tau_0 = \beta_0 d\sqrt{\epsilon}$, and

$$(60) \qquad S_0 = \frac{64}{\pi^4} E_0^2 w^2 \ell^2 \frac{\beta_0^2}{Z_0} \frac{1}{(1 - \frac{\epsilon-1}{\epsilon}\sin^2\tau_0)} \quad .$$

The total power radiated is:

$$(61) \qquad P_{rad} = \int_0^{\pi/2}\int_0^{2\pi} SR^2 \sin\theta \, d\phi \, d\theta \quad .$$

This integral has been evaluated numerically with the result:

$$P_{rad} = S_0 \cdot 2.52 \ .$$

(59) shows the effect of the dielectric on the radiation pattern. For example if $\tau \to 0$, (or $\epsilon \to 1$), the pattern for $\phi = 0$ is independent of θ as it should be. With the dielectric, a null occurs for $\theta = \pi/2$ at all ϕ values. Figure 13 shows the pattern for $\phi = 0$, as given by (59).

b) Surface Wave Fields

Equation (A17) of Appendix II gives for the parameters assumed above $X = 0.392$. According to (A13), (A3), the H_ϕ field of the surface wave is for $Z > 0$ and $\beta_0 r >> \phi$:

$$H_{\phi_s} = (1+j)\frac{16E_0 w\ell}{4\pi^3 Z_0} \frac{\cos\left[\frac{\pi}{2}\frac{4\ell}{\lambda_0}\sqrt{1+X^2}\sin\phi\right]}{\left[1-\left(\frac{4\ell}{\lambda_0}\right)^2(1+X^2)\sin^2\phi\right]}(\cos\phi)\beta_0\sqrt{\frac{\pi\beta_0\sqrt{1+X^2}}{r}}$$

$$\cdot \lim_{u \to \sqrt{1+X^2}} \left[j \frac{(u-\sqrt{1+X^2})\,2\pi j}{\left[\frac{\sqrt{\epsilon-u^2}}{\epsilon}\sin\left[\beta_0 d\sqrt{\epsilon-u^2}\right] - \sqrt{u^2-1}\cos\left[\beta_0 d\sqrt{\epsilon-u^2}\right]\right]} \right] \tag{62}$$

$$\cdot e^{-\beta_0 X z - j\beta_0 r\sqrt{1+X^2}} \ .$$

Performing the limiting process results in

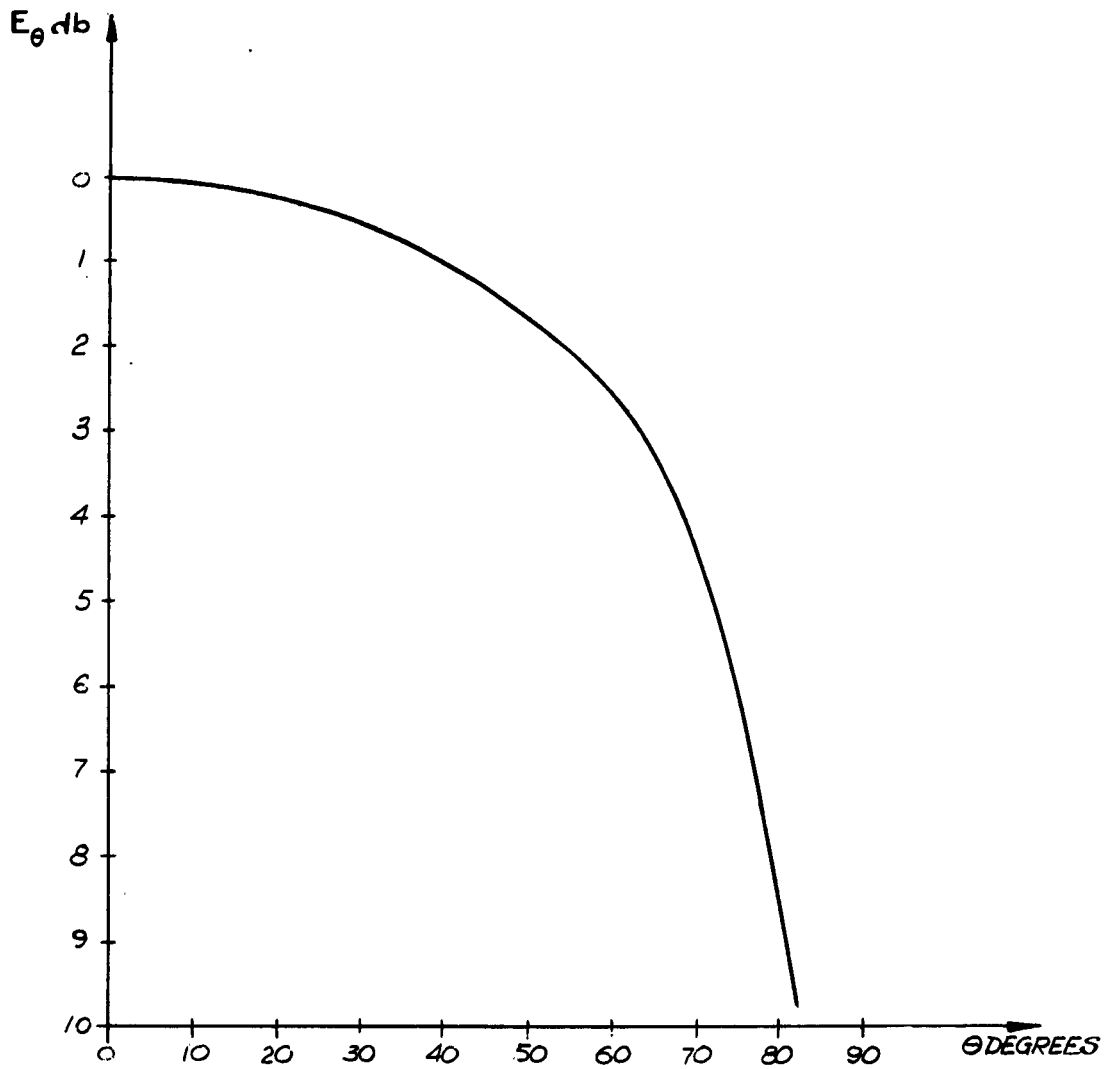

FIGURE 13 - E_θ FOR $\phi = 0$ WITH $d = 1/8"$, $\epsilon = 2.3$, $\lambda_0 = 1.20"$

$$(63) \qquad \lim[\,] = -\frac{2\pi\epsilon X\left[1+(\epsilon+1)X^2\right]\cos\left[\beta_0 d\sqrt{\epsilon-1-x^2}\,\right]}{\sqrt{1+X^2}\,\left[\epsilon+\beta_0 dX\left[1+(\epsilon+1)X^2\right]\right]} \,.$$

The power density in the wave can be written:

$$(64) \qquad S_s = \frac{S_{s_0}}{r}\cos^2\phi\,\frac{\cos^2\left[\frac{\pi}{2}\frac{4\ell}{\lambda_0}\sqrt{1+X^2}\sin\phi\right]}{\left[1-\left(\frac{4\ell}{\lambda_0}\right)^2(1+X^2)\sin^2\phi\right]^2} \,.$$

The surface wave pattern is shown in Figure 14.

The total power in the surface wave is then:

$$(65) \qquad P_s = \int_0^{2\pi} S_s\, d\phi \,.$$

For the assumed parameters, one obtains $P_s = 2.90 S_{s_0}$, and the efficiency is then given by

$$(66) \qquad \eta = \frac{P_s}{P_{rad}+P_s} = \frac{1}{\left[1+0.868\frac{S_0}{S_{s_0}}\right]} \,.$$

A comparison between (62), (63), and (A14) results in a value for K that can be inserted into (A16) in order to obtain S_{s_0}. The result is

$$(67) \qquad S_{s_0} = \frac{64}{\pi^3}E_0^{\,2}w^2\ell^2\frac{\beta_0^2}{Z_0}\left[\frac{\epsilon X\left[1+(\epsilon+1)X^2\right]}{\epsilon+\beta_0 dX(1+(\epsilon+1)X^2)}\right]\left[\frac{\beta_0 d}{\epsilon}+\frac{1}{X\left[1+(\epsilon+1)X^2\right]}\right] \,.$$

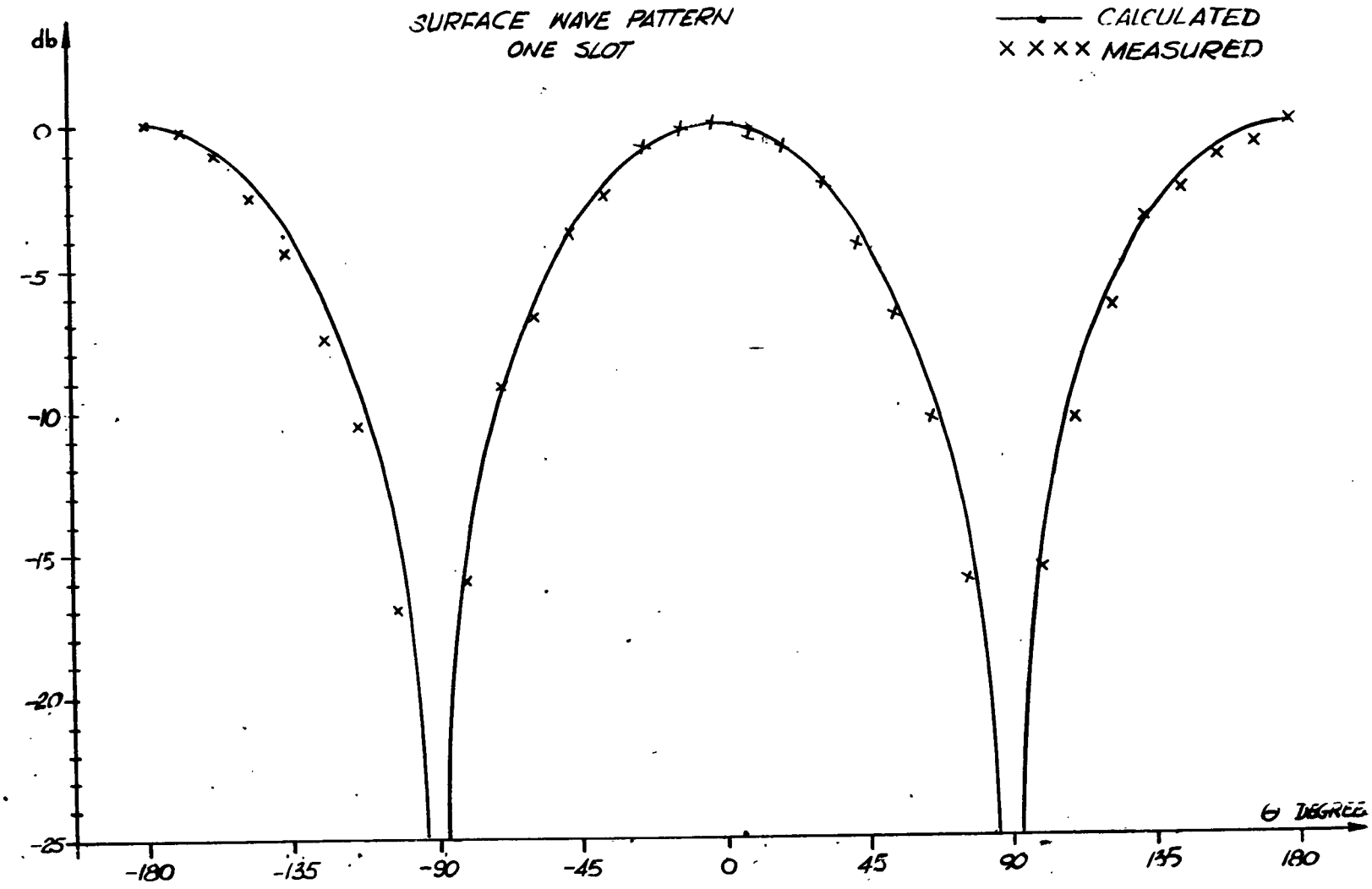
SURFACE WAVE PATTERN
ONE SLOT
CALCULATED
MEASURED
db
0
-5
-10
-15
-20
-25
-180
-135
-90
-45
0
45
90
135
180
θ DEGREE

FIG. 14

Insertion of appropriate numbers in (60) and (67) gives $S_0 = 1.04 S_{s_0}$, and from (66) one obtains $\eta = 0.525$.

The efficiency of one slot plays a vital part in the following, since it is used for relative calibration of surface wave and radiation field probes used to determine efficiency for a 5 slot launcher.

VI. COMBINATION OF SLOTS FOR HIGH EFFICIENCY

On a two-dimensional guiding surface one can use an argument similar to that of "group spectra" used earlier for one-dimensional guides.

If we assume that an array of slots of finite length is placed along the x-axis, the transform function of the array can be written:

$$\tilde{F}(\beta_x, \beta_y) = \tilde{F}_{slot}(\beta_x, \beta_y) \sum_n A_n e^{-j\beta_x x_n} \tag{68}$$

where $\tilde{F}_{slot}$ is the transform for one slot with unit excitation, A_n is the (complex) amplitude of the nth slot, and $\beta_x = \beta_0 \sin\theta \cos\phi$. The notation $\tilde{F}_a$ and the word "array factor" will be used for the series in (68).

Next, assume that the array factor has the shape of a "square wave" as shown in Figure 15. To find the qualitative effect on the radiation pattern that this array factor would give, we recall that the pattern in a direction (ϕ, θ) in space is proportional to $\tilde{F}(\beta_x = \beta_0 \sin\theta \cos\phi,\ \beta_y = \beta_0 \sin\theta \sin\phi)$. Also, the surface wave amplitude in a direction ϕ is proportional to $F[\beta_x = \beta_0 \sqrt{1+X^2} \cos\phi,\ \beta_y = \beta_0 \sqrt{1+X^2} \sin\phi]$.

Figure 16 shows the β_x-β_y plane with shaded areas representing $\tilde{F}_a = 2$.

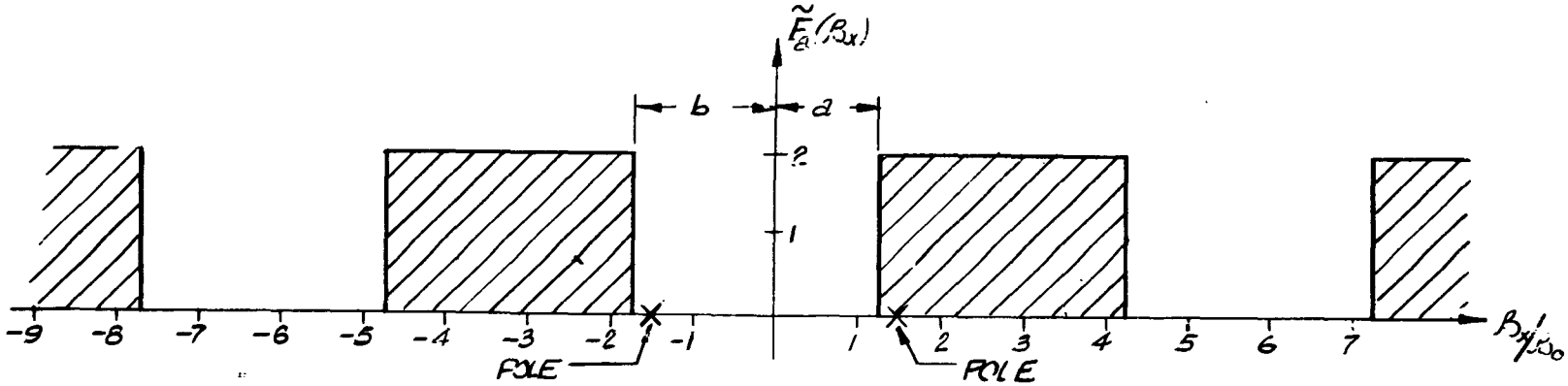

FIGURE 15

SQUARE WAVE SPECTRUM, ONE DIMENSION

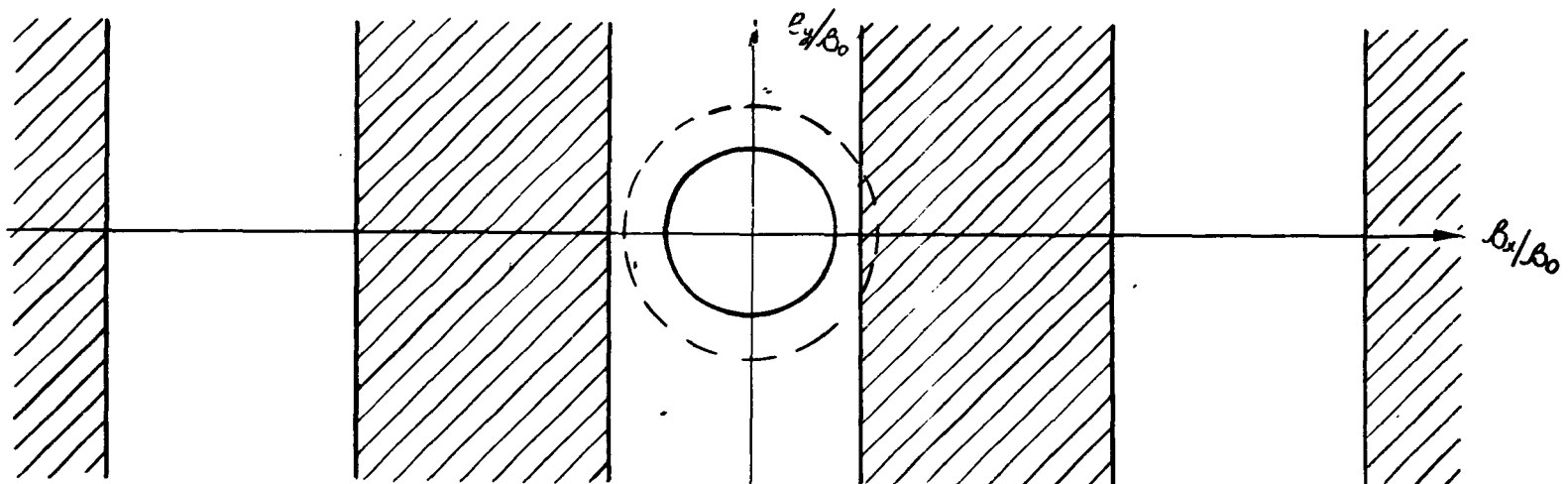

FIGURE 16

SQUARE WAVE SPECTRUM, TWO DIMENSIONS

The inner circle is the boundary for radiation (real θ), and the dotted circle represents the pole at $p = \beta_0\sqrt{1+X^2}$. It is obvious that this $\tilde{F}_a$ will suppress the radiation completely, and the surface wave will be confined to a rather narrow angular region around $\phi = 0$.

Using the two numbers a and b shown in Figure 15 to fix the position and period of the square-wave, $\tilde{F}_a$ gets the form:

$$(69) \qquad \tilde{F}_a(\beta_x) = 1 - \frac{4}{\pi}\sum_{n=0}^{\infty}\frac{(-1)^n}{2n+1}\cos\left[(2n+1)\left[\frac{\beta_x\lambda_0}{2(a+b)} - \frac{\pi}{2}\frac{a-b}{a+b}\right]\right].$$

The relative amplitude and phase of the slots, as well as their location is shown in Figure 17 (a = 1, b = 1.25 is assumed). A comparison with Figure 8 illustrates the close relationship between the continuous distribution for a step-type spectrum and this slot arrangement. The slots can clearly be looked upon as sampling points for the continuous function.

In a practical launcher, one has to use a finite number of slots, and this will have the same effect on the spectrum as a low-pass filter on a square-wave. Once the number of slots is determined, the shape of $\tilde{F}_a$ is given, and a, b can be chosen to suit various conditions on surface wave and radiation fields. This process is best described by an example.

Assume that 5 slots are to be used, and that X = 0.39 as before. We want to suppress the surface wave for negative x ($\phi = \pi$), and place one null of the spectrum function at $\beta_x = -\beta_0\sqrt{1+X^2}$ (Figure 18). This gives us the equation:

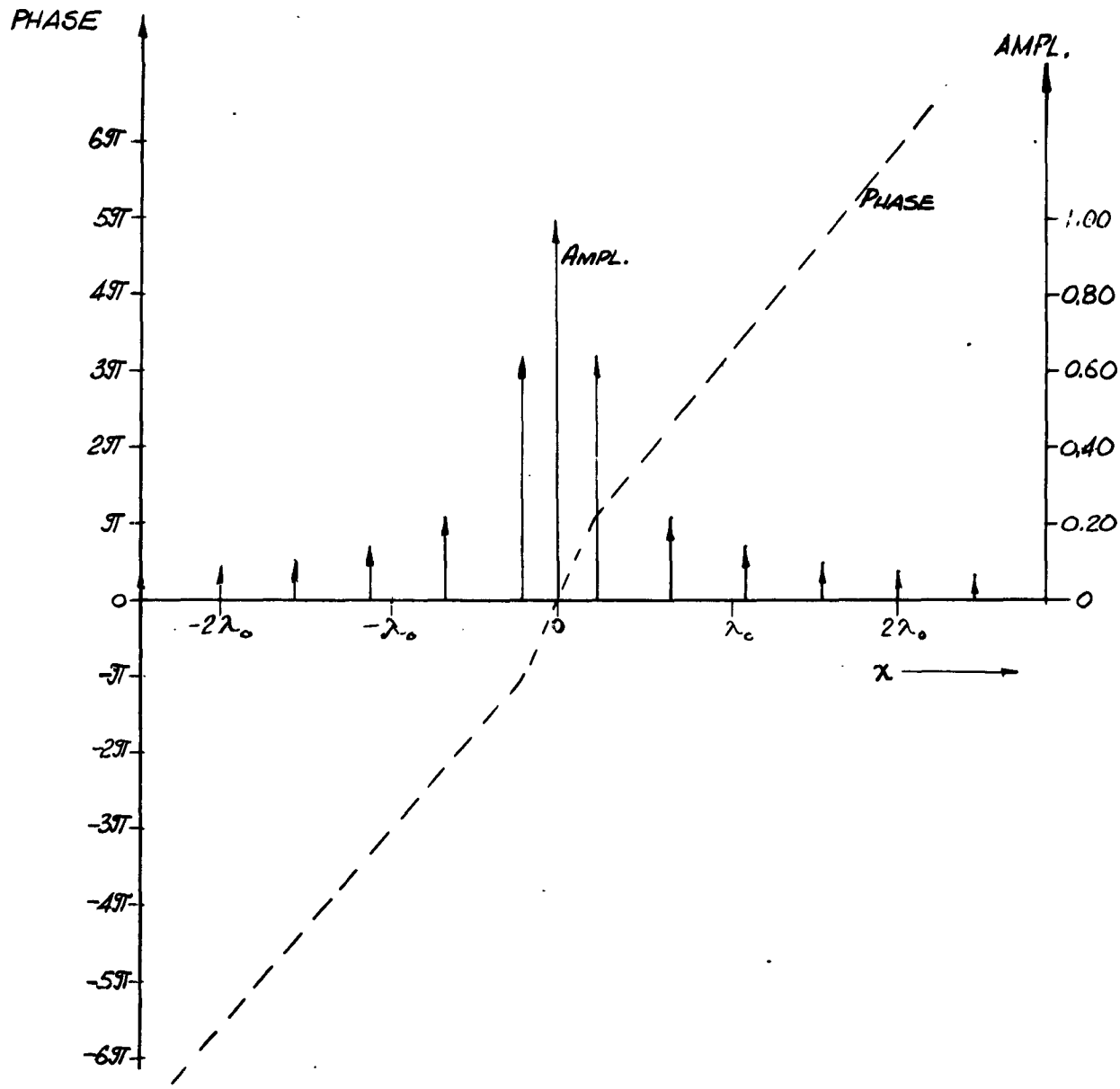

FIGURE 17 - AMPLITUDE AND PHASE DISTRIBUTION IN MULTISLOT LAUNCHER a = 1.0, b = 1.25 (FIGURE 15)

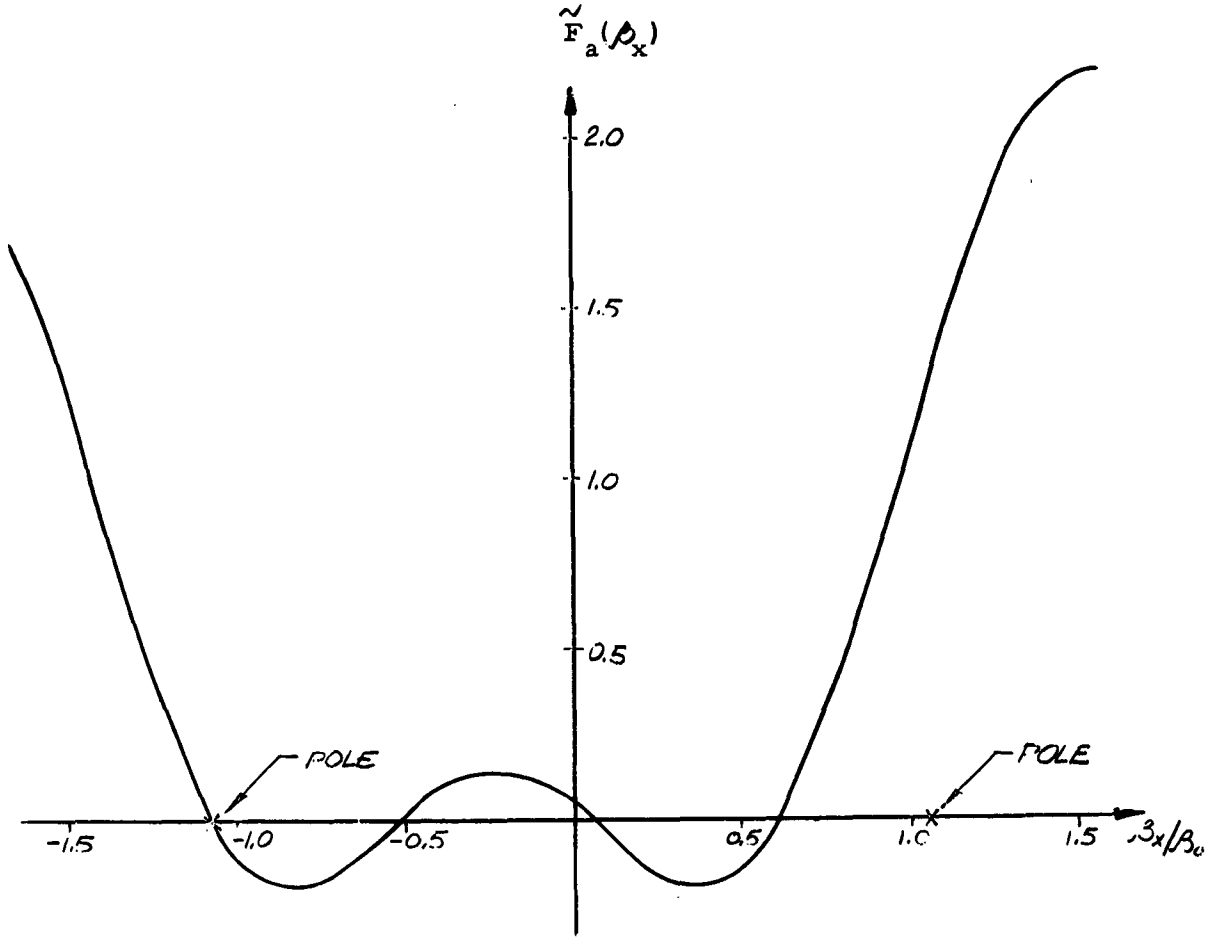

FIGURE 18 - SPECTRUM FOR 5 SLOTS, a = 0.97, b = 1.43 (FIGURE 13)

$$(70) \qquad -\frac{\beta_0\sqrt{1+X^2}\,\lambda_0}{2(a+b)} - \frac{\pi}{2}\left(\frac{a-b}{a+b}\right) = -1.10 .$$

One more condition is needed, and we could for instance assume $a = 1$, which makes $b = 1.43$ and

$$(71) \qquad \frac{\beta_x\lambda_0}{2(a+b)} - \frac{\pi}{2}\left(\frac{a-b}{a+b}\right) = \beta_x\frac{\lambda_0}{4.43} + 0.28 .$$

The three middle slots will thus be about $\lambda_0/4$ apart, and the distance between two of the outer slots is nearly $\lambda_0/2$. The length of the array is less than $1.5\lambda_0$.

VII. DESIGN AND ADJUSTMENT OF 5-SLOT LAUNCHER

It was decided to build a 5-slot launcher using the design principles described in the preceding section. In the final design b was chosen to 1.43, and a was made 0.97. For a wavelength $\lambda_0 = 1.20$ inches, $\lambda_0/2(a+b)$ is then 0.25 inch. Figure 18 shows the resulting spectrum function. The three slots in the middle are then 0.25 inch apart, and regular X-band waveguide (RG52 or WR90) cannot be used to feed these slots. Waveguides with inner dimensions .200 x .900 inches("1/2 height X-band guide") were therefore used for all the slots.

Phase-shifters of the dielectric-slab type were introduced in all the feeding guides, except the guide feeding the middle slot.

The power division network is shown in Figure 19. To the two outer

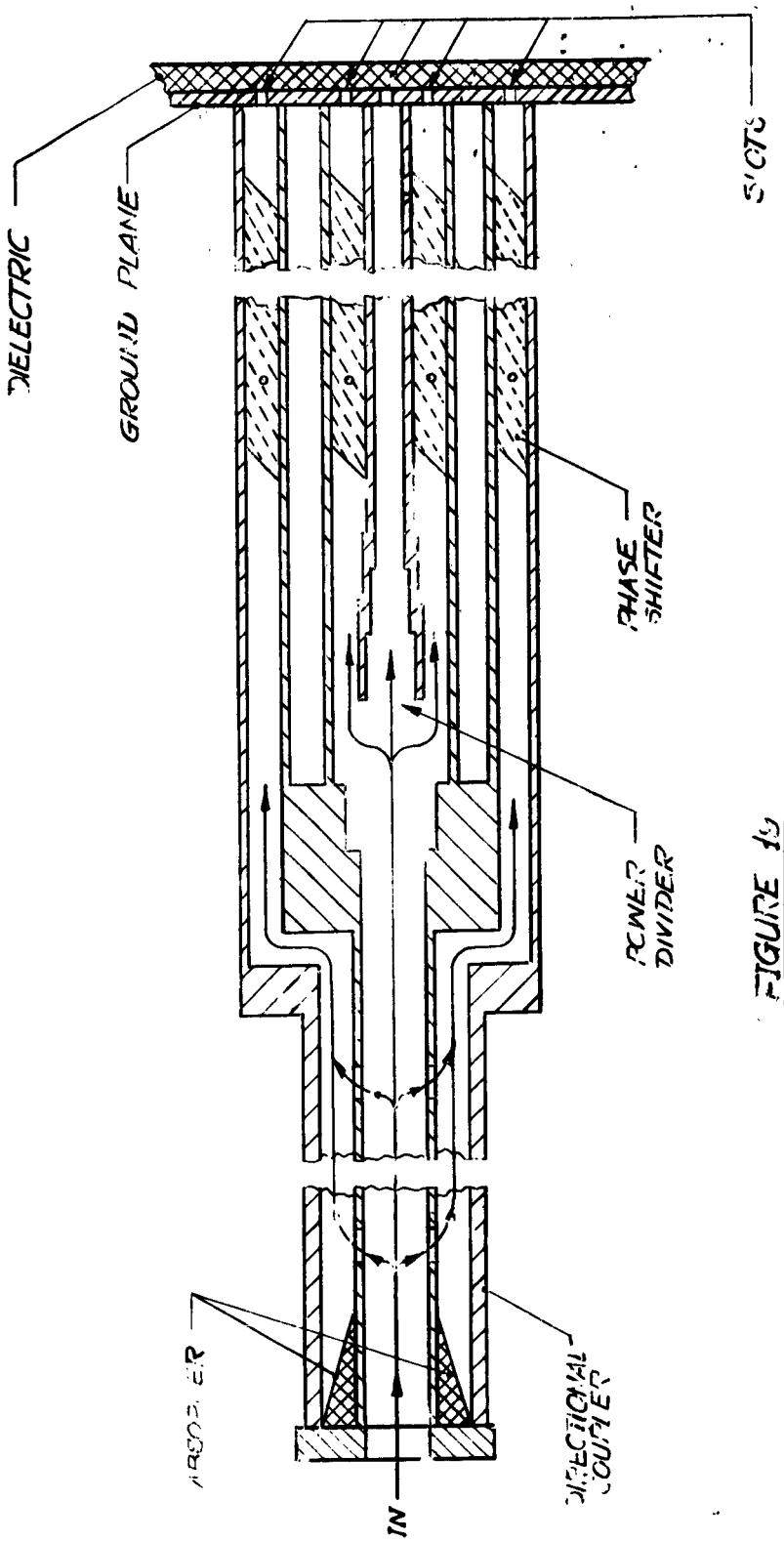

FIGURE 15

FEEDING ARRANGEMENT FOR THE 5 SLOT LAUNCHER

slots power is taken from the input guide via directional couplers. The remaining power is split up between the three middle guides in the way shown in Figure 19. The power ratios were thus not variable, but designed to provide the correct power ratios if no coupling between the slots takes place. This is, of course, not a realistic assumption, but on the other hand it is extremely difficult to anticipate the coupling effects, and some assumptions had to be made. In the first try we were also prepared to waste power if necessary by introducing lossy devices in order to obtain the desired slot fields (Figure 20). The important question is not the overall efficiency, but the launching efficiency in terms of the relation between surface wave power and radiation emitted by the launcher.

The slots were cut in a 1/16 inch thick aluminum plate with the dimensions 6x4 inches The slot-width was 1/16 inch and length was adjusted to present a good match to the feeding guide when covered by a polyethylene slab of thickness 1/8 inch. This length was experimentally determined to 0.54 inch or $0.45\lambda_0$ for a VSWR < 1.2.

Grooves were cut 1/32 inch deep on the side of the plate facing the feeding guides, mating their walls, in order to ensure good contact between the walls and the plate, so as to prevent leakage between individual guides.

To make measurements on a single slot possible, a similar plate was made with one slot. The groundplane was a circular aluminum plate, 1/8 inch thick and 36 inches in diameter. In the center a rectangular hole was cut to accept the slotted plates. Good contact between the circular and rectangular

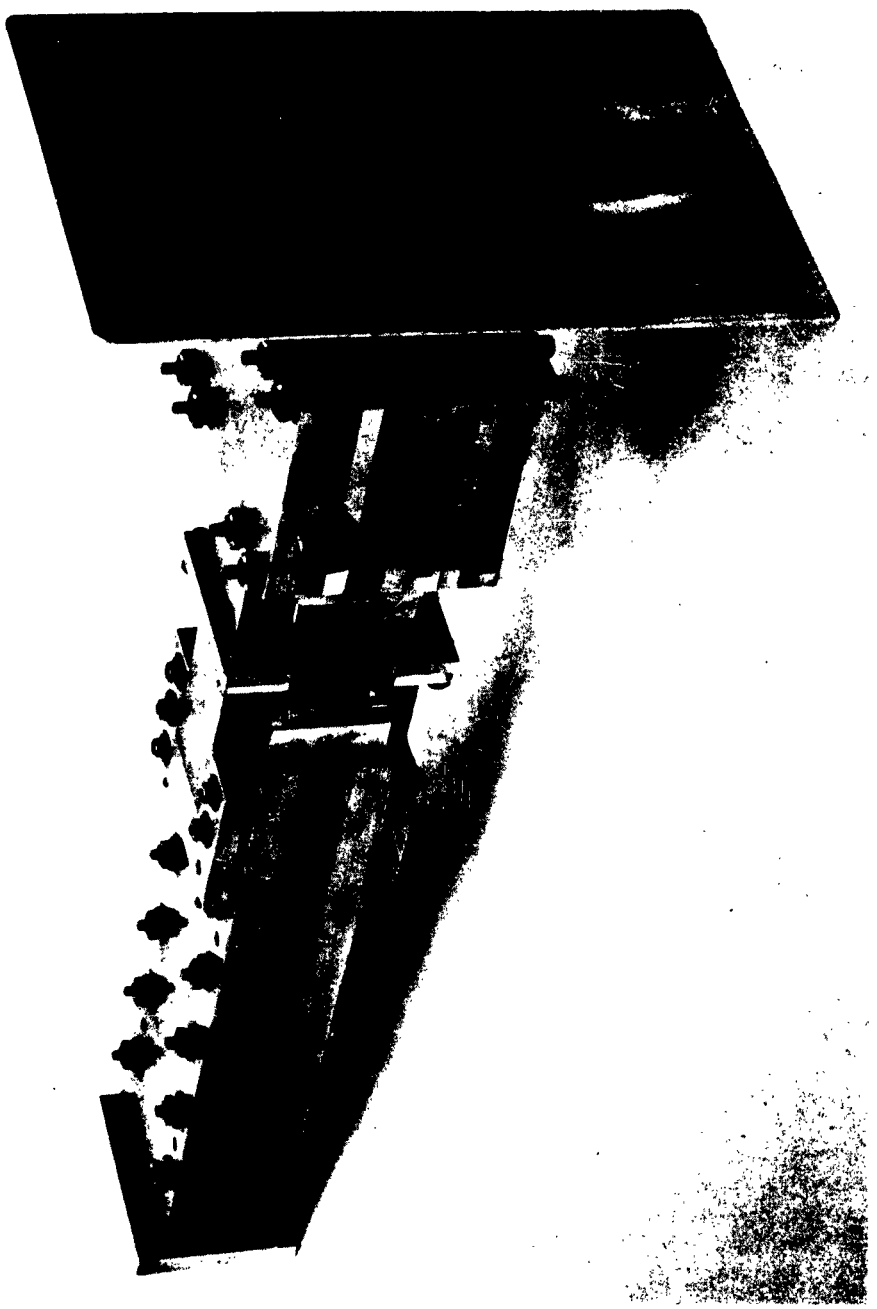

FIGURE 20 - FIVE SLOT LAUNCHER (NOTE STRIPS OF ABSORBING FILM TAPED ACROSS TWO OF THE SLOTS).

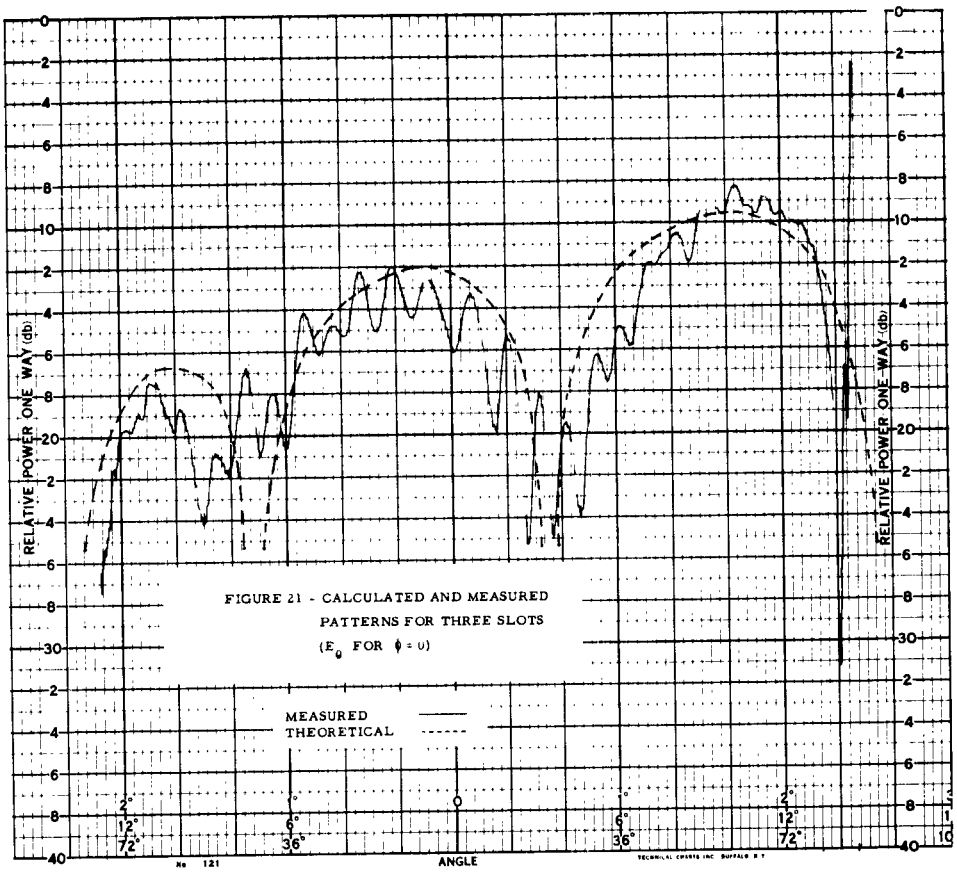

FIGURE 21 - CALCULATED AND MEASURED PATTERNS FOR THREE SLOTS (E_θ FOR $\phi = 0$)

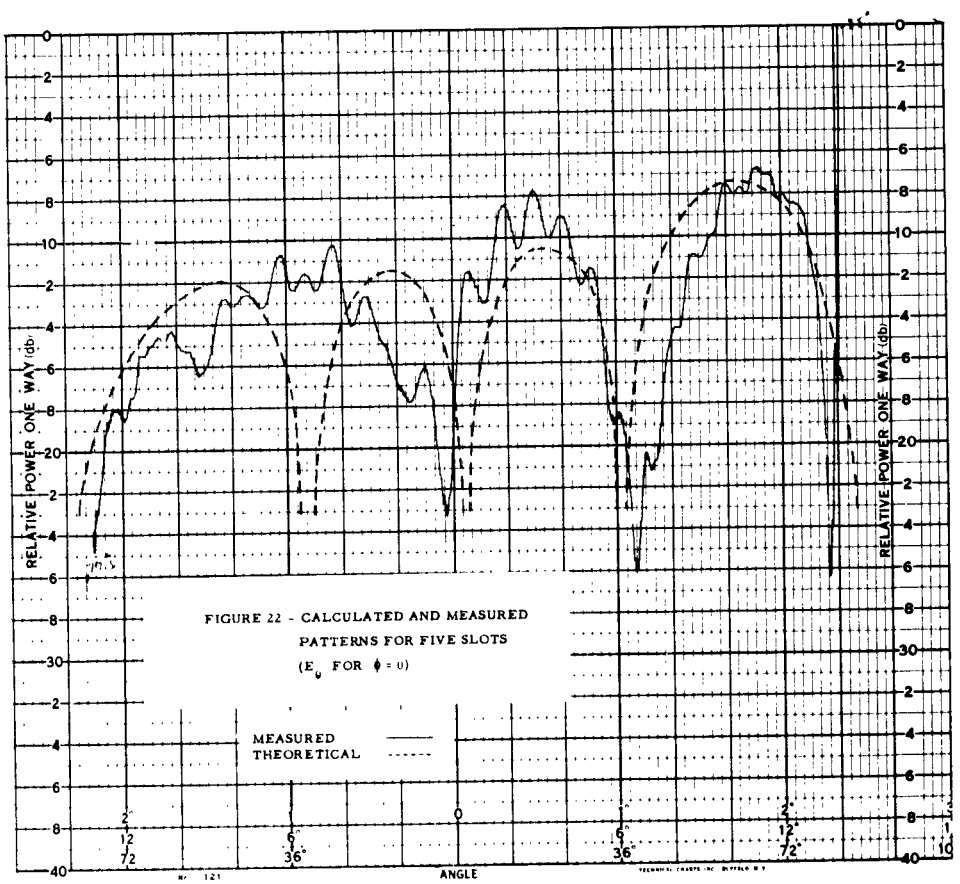

FIGURE 22 - CALCULATED AND MEASURED PATTERNS FOR FIVE SLOTS (E_θ FOR $\phi = 0$)

plates was ensured by covering the gap between them with aluminum foil.

To measure radiation patterns, a probe arm was erected, permitting the measurement of E_ϕ or E_θ as a function of θ for any ϕ. A synchro was attached to the probe arm to permit use of a pattern recorder. The same arrangement was used to measure surface wave distribution as a function of ϕ.

The probe was an open-ended WR90 waveguide that could be turned to accept the desired polarization and the distance probe-launcher was about 11 inches. The setup, including a parabolic reflector and with the ground-plane extended for the experiments described in Section IX, is shown in Figure 24.

Adjustment of the launcher had to be made in two steps. First the two outer slots were covered with aluminum foil and the pattern for the three middle slots was taken for $\phi = 0$ (Figure 21). A direct way of measuring relative phase and amplitude in the slots would have been preferable. However, such a method is very hard to conceive, since the measurements have to be made with the dielectric slab in place and without disturbing the coupling between the slots.

The desired pattern had been computed in advance, using the previously presented theory. The phase shifters were adjusted for closest agreement between theoretical and measured patterns, but at first the agreement was rather poor. By calculating and plotting the spectrum from the measured pattern it was found that this was due to higher fields in the side slots than desired. Small strips of lossy film were placed across the ends of these slots, and after a few

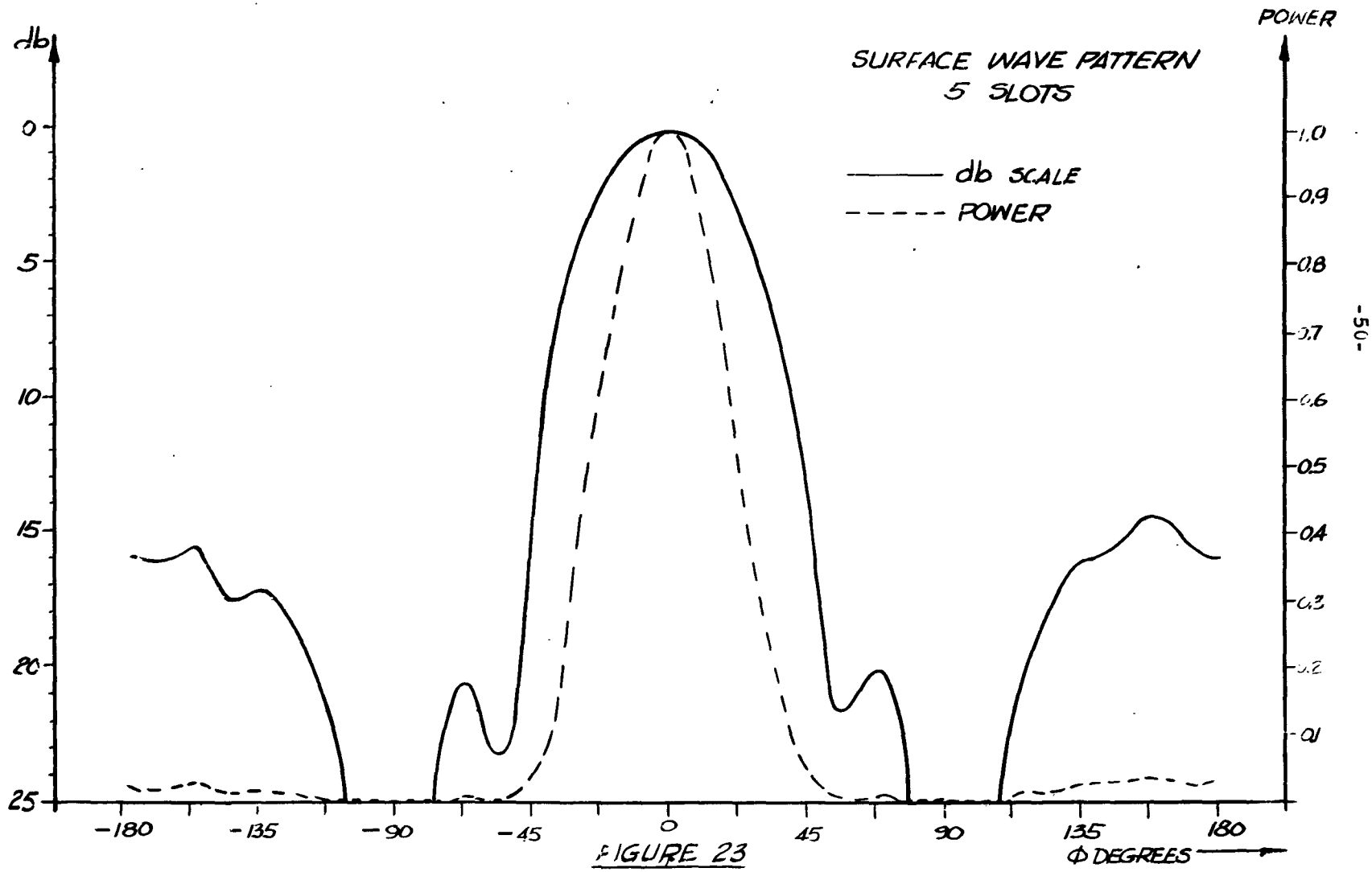
SURFACE WAVE PATTERN
5 SLOTS
db SCALE
POWER
db
POWER
0
5
10
15
20
25
1.0
0.9
0.8
0.7
0.6
0.5
0.4
0.3
0.2
0.1
-180
-135
-90
-45
0
45
90
135
180
Φ DEGREES

FIGURE 23

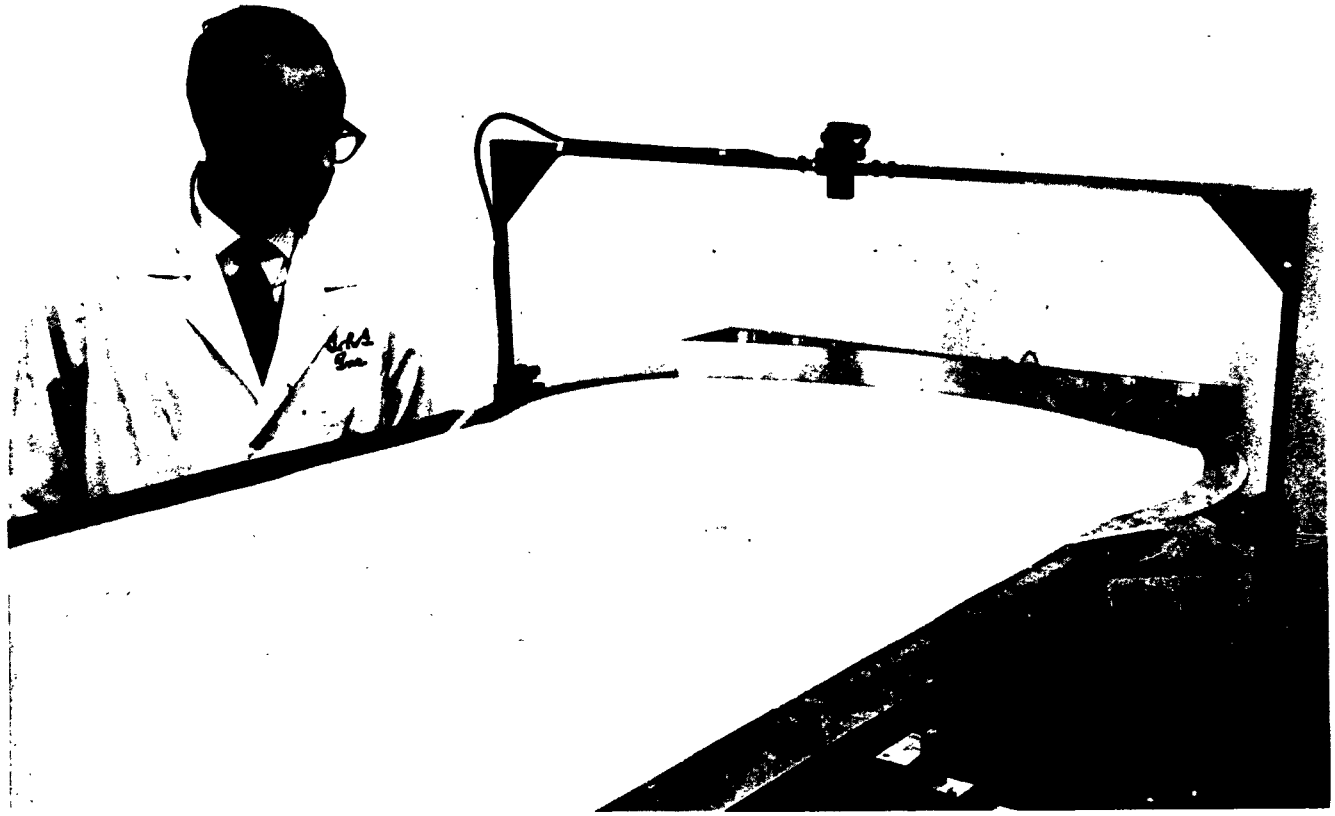

FIGURE 24 - SETUP USED FOR MEASUREMENT OF RADIATION PATTERNS FOR LINE DISCONTINUITIES ACROSS A SURFACE WAVEGUIDE

The discontinuities were placed along the dark line in the foreground, and the probe arm was fastened in the empty support, also in the foreground. The circular ground plane used for measurements of feed patterns can be seen in outline as well as the arrangement for moving the the probe-arm in the ϕ-direction.

changes the desired pattern was obtained.

Next step was to remove the foil from the outer slots and vary their phase shifters until the desired pattern was achieved. This was not pursued to the point of exact agreement. Adjustments were made up to a point where the pattern at all θ had approximately the correct level and the surface wave for $\phi = \pi$ was brought down more than 15 db below the value at $\phi = 0$. Theoretical and measured patterns for three and five slots are shown in Figures 21 and 22. Surface wave distribution for five slots is shown in Figure 23.

The VSWR of the complete launcher was less than 1.4.

VIII. EXPERIMENTAL DETERMINATION OF LAUNCHING EFFICIENCY FOR 5-SLOT LAUNCHER

The radiation pattern and the surface wave distribution were measured with the setup described in the previous section. To determine the efficiency from these measurements, it was necessary to calibrate the probe. To be more specific, the power received by the probe when placed in the radiation field is proportional to the power density (watts per unit solid angle), but in the surface wave field the power received by the probe will be proportional to the power content in the surface wave per unit interval in ϕ. To interpret the measured data from the 5-slot launcher the relative meaning of the radiation field and surface wave field readings must be known. If one can make the corresponding measurements on a launcher with known ratio between the two kinds of power (e.g. a launcher with known launching efficiency) this relationship can be established. A single slot is in our case a convenient reference and radiation as well as surface wave patterns were measured for both a single slot

and for the 5-slot launcher, with the output from a directional coupler sampling the input power as reference. For the single slot, patterns were also taken without the dielectric cover. The single slot patterns were compared to those computed from theoretical expressions, and the agreement was found to be good (see Figure 25 for example). Writing the power radiated without dielectric *

$$P_1 = \int_0^{\pi/2} \int_0^{2\pi} S_{10} F(\theta, \phi) \sin\theta \, d\phi \, d\theta \tag{72}$$

and that radiated when the dielectric is present:

$$P_2 = \int_0^{\pi/2} \int_0^{2\pi} S_{20} G(\theta, \phi) \sin\theta \, d\phi \, d\theta \tag{73}$$

we obtain by numerical integration of the theoretical expressions:

$$P_1 = S_{10} \cdot 3.896 \tag{74}$$

$$P_2 = S_{20} \cdot 2.516 \, . \tag{75}$$

Since the measured patterns agree very well with those derived from theory, (74) and (75) can be considered correct. If now S_{10} and S_{20} are measured for the same incident power, the surface wave power with dielectric is

* $F(\theta, \phi)$ and $G(\theta, \phi)$ are both the sum of the power radiated in the two polarizations, and $F(\theta = 0) = G(\theta = 0) = 1$

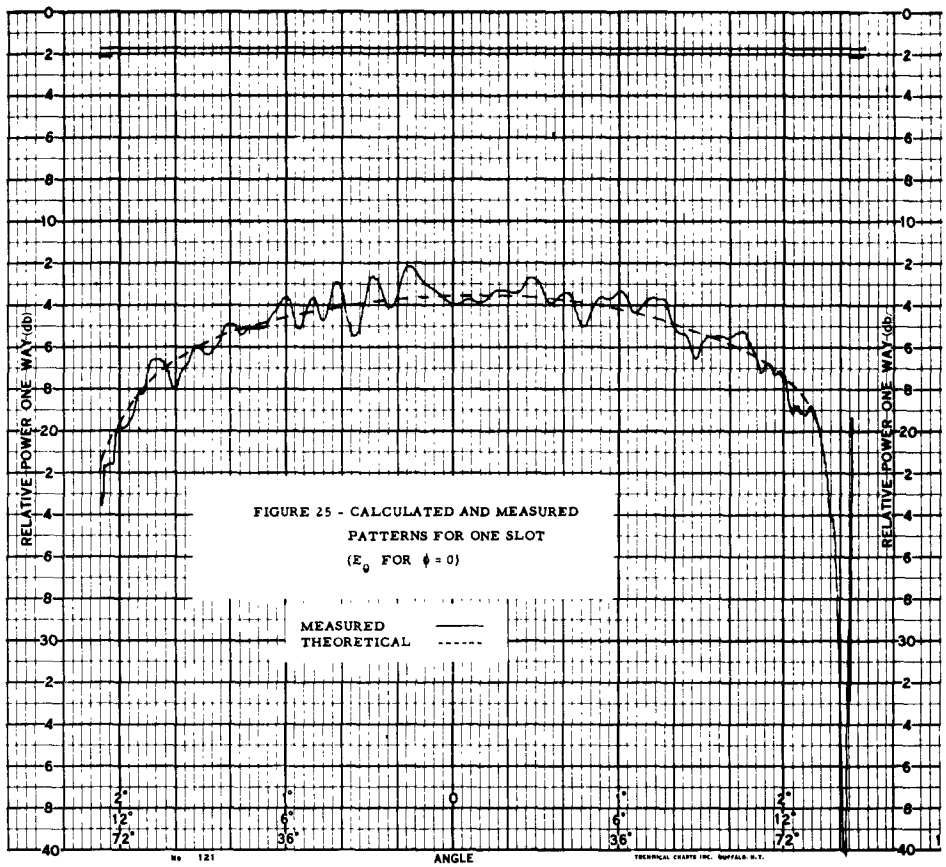

FIGURE 25 - CALCULATED AND MEASURED PATTERNS FOR ONE SLOT (E_θ FOR $\phi = 0$)

MEASURED ——
THEORETICAL ------

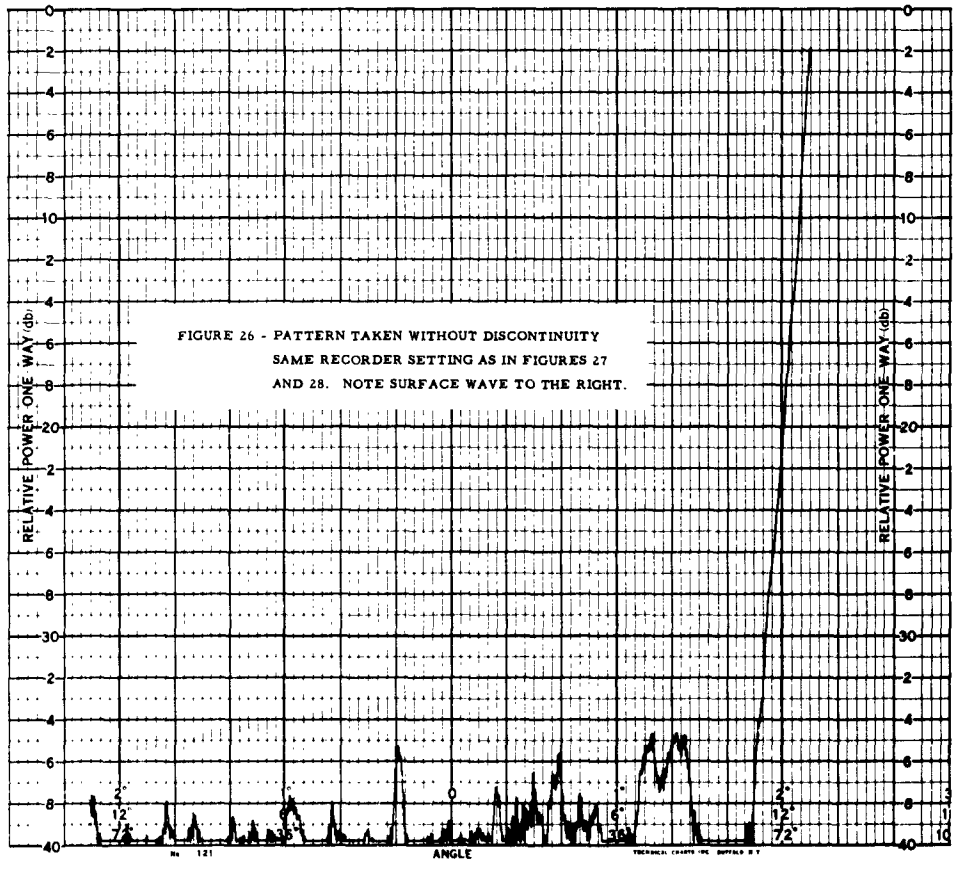

FIGURE 26 - PATTERN TAKEN WITHOUT DISCONTINUITY SAME RECORDER SETTING AS IN FIGURES 27 AND 28. NOTE SURFACE WAVE TO THE RIGHT.

$P_1 - P_2$, and the launching efficiency for one slot is given by

$$\eta_1 = \frac{P_1 - P_2}{P_1} = 1 - \frac{S_{20}}{S_{10}} \cdot 0.646 \tag{76}$$

conversely, (76) gives

$$\frac{S_{20}}{S_{10}} = \frac{1 - \eta_1}{0.646} . \tag{77}$$

Inserting the previously computed value $\eta_1 = 0.525$ in (77) makes $S_{20} = 0.725\ S_{10}$. In other words, theory predicts that S_{20} should be about 1.3 db below S_{10}. The results of the measurements show a S_{20} value only 0.5 db below S_{10}. This difference of 0.8 db is partially due to the fact that the slot was severely mismatched when the dielectric was removed (VSWR = 6.5). A slide-screw tuner was used to cancel the reflections, and some extra loss was introduced this way. The waveguide attenuation between the slot and the tuner was about 0.1 - 0.2 db, and the increase in attenuation due to extra losses in this section is about twice this value when the VSWR is 6.5 before tuning. However, this leaves 0.2 - 0.5 db unaccounted for, and it is hard to tell what caused this discrepancy between theory and experiment. Some loss in the tuning screw itself can be expected, but not quite of this magnitude. An accumulative error in the numerical integration could be the explanation, as well as deviations in X, ϵ or d from the assumed values.

If we accept the measured values of S_{10} and S_{20}, including corrections

for extra tuning loss of 0.4 db* the efficiency of the one slot launcher is:

$\eta_1 \geq 0.475$.

The surface wave power can be written:

$$P_{sw} = \int_0^{2\pi} S_{sw} g(\phi) d\phi \tag{78}$$

where $g(0) = 1$. Numerical integration of (78) gives

$$P_{sw} = S_{sw} \cdot 2.896 \tag{79}$$

and we have

$$\eta_1 = \frac{P_{sw}}{P_s + P_{sw}} = \frac{1}{1 + \frac{S_{20}}{S_{sw}} 0.870} \tag{80}$$

For $\eta_1 = 0.475$, (80) gives $S_{sw} = 0.787 S_{20}$, or in terms of logarithmic measure, S_{sw} is about 1 db below S_{20}.

When the probe was set to measure the peak of the surface wave pattern, the indicator showed a reading 9.2 db higher than that obtained at the peak of the radiation pattern. This means that the readings of surface wave power should be decreased 10.2 db in order to be comparable to the radiation levels in the sense indicated by (77) and (78).

For the 5-slot launcher, the radiation patterns for both polarizations and the surface wave distribution were again measured, and in terms of two

* at least

new reference power densities S'_{20} and S'_{sw} numerical pattern integrations were performed with the results:

(81) $$P_{rad} = S'_{20} \cdot 1.73$$

(82) $$P_{sw} = S'_{sw} \cdot 0.940.$$

The indicator readings of the reference levels differed 17.5 db, with the surface wave level higher than the radiation field reading. According to the previous calibration, 10.2 db should be subtracted from this value for obtaining the ratio between S'_{sw} and S'_{20}, which gives $S'_{20} = 0.186 \cdot S'_{sw}$. The efficiency of the 5-slot launcher is then $\eta_5 = (1.186)^{-1} = 0.84$.

The accuracy of this value is naturally not very good, because of the great number of measurements and numerical integrations performed. However, great care has been taken in each step of the procedure, and it should be safe to assume that the actual efficiency lies in the immediate vicinity of 0.8 or higher.

This may not seem extremely high, but in view of the low reactance (≈ 0.4) and the small size of the launcher ($1.25\lambda_0 \cdot 0.45\lambda_0$) this result must be considered as good. Of major importance is also that the conceived design method has been proved feasible at least for laboratory use, and it is undoubtedly possible to increase the efficiency by adding more slots. As will be described in the next section, the designed launcher has already been used for

measuring the pattern of radiation from step-type changes in the thickness of the dielectric and other radiating discontinuities with good results.

IX. EXPERIMENTS PERFORMED WITH THE 5-SLOT LAUNCHER

Radiation and surface wave patterns, as well as efficiency, do not in themselves form a very convenient basis for judging the usefulness of a launcher. Until actual experiments have been performed to demonstrate the capability of the launcher in a specific application, this investigation would not be complete. As has been pointed out before in this report, one of the major applications for a launcher of this type is its use in connection with pattern measurements on radiating elements placed on a surface waveguide. The main problem here is to avoid interference between the element radiation and radiation from the launcher. The latter can be due to either radiation direct from the feed or to room reflections and to prevent both, a high efficiency is desirable. Since the radiation is mainly concentrated in the direction of maximum surface wave intensity for all endfire-type launchers, the requirements on efficiency become very strict. To circumvent this difficulty, and in order to obtain a collimated surface wave "beam" simulating a one-dimensional structure, the arrangement shown in Figure 24 was used. The reflector is a parabolic cylinder with 12 inches focal length, and its height and position was chosen so that the surface wave is reflected with good efficiency, but very little radiation is intercepted by the reflector due to the null in the radiation pattern for $\theta = \pi/2$.

The ground plane was extended in the direction of the reflected surface wave "beam", and provisions were made for a radiation probe to be moved on

a circle with 11 inches radius and with its center located on the surface 30 inches away from the feed. The pattern of a line discontinuity placed across the guide at this point can then be measured in a plane parallel to the direction of surface wave propagation. The setup is shown in Figure 24 except that the probe here is mounted for taking patterns of the launcher. The supports for the probe arm used for taking patterns of discontinuities can be seen near the edge of the extended ground plane.

Two kinds of discontinuities were investigated: (1) abrupt changes in the thickness of the dielectric (from 1/8 inch to 1/4 inch, and from 1/8 inch to zero) and (2) metallic rods of different cross-sections. Figure 21 shows the pattern obtained without discontinuity, Figures 27 to 36 show the patterns measured for the various discontinuities.

In Figures 27 and 28 curves marked theory have been superimposed on the measured patterns. These curves have been computed from [14] where the pattern from an abrupt change of reactance X from X_0 to X_1 is derived. Changing the notation for polar angle to conform with that used in this report, the theoretical power pattern expression reads:

$$(83) \qquad S(\theta) = \frac{(X_0 - X_1)^2 \sqrt{1+X_0^2}}{\pi k r} \cdot \frac{\cos^2\theta}{(\sqrt{1+X_1^2} - \sin\theta)(\sqrt{1+X_0^2} - \sin\theta)(X_0^2 + \cos^2\theta)} .$$

X_0 is in our case 0.392. For d = 1/4 inch X_1 becomes 0.758, and when the dielectric is terminated $X_1 = 0$ should be used in (83). From Figures 27 and 28 it can be seen that (83) gives the correct difference in level between

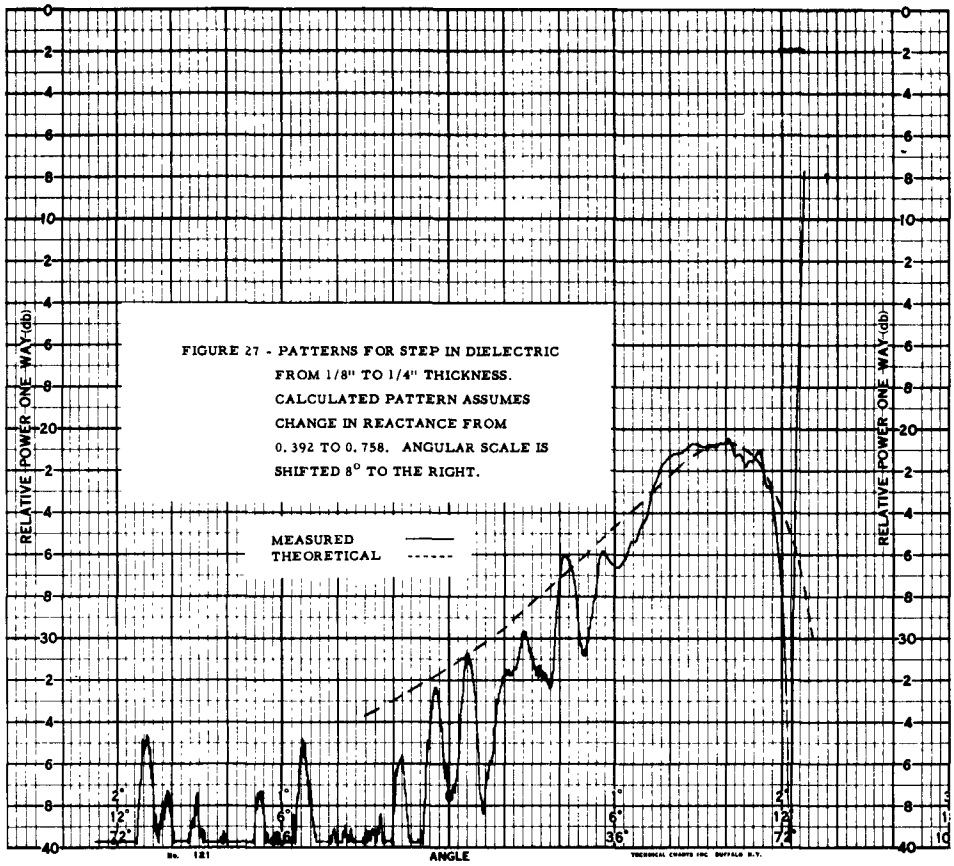

FIGURE 27 - PATTERNS FOR STEP IN DIELECTRIC FROM 1/8" TO 1/4" THICKNESS. CALCULATED PATTERN ASSUMES CHANGE IN REACTANCE FROM 0.392 TO 0.758. ANGULAR SCALE IS SHIFTED 8° TO THE RIGHT.

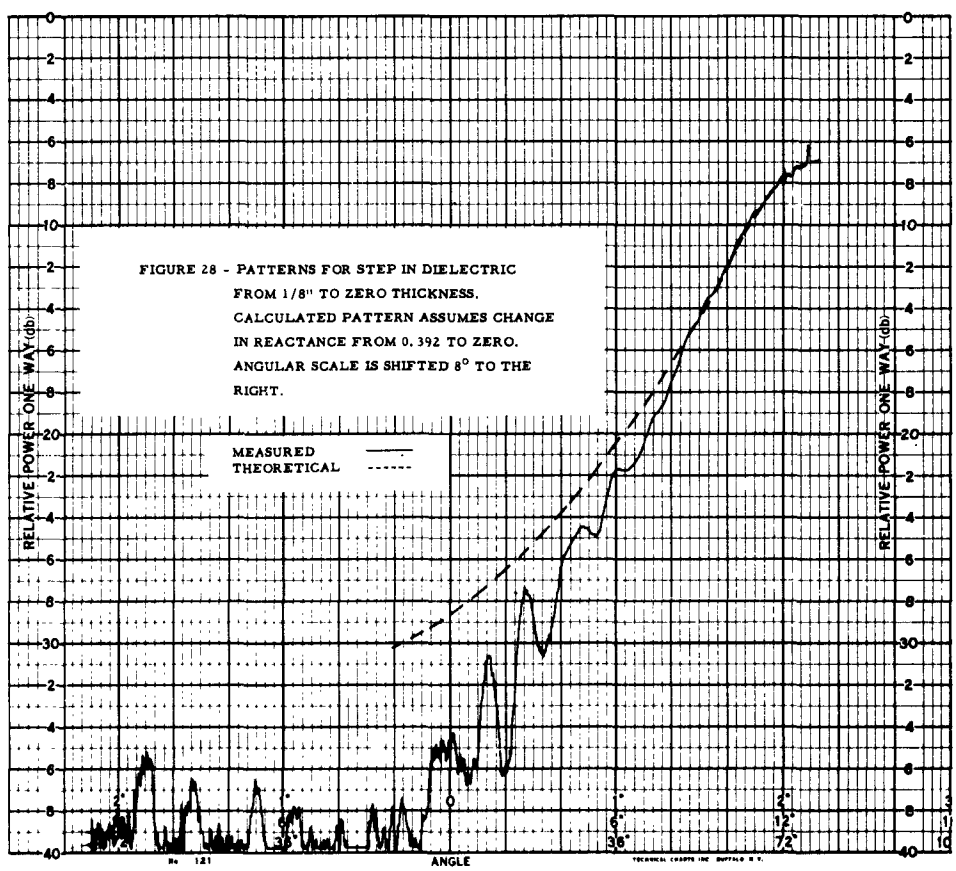

FIGURE 28 - PATTERNS FOR STEP IN DIELECTRIC FROM 1/8" TO ZERO THICKNESS. CALCULATED PATTERN ASSUMES CHANGE IN REACTANCE FROM 0.392 TO ZERO. ANGULAR SCALE IS SHIFTED 8° TO THE RIGHT.

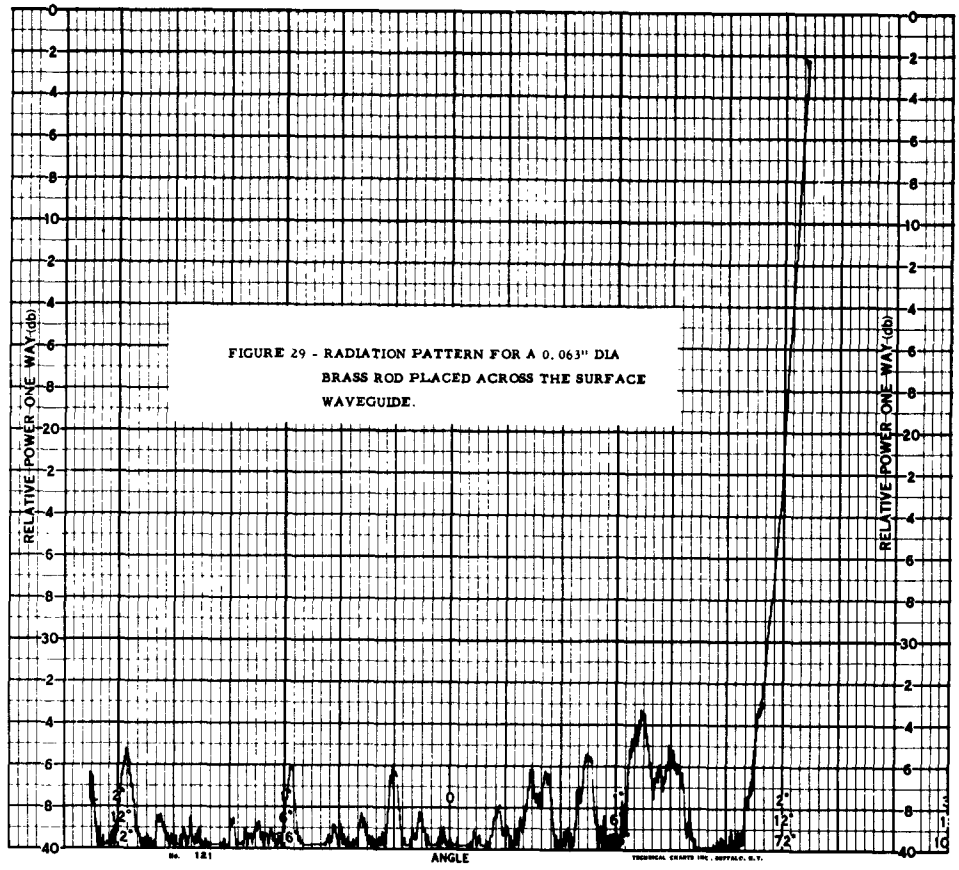

FIGURE 29 - RADIATION PATTERN FOR A 0.063" DIA BRASS ROD PLACED ACROSS THE SURFACE WAVEGUIDE.

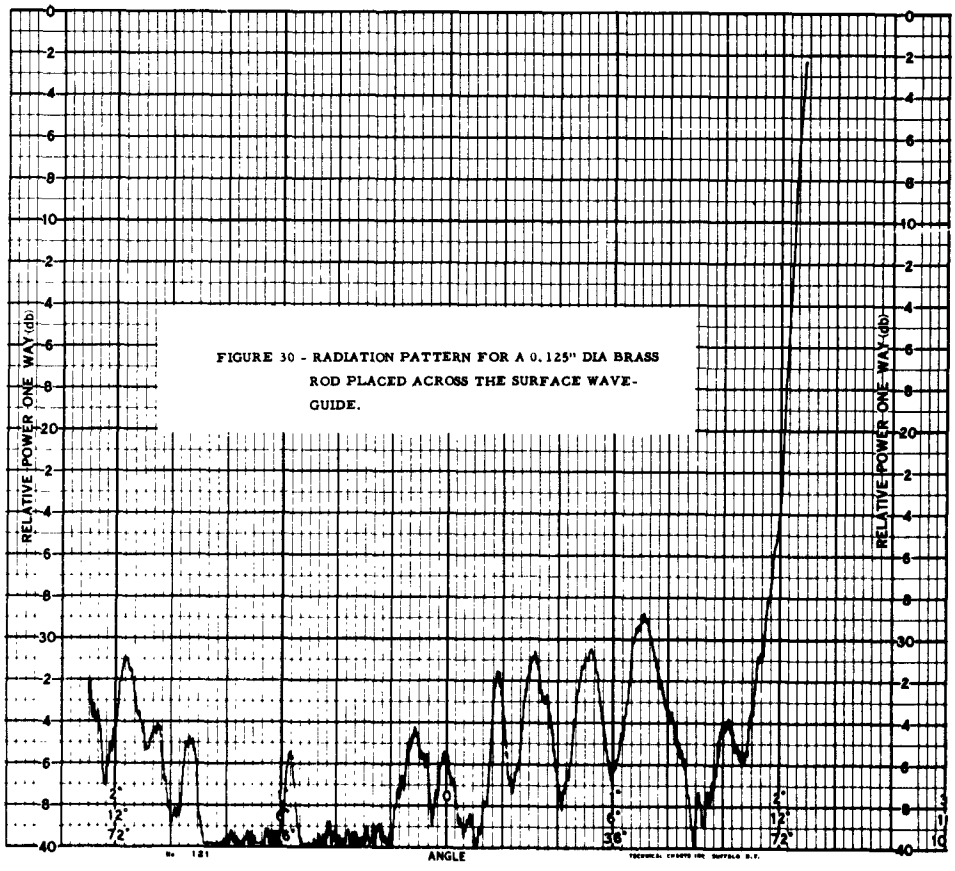

FIGURE 30 - RADIATION PATTERN FOR A 0.125" DIA BRASS ROD PLACED ACROSS THE SURFACE WAVEGUIDE.

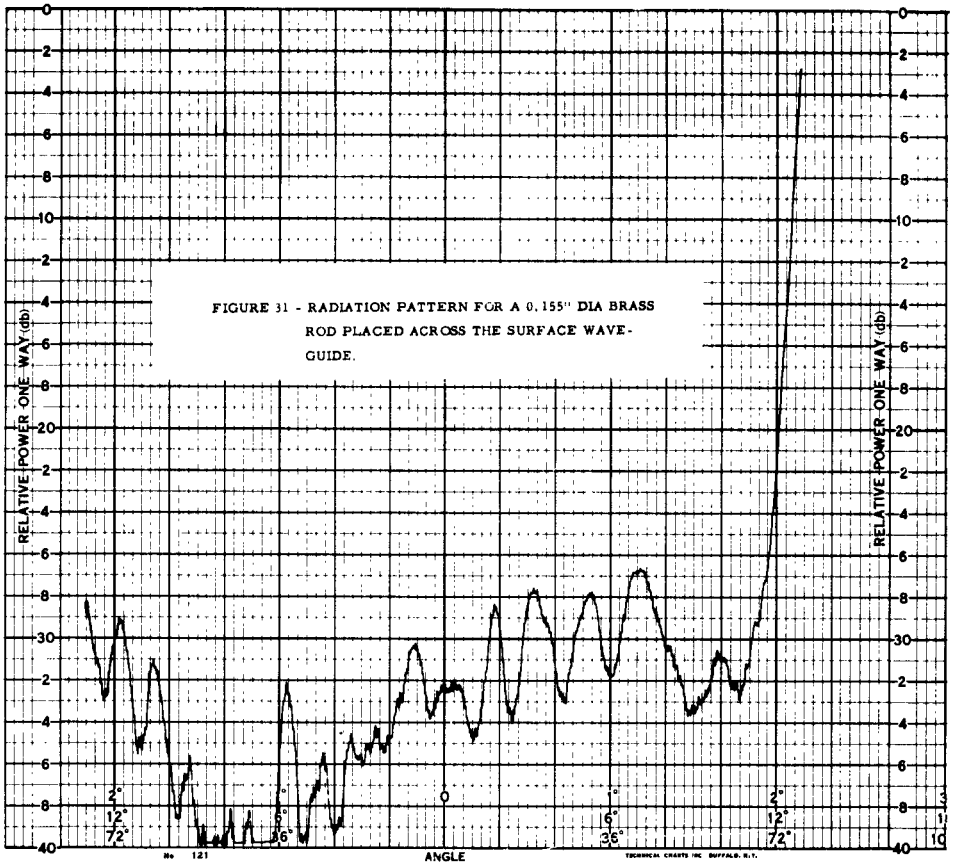

FIGURE 31 - RADIATION PATTERN FOR A 0.155" DIA BRASS ROD PLACED ACROSS THE SURFACE WAVE-GUIDE.

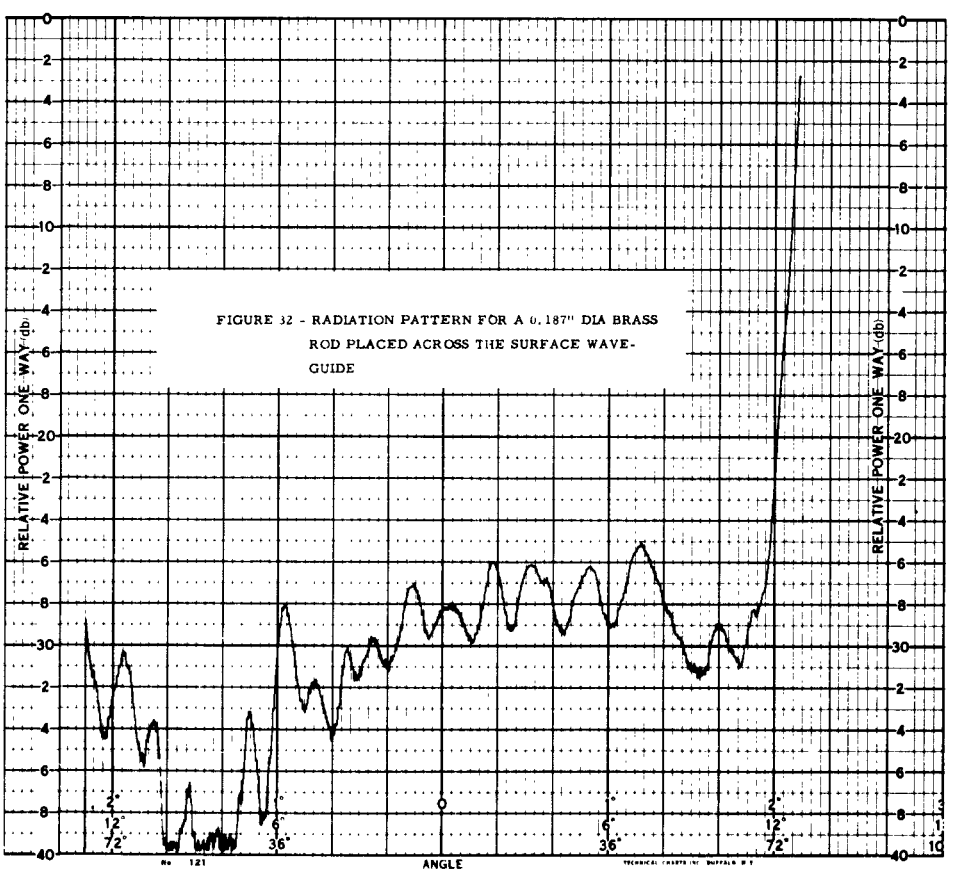

FIGURE 32 - RADIATION PATTERN FOR A 0.187" DIA BRASS ROD PLACED ACROSS THE SURFACE WAVE-GUIDE

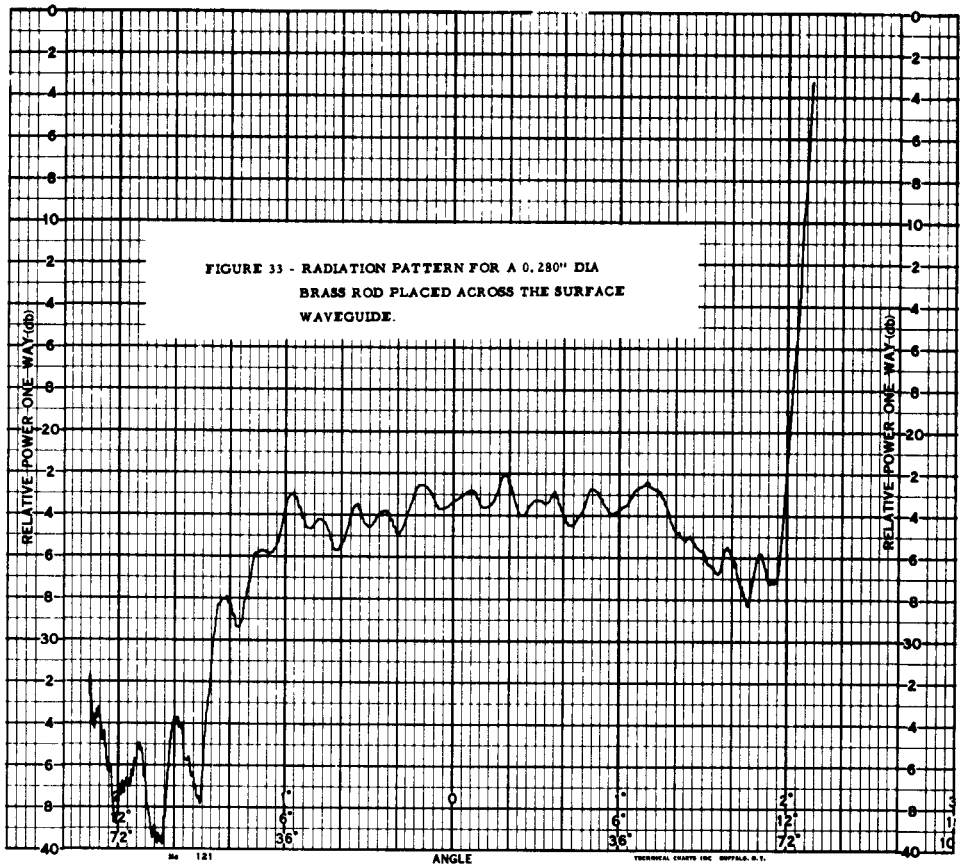

FIGURE 33 - RADIATION PATTERN FOR A 0.280" DIA BRASS ROD PLACED ACROSS THE SURFACE WAVEGUIDE.

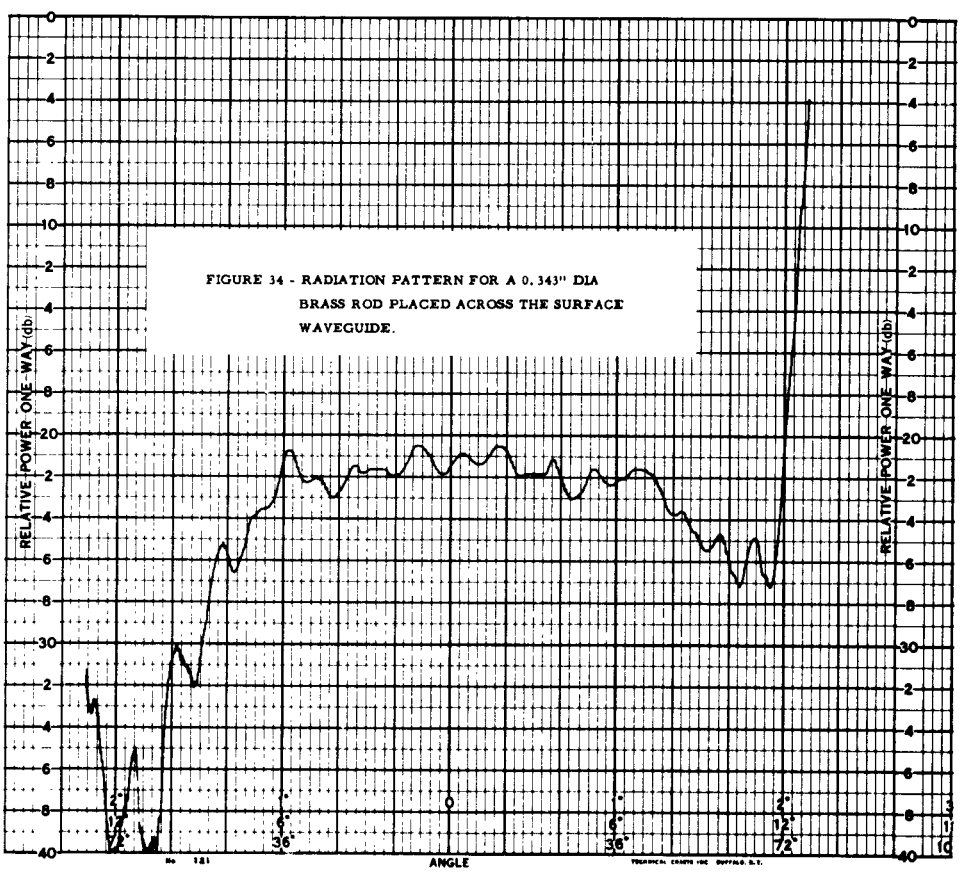

FIGURE 34 - RADIATION PATTERN FOR A 0.343" DIA BRASS ROD PLACED ACROSS THE SURFACE WAVEGUIDE.

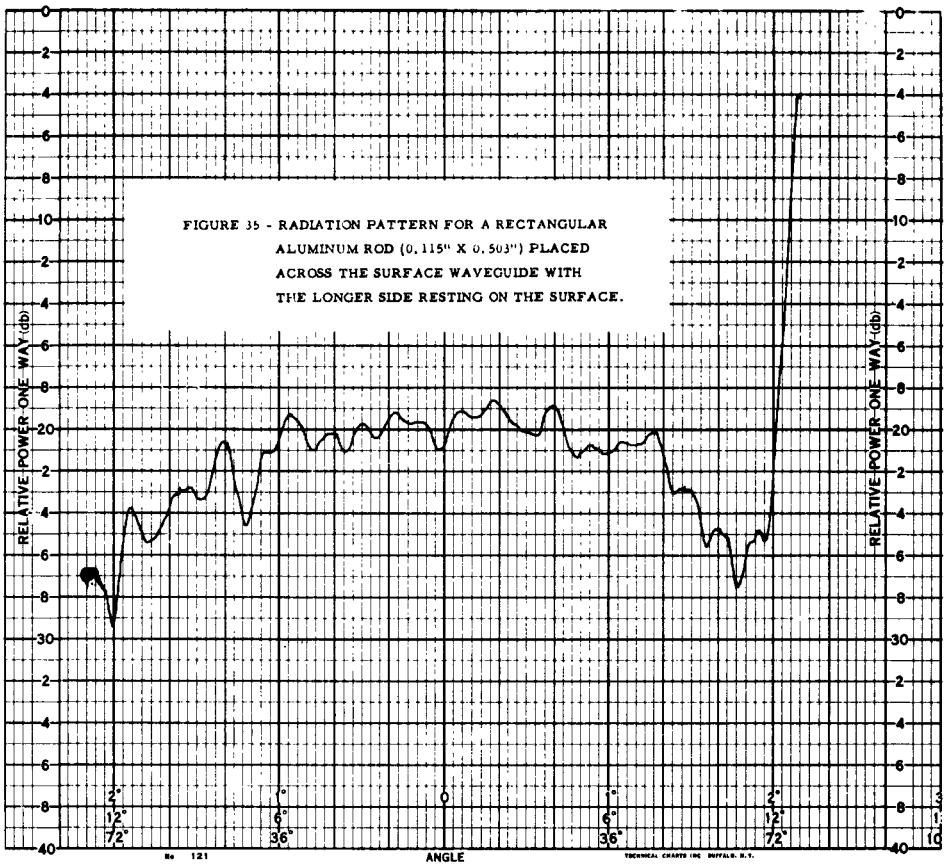

FIGURE 35 - RADIATION PATTERN FOR A RECTANGULAR ALUMINUM ROD (0.115" X 0.503") PLACED ACROSS THE SURFACE WAVEGUIDE WITH THE LONGER SIDE RESTING ON THE SURFACE.

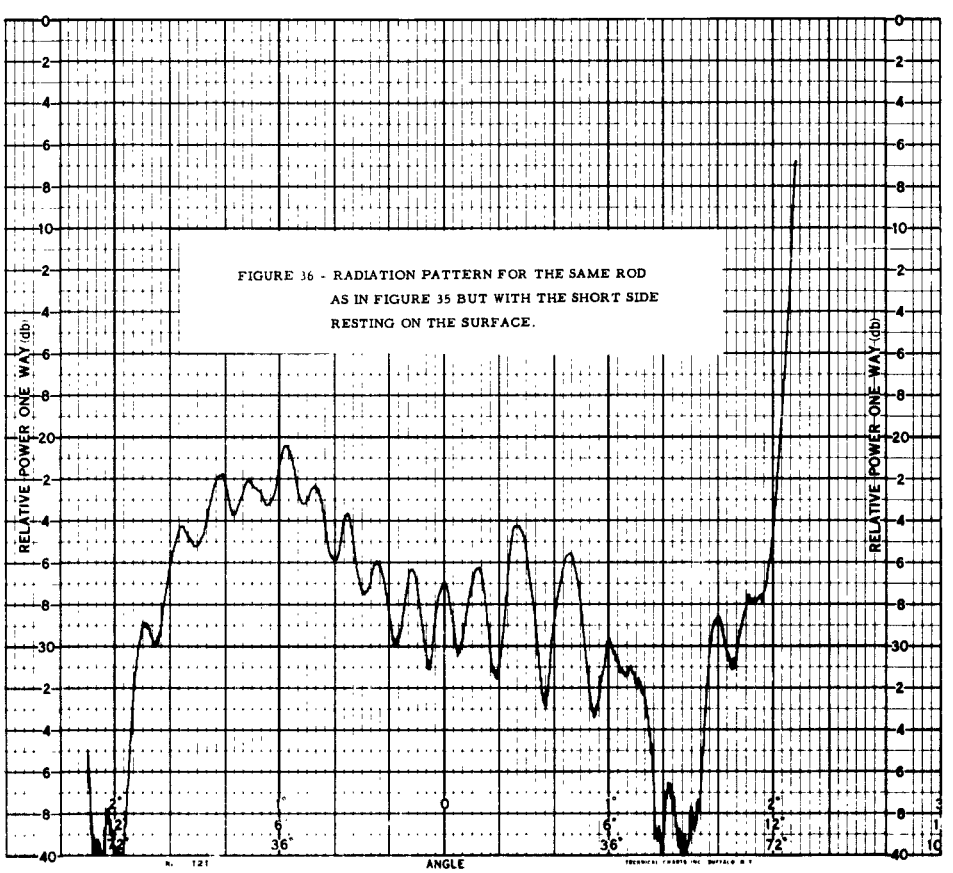

FIGURE 36 - RADIATION PATTERN FOR THE SAME ROD AS IN FIGURE 35 BUT WITH THE SHORT SIDE RESTING ON THE SURFACE.

the peaks of the two patterns, and that the theory agrees well with the measurements for $\theta > 60^{\circ}$. However, the measured radiation patterns decrease faster for $\theta < 60^{\circ}$ than the theory predicts. This indicates that the radiation near endfire from step discontinuities on dielectric-clad surfaces can be accurately obtained with the theory put forward in [14]. The discrepancy for angles near broadside is an example of the known fact that a dielectric clad ground plane in certain respects does not behave as a surface with constant normal impedance.

The experiments reported here are of course only a small fraction of those that could be performed using the launcher. The capabilities of the launcher for this type of measurement has however been convincingly demonstrated.

APPENDIX I

Evaluation of the Integrals (51) and (52)

In order to keep (x, y, z) -space and (β_x, β_y, β_z)-space separate, we introduce the following notations in (51) and (52):

(A1)
$$\begin{aligned} \beta_x &= p\cos\varphi & x &= r\cos\phi \\ \beta_y &= p\sin\varphi & y &= r\sin\phi \\ \beta_z &= \beta_0\cos\theta & z &= R\cos\theta \\ p &= \beta_0\sin\theta & r &= R\sin\theta \end{aligned}$$

(51) and (52) then both take the following form:

(A2)
$$f(x,y,z) = \frac{1}{4\pi^2}\int_0^{\infty} F_1(p)\left[\int_{\varphi_0}^{\varphi_0+2\pi} F_2(p,\varphi)e^{-jpr\cos(\phi-\varphi)}d\varphi\right]e^{-jz\sqrt{\beta_0^2-p^2}}\,p\,dp$$

where φ_0 is an arbitrary angle.

The inner integrals will first be carried out under the assumption that $pr >> 1$.

We have

(A3)
$$\tilde{E}_{x0} = 2WE_0\frac{\sin(pw\cos\varphi)}{pw\cos\varphi}\,\frac{2\ell}{\pi}\,\frac{4\cos(\frac{\pi}{2}\cdot\frac{2\ell}{\pi}p\sin\varphi)}{\left|1-(\frac{2\ell}{\pi}p\sin\varphi)^2\right|}\ .$$

We observe that $\tilde{E}_{x0}$ is an even function of both φ and p. For the two integrals, F_2 is:

(A4)
$$(51)\quad F_2 = -\sin\phi\,\tilde{E}_{x0}$$

$$(52)\quad F_2 = \frac{\cos\varphi}{\sqrt{1-p^2/\beta_0^2}}\cdot\tilde{E}_{x0}\ .$$

We also observe that a change of φ with $\pm\pi$ has exactly the same effect on the integrands as changing the sign of p. We can therefore write:

$$(A5) \qquad f(x,y,z) = \frac{1}{4\pi^2} \int_{-\infty}^{+\infty} F_1(p) \left[\int_{\varphi_0}^{\varphi_0+\pi} F_2(p,\varphi) e^{-jpr\cos(\varphi-\phi)} d\varphi \right] e^{-jz\sqrt{\beta_0^2-p^2}} \, p \, dp .$$

Next, a new variable is introduced: $\psi = \psi_1 + j\psi_2 = \varphi - \phi$ and we have $\psi_0 = \varphi_0 - \phi$. The exponent in the integrand then becomes:

$$(A6) \qquad -jpr\cos(\varphi-\phi) = -pr\sin\psi_1\sinh\psi_2 - jpr\cos\psi_1\cosh\psi_2 .$$

The case $p > 0$, $r > 0$ will be treated first, and for this case the real part of (A6) is negative in the shaded areas of the ψ-plane, shown in Figure A1.

If the integration path is augmented as shown in Figure A1, the value of the integral (51) will not change since $\sin\varphi = \sin(\psi+\phi) = 0$ along the added portions. The same is true for (52), if ψ_0 has the values shown in Figure A1.

Figure A2 shows the contour in the ψ = plane for which the imaginary part of the exponent (A6) is constant and equals -jpr. The real part of (A6) is either negative or zero (at $\psi = 0$). Since the integration path of Figure A1 has its endpoints in the shaded areas of the ψ-plane. it can be deformed into the path of constant phase close to $\psi = 0$ (if $pr >> 1$) without noticeable change in the value of the integral. Contributions to this value are only obtained close to = 0, where the path is a straight line ($\psi_1 = \psi_2$) and if $F_2(p, \psi + \phi)$ varies

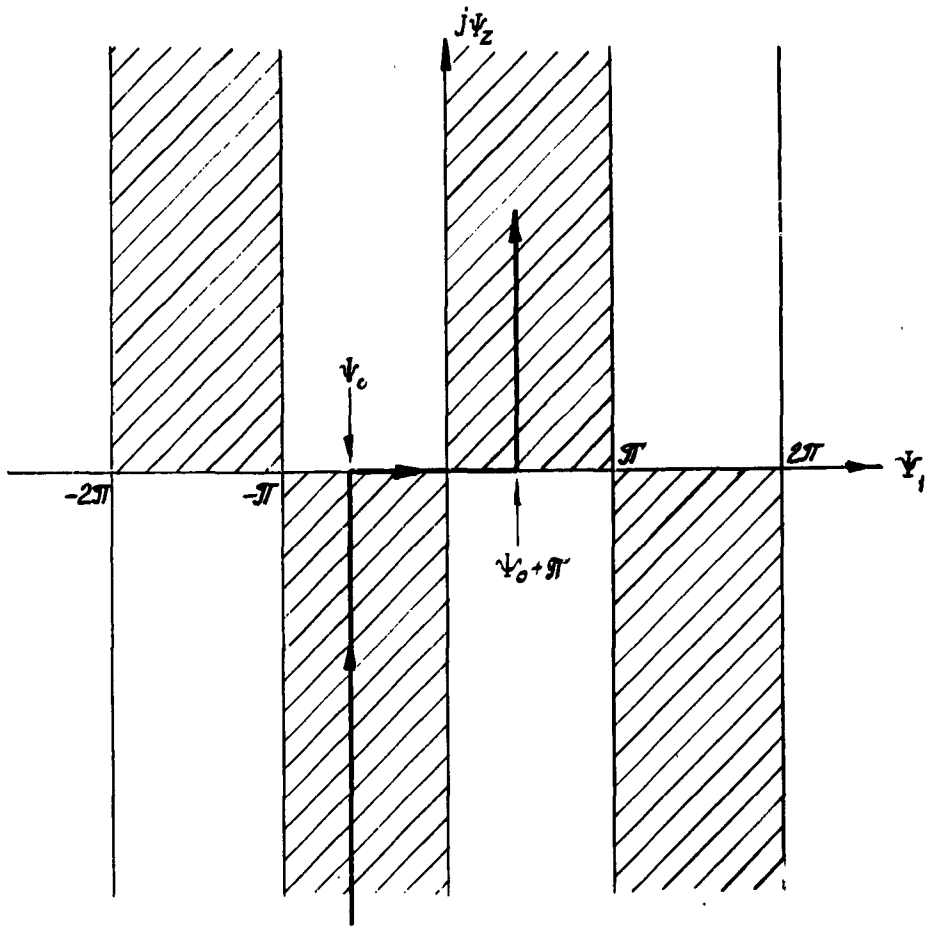

FIGURE A1 - INTEGRATION PATH FOR (51) AND (52)

(51) $\sin \psi_0 = \sin(\gamma_0 + \pi) = 0$ if $\gamma_0 = -\phi$ for $0 < \phi \pi$

$\gamma_0 = \pi - \phi$ for $\pi < \phi < 2\pi$

(52) $\cos \psi_0 = \cos(\gamma_0 + \pi) = 0$ if $\gamma_0 = -\frac{\pi}{2} - \phi$ for $-\frac{\pi}{2} < \phi < \frac{\pi}{2}$

$\gamma_0 = \frac{\pi}{2} - \phi$ for $\frac{\pi}{2} < \phi < \frac{3\pi}{2}$

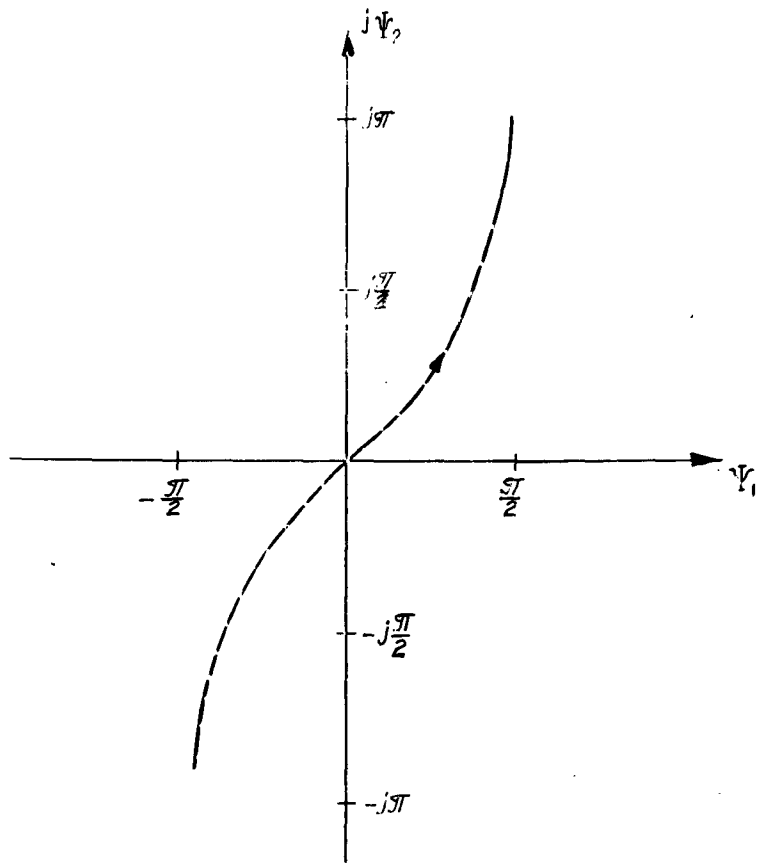

FIGURE A2 - CONSTANT-PHASE CURVE FOR (51), (52)

slowly in this region, we can write:

$$(A7)\qquad \int_{\phi_0}^{\phi_0+\pi} F_2(\phi, p)e^{-jpr\cos\psi}\,d\psi \approx F_2(\phi, p)e^{-jpr}\int_{-\infty}^{+\infty} e^{-pr\psi_2^2}(1+j)\,d\psi_2$$

$$= F_2(\phi, p)e^{-jpr}\sqrt{\frac{\pi}{pr}}(1+j)\,.$$

In the case $p < 0$, $r > 0$, one has to select a different path of integration, and the saddle-point is then located at $\psi = \pi$. The result differs from (A7) by a change of sign for pr, and to include negative p in (A7) we have to exchange p with its magnitude $|p|$ in the square root. Negative r can also be included by writing (A7)

$$(A8)\qquad F_2(\phi, p)e^{-jpr}\sqrt{\frac{\pi}{|pr|}}(1+j)\,.$$

Introducing (A8) into (A5) gives

$$(A9)\qquad f(x, y, z) = \frac{1+j}{4\pi^2}\int_{-\infty}^{+\infty} F_1(p)F_2(\phi, p)\sqrt{\frac{\pi}{|pr|}}\,e^{-j(pr+z\sqrt{\beta_0^2+p^2})}\,p\,dp\,.$$

In the discussion of (A9) p will be regarded as a complex variable. $p = 0$ is neither a branch-point nor a pole, but $F_1(p)$ may contain two or more poles, and $p = \pm\beta_0$ are branch-points. For the function $\sqrt{\beta_0^2 - p^2}$, we choose the branch that is real and positive for p-values on the real

axis between $-\beta_0$ and $+\beta_0$, and is negative imaginary for all other real values of p. The poles will appear in symmetrical pairs on the real p-axis, in the intervals $-\beta_0\sqrt{\epsilon} < p < \beta_0$ and $\beta_0 < p < \beta_0\sqrt{\epsilon}$. Figure A3 shows the proper position of the branchcuts and the integration-path, and three pairs of poles are shown in typical positions.

It is convenient to introduce polar coordinates in (A9), according to (A1), and this gives:

$$\text{(A10)} \qquad \begin{aligned} pr &= \beta_0 R \sin\theta \sin\vartheta \\ z\sqrt{\beta_0^2 - p^2} &= \beta_0 R \cos\theta \cos\vartheta. \end{aligned}$$

From (A10) follows, that the exponent in (A9) can be written:

$$\text{(A11)} \qquad -j\beta_0 R \cos(\vartheta - \theta) .$$

Assuming ϑ to be complex ($\vartheta = \vartheta_1 + j\vartheta_2$) Figure A3 now transforms to Figure A4. The integrand of (A9) has a saddlepoint at $\vartheta_1 = \theta$, $\vartheta_2 = 0$, and the constant-phase contour is of the same shape as the contour in Figure A2. If we now deform the solid integration path of Figure A4 into the constant-phase contour, and $0 < \theta << \pi/2$, the contribution at the saddle-point will be a good approximation to the integral, provided $\beta_0 R >> 1$. This contribution becomes:

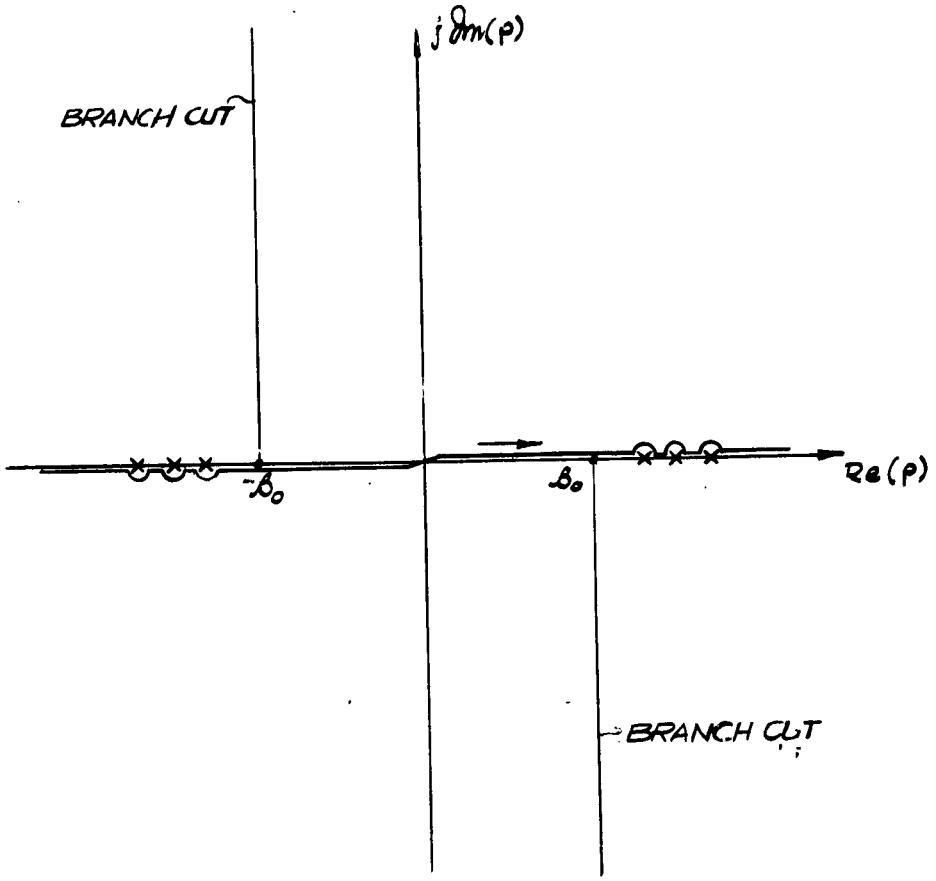

FIGURE A3 - BRANCH CUTS, POLES AND INTEGRATION PATH FOR (A9)

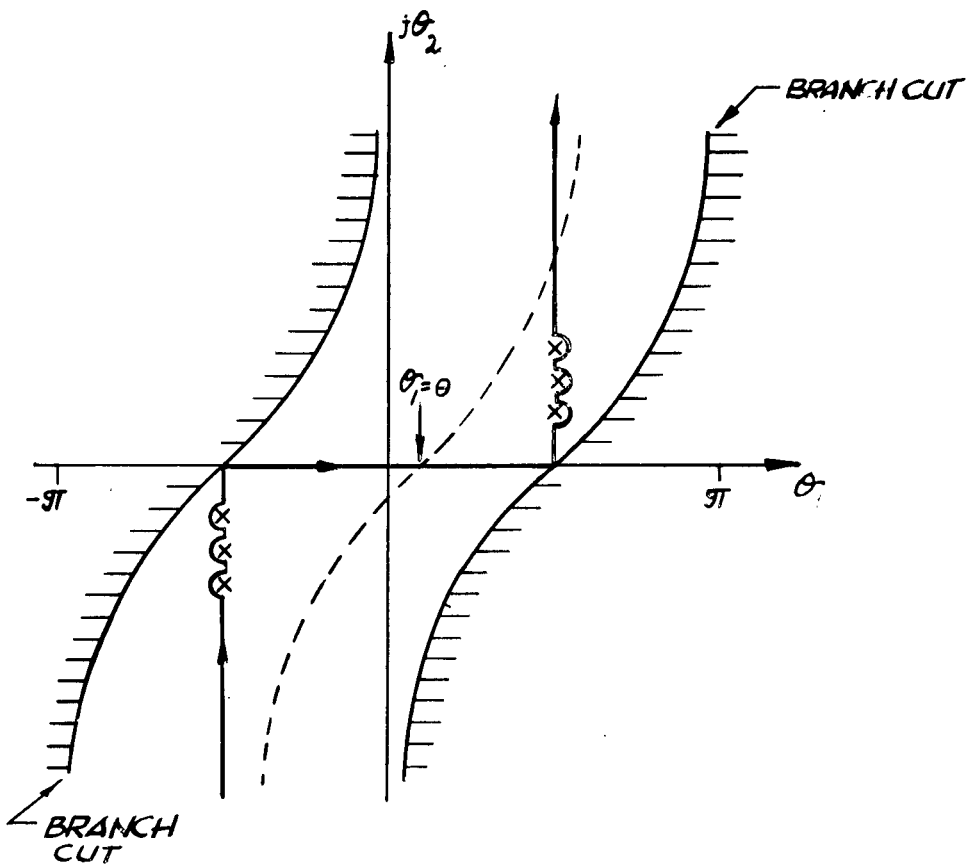

FIGURE A4 - INTEGRATION PATHS FOR (A9) IN THE COMPLEX θ-PLANE

Solid Curve: Integration path equivalent to that in Figure A3

Broken Curve: Saddle-point path

$$f_1(x,y,z) \approx \frac{(1+j)^2}{4\pi^2} F_1(\beta_0 \sin\theta) F_2(\phi, \beta_0 \sin\theta) \sqrt{\frac{\pi|\beta_0 \sin\theta|}{|R \sin\theta|}}\, e^{-j\beta_0 R} \beta_0 \cos\theta \int_{-\infty}^{+\infty} e^{-\beta_0 R \theta_2^2} d\theta_2$$

(A12)

$$= \frac{j\beta_0}{2\pi} \cos\theta F_1(\beta_0 \sin\theta) F_2(\phi, \beta_0 \sin\theta) \frac{e^{-j\beta_0 R}}{R} \quad .$$

The factor $\beta_0 \cos\theta$ comes from the differential: $dp = d(\beta_0 \sin\theta) = \beta_0 \cos\theta d\theta$ and otherwise the operations performed are identical to (A7).

For θ-values close to $\pi/2$, however, the poles come close to the integration path, and will give an appreciable contribution to the integral. For $\theta = \pi/2$, the constant-phase contour follows the branchcut, and within the approximations used, the integral along the cut is zero, since (A12) contains the factor $\cos\theta$. This makes it possible to close the original contour in Figure A4 as shown in Figure A5. Now, the integral is given by the residues at the poles.

From a pole at $p = \beta_0 \sqrt{1+X^2}$, the contribution is

$$f_2(x,y,z) = \frac{1+j}{4\pi^2} 2\pi j \lim_{p \to \beta_0\sqrt{1+X^2}} \left[(p - \beta_0\sqrt{1+X^2}) F_1(p)\right]$$

(A13)

$$F_2(\phi, \beta_0\sqrt{1+X^2}) \sqrt{\frac{\pi\beta_0\sqrt{1+X^2}}{r}}\, e^{-j\beta_0\sqrt{1+X^2}\, r} \quad .$$

(A13) shows all the characteristic features of a surface wave, and its z-dependence just above $z = 0$ must be:

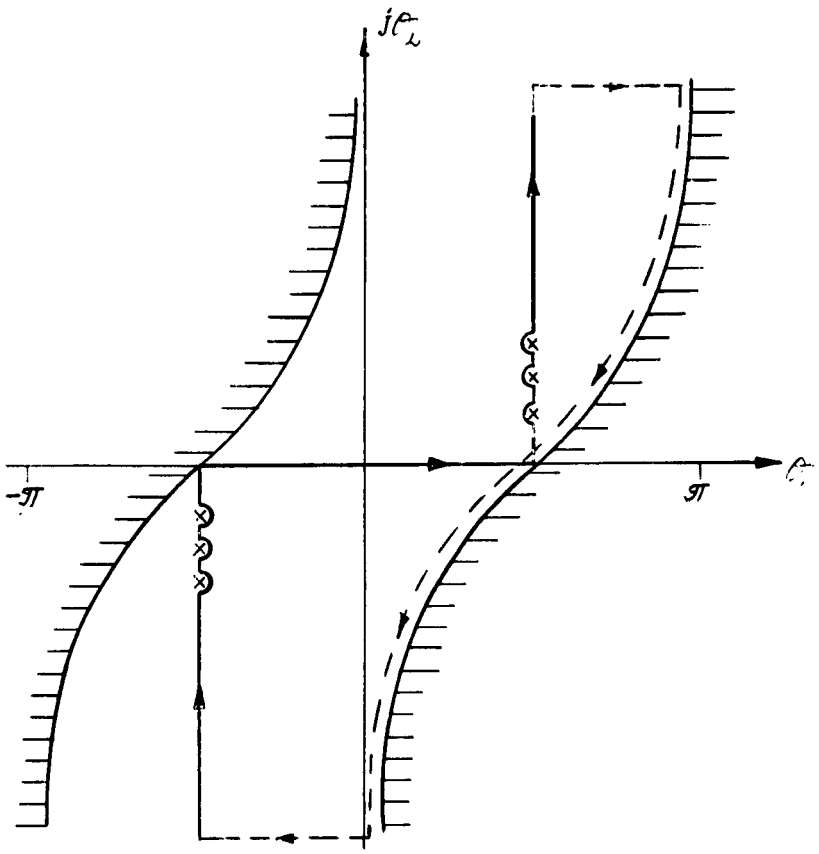

FIGURE A5 - CLOSED INTEGRATION PATH FOR $\theta = 0$

(A13a) $$e^{-\beta_0 X z} \quad .$$

In between the extreme cases $0 < \theta << \frac{\pi}{2}$, and $\theta \approx \frac{\pi}{2}$ the evaluation of the integral becomes more complicated. One can however assume that (A12) represents the radiation field for all points in space where $\beta_0 R >> 1$, and that (A13) combined with (A13a) represents a surface wave. This assumption is strongly supported by the performed measurements.

APPENDIX II

Basic Properties of Lowest Order TM- type Surface Waves on Dielectric-clad Metallic Surfaces

Far away from the source, we can regard the surface waves as being plane, and we can express the fields as follows:

In the dielectric: $(0 > x > -d)$

$$H_\phi' = \frac{K}{\sqrt{r}} \cos\left[\beta_0 (z+d)\sqrt{\epsilon - 1 - X^2}\right] e^{-j\beta_0 r\sqrt{1+X^2}}$$

(A14)
$$E_r' = -j \frac{K}{\sqrt{r}} \frac{Z_0\sqrt{\epsilon - 1 - X^2}}{\epsilon} \sin\left[\beta_0 (z+d)\sqrt{\epsilon - 1 - X^2}\right] e^{-j\beta_0 r\sqrt{1+X^2}}$$

$$E_z' = -\frac{Z_0\sqrt{1+X^2}}{\epsilon} H_\phi' .$$

Above the dielectric: $(z > 0)$

$$H_\phi'' = \frac{K}{\sqrt{r}} \cos\left[\beta_0 d\sqrt{\epsilon - 1 - X^2}\right] e^{-\beta_0 Xz - j\beta_0 r\sqrt{1+X^2}}$$

(A15)
$$E_r'' = -j \frac{K}{\sqrt{r}} Z_0 X \sin\left[\beta_0 d\sqrt{\epsilon - 1 - X^2}\right] e^{-\beta_0 Xz - j\beta_0 r\sqrt{1+X^2}}$$

$$E_z'' = -Z_0\sqrt{1+X^2}\, H_\phi''$$

where $K/\sqrt{r}$ is the surface current in the groundplane, and $Z_0 = \sqrt{\mu_0/\epsilon_0}$.

The power transported in the two media can be written:

In the dielectric:

$$P' = \frac{KK^*}{r} \frac{Z_0}{\epsilon} \sqrt{1+X^2} \left[\frac{d}{2} + \frac{\sin\left[2\beta_0 d\sqrt{\epsilon-1-X^2}\right]}{4\beta_0\sqrt{\epsilon-1-X^2}} \right] .$$

In the air:

$$P'' = \frac{KK^*}{r} Z_0 \frac{\sqrt{1+X^2}}{2\beta_0 X} \cos^2\left[\beta_0 d\sqrt{\epsilon-1-X^2}\right] . \tag{A16}$$

The dimension of (A16) is watt per unit width of guide.

The quantity X is obtained from:

$$\epsilon X = \sqrt{\epsilon-1-X^2} \tan\left[\beta_0 d\sqrt{\epsilon-1-X^2}\right] . \tag{A17}$$

For small values of $\beta_0 d\sqrt{\epsilon}$ X can be obtained from:

$$X \approx \beta_0 d\frac{\epsilon-1}{\epsilon} . \tag{A18}$$

When this approximation is too crude, one has to use graphical or numerical methods to solve (A17) for X.

REFERENCES

1. Cullen, A.L., "The Excitation of Plane Surface Waves," Monograph no. 93, Proc. I.E.E., Vol. 101, Part IV, 1954.

2. Tai, C.T., "The Effect of a Grounded Slab on the Radiation From a Line Source," Journ. Appl. Phys., Vol. 22, 1951 p. 405.

3. Kay, A.F., and Zucker, F.J., "Efficiency of Surface Wave Excitation," IRE Convention Record, Vol. 1955.

4. Kay, A.F., "The Excitation of Surface Waves in Multi-layered Media," Final Report, Section No. 1 on Contract AF19(604)-1126, October 1954.

5. Booker, H.G., and Clemmow, P.C., "The Concept of Angular Spectrum of Plane Waves and Its Relation to that of a Polar Diagram for Aperture Distribution," Proc. I.E.E., Vol. 97, Part III, 1950, p. 11.

6. Elliott, R.S., "On the Theory of Corrugated Surfaces," IRE Trans. PGAP No. 2, April 1954.

7. Attwood, S.S., "Surface Wave Propagation Over a Coated Plane Conductor," Journ. Appl. Physics, Vol. 22, 1951, p. 504.

8. Kay, A.F., "Applied Problems in Electromagnetic Theory," Final Report on Contract AF19(604)-3476 dated April 1961.

9. Viggh, M.E., "Investigation Regarding Surface Waves Over Conducting Surfaces," FOA 3 Report A 348, July 1958 (In Swedish with a summary in English, the report can be obtained from: FOA 3 Library, Stockholm 80. Sweden.

10. Kraus: "Antennas." Section 17 of Appendix, McGraw-Hill, 1950.

11. Woodward, P.M., "Probability and Information Theory," McGraw Hill 1953.

12. Brick, D.B., "The Radiation of a Hertzian Dipole Over a Coated Conductor," Technical Report No. 172, Cruft Laboratory, Harvard University, May 1953.

13. Andreasen, M.G., "Flush-Mounted Surface Wave Launcher," Scientific Report No. 11, Contract AF19(604)-3502, Stanford Research Institute, March 1961.

14. Kay, A.F., "Scattering of a Surface Wave by a Discontinuity in Reactance," IRE Trans. Vol. AP-7. January 1959, p. 22.

DISTRIBUTION LIST

AFCRL-63-63

APGC (PGAPI)
Eglin AFB, Florida

RADC(RCE)
Attn/ Dr. J.S. Burgess
Griffiss AFB, New York

Director of Resident Training
3380th Technical Training Group
Keesler AFB, Mississippi
Attn/ OA-3011 Course

AUL
Maxwell AFB, Alabama

USAF Security Service (CLR)
San Antonio, Texas

OAR (RROS, Col John R. Fowler)
Tempo D
4th and Independence Ave.
Washington 25, D.C.

Hq. OAR (RROSP, Maj. R.W. Nelson)
Tempo D, 4th and Independent Ave.
Washington 25, D.C.

WADD (WCLRSA, Mr. Portune)
Wright-Patterson AFB, Ohio

Director, Electronics Division
Air Technical Intelligence Center
Attn/ AFCIN-4E1, Col. H.K. Gilbert
Wright-Patterson AFB, Ohio

Lt. Col. Jensen (SSRTW)
Space Systems Division
Air Force Unit Post Office
Los Angeles 45, California

RADC (RAYLD)
Attn/ Documents Library
Griffiss AFB, New York

AF Missile Dev. Cent.
(MDGRT)
Holloman AFB, New Mexico

SAC (Operations Analysis Office)
Offutt AFB, Nebraska

AF Missile Test Center
Patrick AFB, Florida

Technical Information Office
European Office, Aerospace Res.
Shell Building, 47 Cantersteen
Brussels, Belgium

AFOSR, OAR (SRYP)
Tempo D
4th and Independence Ave.
Washington 25, D.C.

ASD (ASAPRD-Distr.)
Wright-Patterson AFB, Ohio

ASD (ASRNRE-3)
Attn/ Mr. Paul Springer
Wright-Patterson AFB, Ohio

WADD (WWDRTR, Mr. A.D. Clark)
Directorate of System Engineering
Dyna Soar Engineering Office
Wright-Patterson AFB, Ohio

Director
Evans Signal Laboratory
Belmar, New Jersey
Attn/ Mr. O.C. Woodyard

Hq. USAF (AFOAC-S/E)
Communications-Electronics Directorate
Washington 25, D.C.

Department of the Army
Office of the Chief Signal Officer
Washington 25, D.C.
Attn/ SIGRD-4a-2

Commanding General
USASRDL
Fort Monmouth, New Jersey
Attn/ Mr. F.J. Triola

Director
U.S. Army Ordnance
Ballistic Research Laboratories
Aberdeen Proving Ground, Maryland
Attn/ Ballistic Measurement Laboratory

Guided Missile Fuze Library
Diamond Ordnance Fuze Laboratories
Washington 25, D.C.
Attn/ R.D. Hatcher, Chief Micr. Dev. Sect.

Redstone Scientific Information Ctr.
U.S. Army Missile Command
Redstone Arsenal, Alabama

ASTIA (TIPAA)
Arlington Hall Station
Arlington 12, Virginia (10 copies)

Defence Research Member
Canadian Joint Staff
2450 Massachusetts Ave. NW
Washington 8, D.C.

Office of Scientific Intelligence
Central Intelligence Agency
2430 E. Street NW
Washington 25, D.C.

Commanding General
USASRDL
Ft. Monmouth, New Jersey
Attn/ Tech. Doc. Center
SIGRA/SL-ADT

Mass. Institute of Technology
Signal Corps Liaison Officer
Cambridge 39, Mass.
Attn/ A.D. Bedrosian, Rm26-131

Office of Chief Signal Officer
Engineering and Technical Division
Washington 25, D.C.
Attn/SIGNET-5

Ballistic Research Laboratories
Aberdeen Proving Ground, Maryland
Attn/ Technical Information Branch

Commanding General
USASRDL
Fort Monmouth, New Jersey
Attn/ SIGFM/EL-AT

Commanding General, SIGFM/EL-PC
USASRDL
Fort Monmouth, New Jersey
Attn/ Dr. H.H. Kedesdy,
Deputy Chief, Chem-Physics Br.

Library
National Bureau of Standards
Boulder, Colorado (2 copies)

National Bureau of Standards
U.S. Department of Commerce
Washington D.C.
Attn/ Gustave Shapiro, Chf. E.E. Sect.

Director
National Security Agency
Ft. George G. Meade, Maryland
Attn/ C3/TDL

National Aeronautical Space Agency
Langley Aeronautical Research Laboratory
Langley, Virginia
Attn/ Mr. Cliff Nelson

AFCRL, Office of Aerospace Res.
Attn/ Contract Files
L.G. Hanscom Field,
Bedford, Mass. (2 copies)

Hq. ESD (ESRDW, Maj. J.J. Hobson)
L.G. Hanscom Field
Bedford, Mass.

Hq. AFCRL, OAR (CRXR, J.R. Marple)
L.G. Hanscom Field
Bedford, Mass.

Chief, Bureau of Naval Weapons
Dept. of the Navy
Washington 25, D.C.
Attn/ DLI-31 (2 copies)

U.S. Naval Ordnance Laboratory
White Oak, Silver Spring 19, Maryland
Attn/ Library

Librarian
U.S. Naval Postgraduate School
Monterey, California

Director
U.S. Naval Research Laboratory
Washington 25, D.C.
Attn/ Code 2027 (2 copies)

Commanding Officer and Director
U.S. Navy Underwater Sound Laboratory
Fort Trumbull, New London, Connecticut

AFCRL, OAR (CRXRA-Stop 39)
L.G. Hanscom Field, Bedford, Mass.

(ship under separate cover - 10 copies

AFCRL, Office of Aerospace Res.
Attn/ C.J. Sletten
L.G. Hanscom Field
Bedford, Mass. (3 copies)

Electronic Systems Div. (AFSC)
Technical Information Serv. Div. (ESAT
L.G. Hanscom Field,
Bedford, Mass.

Chief, Bureau of Ships
Department of the Navy
Washington 25, D.C.
Attn/ Code 690

Commander
U.S. Naval Air Missile Test Center
Point Mugu, California
Attn/ Code 366

Commander
U.S. Naval Ordnance Test Station
China Lake, California
Attn/ Code 753

National Aeronautics and Space Adm.
Attn/ Antenna Systems Branch
Goddard Space Flight Center
Greenbelt, Maryland

Dr. J.I. Bohnert, Code 5210
U.S. Naval Research Laboratory
Washington 25, D.C.

Chief of Naval Research
Department of the Navy
Washington 25, D.C.
Attn/ Code 427

Commanding Officer
U.S. Naval Air Development
Johnsville, Pennsylvania
Attn/ NADC Library

Commanding Officer and Director
U.S. Navy Electronics Laboratory (Library)
San Diego 52, California

Material Laboratory, Code 932
New York Naval Shipyard
Brooklyn 1, New York
Attn/ Mr. Douglas First

Chief, Bureau of Ships
Department of the Navy
Washington 25, D.C.
Attn/ Code 817B

Aero Geo Astro Corporation
1200 Duke Street
Alexandria, Virginia
Attn/ Librarian

Airborne Instruments laboratory, Inc.
Division of Cutler Hammer
Walt Whitman Road
Melville, L.I., New York
Attn/ Library

Andrew Alford, Consulting Engineers
299 Atlantic Avenue
Boston 10, Mass.

ACF Electronics Division
Bladensburg Plant
52nd Ave and Jackson Street
Bladensburg, Maryland

Bell Aircraft Corporation
P.O. Box 1
Buffalo 5, New York
Attn/ E.P. Haselton, Librarian

Office of Naval Research
Branch Office, London
Navy 100, Box 39
F.P.O. New York, New York

Commander
U.S. Naval Air Test Center
Patuxent River, Maryland
Attn/ ET-315, Antenna Branch

Commanding Officer
U.S. Naval Ordnance Laboratory
Corona, California
Attn/ Documents Librarian

AFSC Scientific and Tech. Liaison Of.
c/o Department of the Navy
Room 2305, Munitions Building
Washington 25, D.C.

Aerospace Corporation
Box 95085
Los Angeles 45, California
Attn/ Librarian

Aircom, Inc.
48 Cummington Street
Boston, Mass.

Aerospace Corporation
Satellite Control
Attn/ Mr. R.C. Hansen
P.O. Box 95085
Los Angeles 45, California

Battelle Memorial Institute
505 King Avenue
Columbus 1, Ohio
Attn/ W.E. Rife, Project Engr.

Bell Telephone Laboratories
Murray Hill, New Jersey

Bell Telephone Laboratories, Inc.
Technical Information Library
Whippany Laboratory
Attn/ Technical Reports Librarian

Bendix Radio Division
Bendix Aviation Corporation
E. Joppa Road
Towson 4, Maryland
Attn/ Dr. D.M. Allison, Jr.

Boeing Airplane Company
Pilotless Aircraft Division
P.O. Box 3707
Seattle 24, Washington
Attn/ R.R. Barber, Libr. Supervisor

Brush Beryllium Company
4301 Perkins Aven
Cleveland 3, Ohio
Attn/ N.W. Bass

Chance Vought Corporation
Vought Electronics Division
P.O. Box 5907
Dallas 22, Texas

Collins Radio Co.
855 35th Street NE
Cedar Rapids, Iowa
Attn/ Dr. R.L. McCreary

Convair, A Division of General Dynamics
3165 Pacific Highway
San Diego 12, California
Attn/ Mrs. D.B. Burke

Dalmo Victor Company
A Division of Textron, Inc.
1515 Industrial Way
Belmont, California
Attn/ Mary Ellen Addoms, Tech. Libr.

Aircraft Division
Douglas Aircraft Company, Inc.
3855 Lakewood Boulevard
Long Beach, California
Attn/ Technical Library

Bendix Pacific Division
11600 Sherman Way
North Hollywood, California
Attn/ Engineering Library

Bjorksten Research Labs, Inc.
P.O. Box 265
Madison, Wisconsin
Attn/ Librarian

Boeing Company
3801 Oliver Street (South)
Wichita 1, Kansas
Attn/ K.C. Knight, Libr. Supervisor

Chance Vought Corporation
9314 West Jefferson Boulevard
Dallas, Texas
Attn/ A.D. Pattullo, Librarian

Chu Associates
P.O. Box 387
Whitcomb Avenue
Littleton, Mass.

Convair, A Division of General Dynam
Fort Worth, Texas
Attn/ K.G. Brown, Div. Res. Librarian

Corneli Aeronautical Lab, Inc.
4455 Genesee Street
Buffalo 21, New York
Attn/ Librarian

Dorne and Margolin, Inc.
29 New York Avenue
Westbury, Long Island, New York

Douglas Aircraft Company, Inc.
3000 Ocean Park Boulevard
Santa Monica, California
Attn/ Peter Duyan, Jr. Chief Electr.

Douglas Aircraft Company, Inc.
2000 North Memorial Drive
Tulsa, Oklahoma
Attn/ Engr. Librarian, D-250

Electronics Communication
1830 York Road
Timonium, Maryland

Emerson and Cuming, Inc.
Canton, Mass.
Attn/ Mr. W. Cuming

Emerson Radio-Phonograph Corp.
Emerson Res. Labs.
1140 Eastwest Highway
Silver Springs, Maryland
Attn/ Mrs. R. Corkin, Librarian

ITT Federal Laboratories
Technical Library
500 Washington Ave.
Nutley 10, New Jersey

General Electric Company
Electronics Park
Syracuse, New York
Attn/ Documents Library
B. Fletcher, Bldg. 3-143A

General Electric Company
3750 D Street
Philadelphia, Pa.
Attn/ H.G. Lew, Missile and Space Dept.

Goodyear Aircraft Corporation
1210 Massillon Road
Akron 15, Ohio
Attn/ Librarian, Plant G

Grumman Aircraft Engineering Corp.
Bethpage, Long Island, New York
Attn Engr. Librarian, Plant 5

Electromagnetic Res. Corp.
5001 College Avenue
College Park, Maryland
Attn/ Mr. Martin Katzin

Electronic Specialty Company
5121 San Fernando Road
Los Angeles 39, California
Attn/ D.L. Margerum, Chief Engr.

Emerson Electric Mfg. Co.
8100 West Florissant Ave.
St. Louis 21, Missouri
Attn/ Mr. E.R. Breslin, Librarian

Fairchild Aircraft-Missile Div.
Fairchild Engr. and Airplane Corp.
Hagerstown, Maryland
Attn/ Library

Gabriel Electronics Division
Main and Pleasant Streets
Millis, Mass.
Attn/ Dr. Edward Altshuler

General Electric Company
Missile and Space Vehicle Dept.
3198 Chestnut Street
Philadelphia, Pa.
Attn/ Librarian

General Precision Laboratory, Inc.
63 Bedford Road
Pleasantville, New York
Attn/ Librarian

Granger Associates
Electronics Systems
974 Commercial Street
Palo Alto, California
Attn/ J.V.N. Granger, President

Hallicrafters Company
4401 West 5th Avenue
Chicago 24, Illinois
Attn/ L. Lagioia, Librarian

The Hallicrafters Co.
5th and Kostner Avenues
Chicago 24, Illinois
Attn/ Henri Hodara

Hoffman Electronics Corp.
3761 South Hill Street
Los Angeles 7, California
Attn/ Engineering Library

Hughes Aircraft Company
Antenna Department
Building 12, Mail Station 2714
Culver City, California
Attn/ Dr. W. H. Kummer

Hughes Aircraft Company
Florence Ave. and Teale Streets
Culver City, California
Attn/ Louis L. Bailin, Mgr. Antenna Dept.

Hughes Aircraft Company
Attn/ Mr. L. Stark, M/W Dept.
Radar Laboratory, P.O. Box 2097
Building 600, Mail Station C-152
Fullerton, California

International Business Machines Corp.
Space Guidance Center-Federal Systems Div.
Owego, Tioga County, New York
Attn/ Technical Reports Center

International Resistance Company
401 N. Broad Street
Philadelphia 8, Pa.
Attn/ Research Library

ITT Federal Laboratories
3700 East Pontiac Street
Fort Wayne 1, Indiana
Attn/ Technical Library

Atlantic Research Corporation
Shirley Highway at Edsall Road
Alexandria, Virginia
Attn/ Delmer C. Ports

Dr. Henry Jasik,
Consulting Engineer
298 Shames Drive
Brush Hollow Industrial Park
Westbury, New York

Lockheed Aircraft Corporation
2555 N. Hollywood Way
Calif. Div. Eng. Library
Dept. 72-25, Plant A-1,
Building 63-1
Burbank, California
Attn/ N. C. Harnois

Lockheed Aircraft Corporation
Missiles and Space Division
Technical Information Center
3251 Hanover Street
Palo Alto, California

Martin-Marietta Corp.
12250 S. State Highway 65
Jefferson County, Colorado
Attn/ Jack McCormick

The Martin Company
Baltimore 3, Maryland
Attn/ Engineering Library
Antenna Design Group

Mathematical Reviews
190 Hope Street
Providence 6, Rhode Island

The W. L. Maxson Corporation
475 10th Avenue
New York, New York
Attn/ Miss Dorothy Clark

McDonnell Aircraft Corporation
Dept. 644, Box 516
St. Louis 66, Missouri
Attn/ C. E. Zoller
Engineering Library

McMillan Laboratory, Inc.
Brownville Avenue
Ipswich, Mass.
Attn/ Security Officer,
Document Room

Melpar, Inc.
3000 Arlington Boulevard
Falls Church, Virginia
Attn/ Engineering Tech. Library

Microwave Associates, Inc.
South Avenue
Burlington, Mass.

Microwave Development Laboratories, Inc.
92 Broad Street
Wellesley 57, Mass.
Attn/ N. Tucker, General Manager

The Mitre Corporation
244 Wood Street
Lexington 73, Mass.
Attn/ Mrs. Jean E. Claflin, Librarian

Motorola, Inc.
8201 East McDowell Road
Phoenix, Arizona
Attn/ Dr. Thomas E. Tice

Motorola, Inc.
Phoenix Research Laboratory
3102 N. 56th Street
Phoenix, Arizona
Attn/ Dr. A. L. Aden

National Research Council
Radio and Electrical Eng. Div.
Ottawa, Ontario, Canada
Attn/ Dr. G. A. Miller, Head
Microwave Section

North American Aviation, Inc.
12214 Lakewood Boulevard
Downey, California
Attn/ Technical Information Center
(495-12) Space and Information
Systems Division

North American Aviation, Inc.
Los Angeles International
Airport
Los Angeles 45, California
Attn/ Engineering Technical File

Page Communications Engineers
2001 Wisconsin Avenue, N.W.
Washington 7, D.C.
Attn/ (Mrs.) Ruth Temple,
Librarian

Northrop Corporation
Norair Division
1001 East Broadway
Hawthorne, California
Attn/ Technical Information
3924-31

Philco Corporation
Research Division
Union Meeting Pond
Blue Bell, Pa.
Attn/ Research Librarian

Pickard and Burns, Inc.
103 Fourth Avenue
Waltham 54, Mass.
Attn/ Dr. Richard H. Woodward

Polytechnic Research and
Development Co., Inc.
202 Tillary Street
Brooklyn 1, New York
Attn/ Technical Library

Radiation, Inc.
Melbourne, Florida
Attn/ RF Systems Division
Technical Incormation Center

Radiation Systems, Inc.
440 Swann Avenue
Alexandria, Virginia
Attn/ Library

RCA Laboratories
David Sarnoff Research Center
201 Washington Road
Princeton, New Jersey
Attn/ Miss Fern Cloak, Librarian

Radio Corporation of America
Defense Electronic Products
Building 10, Floor 7
Camden 2, New Jersey
Attn/ Mr. Harold J. Schrader,
Staff Engineer, Organization of
Chief Technical Administrator

Radio Corporation of America
Missile Control and Electronics
Division
Bedford Street
Burlington, Mass.
Attn/ Librarian

Radio Corporation of America
Surface Communications Systems
Laboratory
75 Varick Street
New York 13, New York
Attn/ Mr. S. Krevsky

Radio Corporation of America
West Coast Missile and Surface Radar
Division
Engineering Library, Building 306/2
Attn/ L. R. Hund, Librarian
8500 Balboa Boulevard
Van Nuys, California

Radio Corporation of America
Defense Electronic Products
Advanced Military Systems
Princeton, New Jersey
Attn/ Mr. David Shore

Director, USAF Project RAND
Via: AF Liaison Office
The Rand Corporation
1700 Main Street
Santa Monica, California

The Rand Corporation
1700 Main Street
Santa Monica, California
Attn/ Technical Library

Rantec Corporation
23999 Ventura Boulevard
Calabasas, California
Attn/ Grace Keener, Office Mgr.

Raytheon Company
Boston Post Road
Wayland, Mass.
Attn/ Mr. Robert Borts

Raytheon Company
Wayland Laboratory
Wayland, Mass.
Attn/ Miss Alice G. Anderson,
Librarian

Raytheon Company
Missile Systems Division
Hartwell Road, Bedford, Mass.
Attn/ Donald H. Archer

Remington Rand UNIVAC
Division of Sperry Rand Corp.
P.O. Box 500
Blue Bell, Pennsylvania
Attn/ Engineering Library

Republic Aviation Corporation
Farmingdale, L.I., New York
Attn/ Engineering Library

Ryan Aeronautical Company
2701 Harbor Drive
Lindbergh Field
San Diego 12, California
Attn/ Library

Sage Laboratories, Inc.
3 Huron Drive
Natick, Mass.

Sanders Associates, Inc.
95 Canal Street
Nashua, New Hampshire
Attn/ Mr. Norman R. Wild

Sandia Corporation
P.O. Box 5800
Albuquerque, New Mexico
Attn/ Records Management and
Services Department

Scanwell Laboratories, Inc.
6601 Scanwell Lane
Springfield, Virginia

STL Technical Library
Document Acquisitions
Space Technology Laboratories, Inc.
P. O. Box 95001
Los Angeles 45, California

Sperry Gyroscope Company
Great Neck, L. I., New York
Attn/ Florence W. Turnbull
Engineering Librarian

Stanford Research Institute
Documents Center
Menlo Park, California
Attn/ Acquisitions

Sylvania Electric Products, Inc.
100 First Avenue
Waltham 54, Mass.
Attn/ Charles A. Thornhill,
Report Librarian
Waltham Lab. Library

Sylvania Elec. Prod. Inc.
Electronic Defense Laboratory
P. O. Box 205
Mountain View, California
Attn: Library

Sylvania Reconnaissance Systems Lab.
Box 188
Mountain View, California
Attn/ Marvin D. Waldman

A. S. Thomas, Inc.
355 Providence Highway
Westwood, Mass.
Attn/ A. S. Thomas, President

Texas Instruments, Inc.
6000 Lemmon Avenue
Dallas 9, Texas
Attn/ John B. Travis
Systems Planning Branch

Westinghouse Electric Corp.
Electronics Division
Friendship Int'l. Airport
Box 1897, Baltimore 3, Maryland
Attn/ Engineering Library

Library Geophysical Institute of
the University of Alaska
College, Alaska

Brown University
Department of Elec. Engineering
Providence, Rhode Island
Attn/ Dr. C. M. Angulo

California Institute of Technology
Jet Propulsion Laboratory
4800 Oak Grove Drive
Pasadena, California
Attn/ Mr. I. E. Newlan

California Institute of Technology
1201 E. California Drive
Pasadena, California
Attn/ Dr. C. Papas

Space Sciences Laboratory
Leuschner Observatory
University of California
Berkeley 4, California
Attn/ Dr. Samuel Silver, Prof. of
Eng. Science

University of California
Electronics Research Lab.
332 Cory Hall
Berkeley 4, California
Attn/ J. R. Whinnery

University of Southern California
University Park
Los Angeles, California
Attn/ Dr. Raymond L. Chuan
Dir., Eng. Center

Case Institute of Technology
Electrical Engineering Department
10900 Euclid Avenue
Cleveland, Ohio
Attn/ Professor Robert Plonsey

Columbia University
Department of Electrical Engineering
Morningside Heights, New York, N.Y.
Attn/ Dr. Schlesinger

University of Southern California
University Park
Los Angeles 7, California
Attn: Z. A. Kaprielian
Associate Professor of Elec. Eng.

Cornell University
School of Electrical Engineering
Ithaca, New York
Attn: Prof. G. C. Dalman

University of Florida
Department of Electrical Engineering
Gainesville, Florida
Attn: Prof. M. H. Latour, Library

Library
Georgia Technology Research Institute
Engineering Experiment Station
722 Cherry Street, N.W.
Atlanta, Georgia
Attn/ Mrs. J. H. Crosland, Librarian

Harvard University
Technical Reports Collection
Gordon McKay Library
303 Pierce Hall
Oxford Street
Cambridge 38, Mass.
Attn/ Librarian

Harvard College Observatory
60 Garden Street
Cambridge 39, Mass.
Attn/ Dr. Fred L. Whipple

University of Illinois
Documents Division Library
Urbana, Illinois

University of Illinois
College of Engineering
Urbana, Illinois
Attn: Dr. P. E. Mayes, Dept. of
Electrical Engineering

Illinois Institute of Technology
Technology Center
Department of Electrical Eng.
Chicago 16, Illinois
Attn: Paul C. Yuen, Electronics
Electronics Res. Lab.

The John Hopkins University
Homewood Campus
Baltimore 18, Maryland
Attn/ Dr. Donald E. Kerr,
Dept. of Physics

The John Hopkins University
Applied Physics Laboratory
8621 Georgia Avenue
Silver Spring, Maryland
Attn: Mr. George L. Seielstad

University of Kansas
Electrical Engineering Department
Lawrence, Kansas
Attn/ Dr. H. Unz

Lowell Technological Institute
Research Foundation
P.O. Box 709, Lowell, Mass.
Attn/ Dr. Charles R. Mingins

Massachusetts Institute of Tech.
Res. Laboratory of Electronics
Building 26, Room 327
Cambridge 39, Mass.
Attn/ John H. Hewitt

Massachusetts Institute of Tech.
Lincoln Laboratory
P.O. Box 73
Lexington 73, Mass.
Attn/ Mary A. Granese, Librarian

McGill University
Department of Electrical Eng.
Montreal, Canada
Attn/ Dr. T. Pavlasek

University of Michigan
Electronic Defense Group
Inst. of Science and Technology
Ann Arbor, Michigan
Attn/ J. A. Boyd, Supervisor

University of Michigan
Office of Research Administration
Radiation Laboratory
912 N. Main Street
Ann Arbor, Michigan
Attn/ Mr. Ralph E. Hiatt

University of Michigan
Engineering Res. Institute
Willow Run Laboratories,
Willow Run Airport
Ypsilanti, Michigan
Attn/ Librarian

University of Minnesota
Minneapolis 14, Minnesota
Attn/ Mr. Robert H. Stumm, Library

Physical Science Laboratory
New Mexico State University
University Park, New Mexico
Attn/ Mr. H. W. Haas

New York University
Institute of Mathematical Sciences
Room 802, 25 Waverly Place
New York 3, New York
Attn/ Morris Kline, Dr.

Northwestern University
Microwave Laboratories
Evanston, Illinois
Attn/ R. E. Beam

Antenna Laboratory
Department of Electrical Engineering
The Ohio State University
2024 Neil Avenue
Columbus 10, Ohio

The University of Oklahoma
Research Institute
Norman, Oklahoma
Attn/ Prof. C. L. Farrar, Chairman
Electrical Engineering

University of Pennsylvania
Institute of Cooperative Research
3400 Walnut Street
Philadelphia, Pennsylvania
Attn/ Department of Electrical Eng.

Polytechnic Institute of Brooklyn
Microwave Research Institute
55 Johnson Street
Brooklyn, New York
Attn/ Dr. Arthur A. Oliner

Polytechnic Institute of Brooklyn
Microwave Research Institute
55 Johnson Street
Brooklyn, New York
Attn/ Mr. A. E. Laemmel

The Pennsylvania State University
223 Electrical Engineering
University Park, Pa.
Attn/ A. H. Waynick, Director
Ionosphere Research Lab.

Purdue University
Department of Electrical Engineering
Lafayette, Indiana
Attn/ Dr. Schultz

Library
W. W. Hansen Laboratory of Physics
Stanford, University
Stanford, California

Syracuse University Research Institute
Collendale Campus
Syracuse 10, New York
Attn/ Dr. C. S. Grove, Jr.
Director of Engineering Research

Technical University
Oestervoldgade 10 G
Copenhagen, Denmark
Attn/ Prof. Hans Lottrup Knudsen

University of Tennessee
Ferris Hall
West Cumberland Avenue
Knoxville 16, Tennessee

The University of Texas
Electrical Engineering Research Lab.
P. O. Box 8026, University Station
Austin 12, Texas
Attn/ Mr. John R. Gerhardt
Assistant Director

The University of Texas
Defense Research Laboratory
Austin, Texas
Attn/ Claude W. Horton,
Physics Library

University of Toronto
Department of Electrical Eng.
Toronto, Canada
Attn/ Prof. G. Sinclair

University of Washington
Department of Electrical Eng.
Seattle 5, Washington
Attn/ D. K. Reynolds

University of Wisconsin
Department of Electrical Eng.
Madison, Wisconsin
Attn/ Dr. Scheibe

AD Div. 8/2

TRG, Inc., East Boston, Mass.
EFFICIENT FLUSHMOUNTED SURFACE WAVE LAUNCHER
by Mats E. Viggh, Scientific Report November 28, 1962, 86 p. incl. illus. (Rept. No. 151-4) Contract AF19(604)-8057
Unclassified Report

Various methods for launching surface waves are reviewed, and the basic design principles are outlined for different kinds of launchers.

The case of a slot in a dielectric-clad groundplane is analyzed in detail, and experiments supporting the calculated results are reported. A way of combining several slots for good launching efficiency is derived and a five-slot launcher designed after this principle is described. Results from measurements of radiation patterns and efficiency are reported; as well as from measurements of radiation patterns from discontinuities on a surface waveguide excited by this launcher in combination with a cylindrical parabolic reflector.

In particular, a launching efficiency of over 80 percent was achieved with five slots, as compared to about 48 percent with one slot. Radiation patterns due to abrupt changes in dielectric thickness were measured, and compared with theoretical results for a corresponding change in surface reactance. The agreement was good at least within the main lobe.

UNCLASSIFIED

1. Surfaces - Wave Transmission
2. Antennas - Theory
3. Antennas - Performance
I. Mats E. Viggh
II. Electronic 5 stems Division
Air Force Systems Command
Office of Aerospace Research
Laurence G. Hanscom Field
Bedford, Massachusetts
III. Contract AF19(604)-8057

UNITERMS

Surface
Radiating
Waves
Slots

Armed Services Technical Information Agency

UNCLASSIFIED

AD Div. 8/2

TRG, Inc., East Boston, Mass.
EFFICIENT FLUSHMOUNTED SURFACE WAVE LAUNCHER
by Mats E. Viggh, Scientific Report November 28, 1962, 86 p. incl. illus. (Rept. No. 151-4) Contract AF19(604)-8057
Unclassified Report

Various methods for launching surface waves are reviewed, and the basic design principles are outlined for different kinds of launchers.

The case of a slot in a dielectric-clad groundplane is analyzed in detail, and experiments supporting the calculated results are reported. A way of combining several slots for good launching efficiency is derived and a five-slot launcher designed after this principle is described. Results from measurements of radiation patterns and efficiency are reported; as well as from measurements of radiation patterns from discontinuities on a surface waveguide excited by this launcher in combination with a cylindrical parabolic reflector.

In particular, a launching efficiency of over 80 percent was achieved with five slots, as compared to about 48 percent with one slot. Radiation patterns due to abrupt changes in dielectric thickness were measured, and compared with theoretical results for a corresponding change in surface reactance. The agreement was good at least within the main lobe.

UNCLASSIFIED

1. Surfaces - Wave Transmission
2. Antennas - Theory
3. Antennas - Performance
I. Mats E. Viggh
II. Electronic Systems Division
Air Force Systems Command
Office of Aerospace Research
Laurence G. Hanscom Field
Bedford, Massachusetts
III. Contract AF19(604)-8057

UNITERMS

Surface
Radiating
Waves
Slots

Armed Services Technical Information Agency

UNCLASSIFIED

AD Div. 8/2

TRG, Inc., East Boston, Mass.
EFFICIENT FLUSHMOUNTED SURFACE WAVE LAUNCHER
by Mats E. Viggh, Scientific Report November 28, 1962, 86 p. incl. illus. (Rept. No. 151-4) Contract AF19(604)-80f7
Unclassified Report

Various methods for launching surface waves are reviewed, and the basic design principles are outlined for different kinds of launchers.

The case of a slot in a dielectric-clad groundplane is analyzed in detail, and experiments supporting the calculated results are reported. A way of combining several slots for good launching efficiency is derived and a five-slot launcher designed after this principle is described. Results from measurements of radiation patterns and efficiency are reported; as well as from measurements of radiation patterns from discontinuities on a surface waveguide excited by this launcher in combination with a cylindrical parabolic reflector.

In particular, a launching efficiency of over 80 percent was achieved with five slots, as compared to about 48 percent with one slot. Radiation patterns due to abrupt changes in dielectric thickness were measured, and compared with theoretical results for a corresponding change in surface reactance. The agreement was good at least within the main lobe.

UNCLASSIFIED

1. Surfaces - Wave Transmission
2. Antennas - Theory
3. Antennas - Performance
I. Mats E. Viggh
II. Electronic Systems Division
Air Force Systems Command
Office of Aerospace Research
Laurence G. Hanscom Field
Bedford, Massachusetts
III. Contract AF19(604)-8057

UNITERMS

Surface
Radiating
Waves
Slots

Armed Services Technical Information Agency

UNCLASSIFIED

AD Div. 8/2

TRG, Inc., East Boston, Mass.
EFFICIENT FLUSHMOUNTED SURFACE WAVE LAUNCHER
by Mats E. Viggh, Scientific Report November 28, 1962, 86 p. incl. illus. (Rept. No. 151-4) Contract AF19(604)-8057
Unclassified Report

Various methods for launching surface waves are reviewed, and the basic design principles are outlined for different kinds of launchers.

The case of a slot in a dielectric-clad groundplane is analyzed in detail, and experiments supporting the calculated results are reported. A way of combining several slots for good launching efficiency is derived and a five-slot launcher designed after this principle is described. Results from measurements of radiation patterns and efficiency are reported; as well as from measurements of radiation patterns from discontinuities on a surface waveguide excited by this launcher in combination with a cylindrical parabolic reflector.

In particular, a launching efficiency of over 80 percent was achieved with five slots, as compared to about 48 percent with one slot. Radiation patterns due to abrupt changes in dielectric thickness were measured, and compared with theoretical results for a corresponding change in surface reactance. The agreement was good at least within the main lobe.

UNCLASSIFIED

1. Surfaces - Wave Transmission
2. Antennas - Theory
3. Antennas - Performance
I. Mats E. Viggh
II. Electronic Systems Division
Air Force Systems Command
Office of Aerospace Research
Laurence G. Hanscom Field
Bedford, Massachusetts
III. Contract AF19(604)-8057

UNITERMS

Surface
Radiating
Waves
Slots

Armed Services Technical Information Agency

UNCLASSIFIED

AD Div. 8/2

TRG, Inc., East Boston, Mass.
EFFICIENT FLUSHMOUNTED SURFACE WAVE LAUNCHER
by Mats E. Viggh. Scientific Report November 28, 1962, 86 p. incl. illus. (Rept. No. 151-4) Contract AF19(604)-8057
Unclassified Report

Various methods for launching surface waves are reviewed, and the basic design principles are outlined for different kinds of launchers.

The case of a slot in a dielectric-clad groundplane is analyzed in detail, and experiments supporting the calculated results are reported. A way of combining several slots for good launching efficiency is derived and a five-slot launcher designed after this principle is described. Results from measurements of radiation patterns and efficiency are reported; as well as from measurements of radiation patterns from discontinuities on a surface waveguide excited by this launcher in combination with a cylindrical parabolic reflector.

In particular, a launching efficiency of over 80 percent was achieved with five slots, as compared to about 48 percent with one slot. Radiation patterns due to abrupt changes in dielectric thickness were measured, and compared with theoretical results for a corresponding change in surface reactance. The agreement was good at least within the main lobe.

UNCLASSIFIED

1. Surfaces - Wave Transmission
2. Antennas - Theory
3. Antennas - Performance
I. Mats E. Viggh
II. Electronic Systems Division
Air Force Systems Command
Office of Aerospace Research
Laurence G. Hanscom Field
Bedford, Massachusetts
III. Contract AF19(604)-8057

UNITERMS

Surface
Radiating
Waves
Slots

Armed Services Technical Information Agency

UNCLASSIFIED

AD Div. 8/2

TRG, Inc., East Boston, Mass.
EFFICIENT FLUSHMOUNTED SURFACE WAVE LAUNCHER
by Mats E. Viggh. Scientific Report November 28, 1962, 86 p. incl. illus. (Rept. No. 151-4) Contract AF19(604)-8057
Unclassified Report

Various methods for launching surface waves are reviewed, and the basic design principles are outlined for different kinds of launchers.

The case of a slot in a dielectric-clad groundplane is analyzed in detail, and experiments supporting the calculated results are reported. A way of combining several slots for good launching efficiency is derived and a five-slot launcher designed after this principle is described. Results from measurements of radiation patterns and efficiency are reported; as well as from measurements of radiation patterns from discontinuities on a surface waveguide excited by this launcher in combination with a cylindrical parabolic reflector.

In particular, a launching efficiency of over 80 percent was achieved with five slots, as compared to about 48 percent with one slot. Radiation patterns due to abrupt changes in dielectric thickness were measured, and compared with theoretical results for a corresponding change in surface reactance. The agreement was good at least within the main lobe.

UNCLASSIFIED

1. Surfaces - Wave Transmission
2. Antennas - Theory
3. Antennas - Performance
I. Mats E. Viggh
II. Electronic Systems Division
Air Force Systems Command
Office of Aerospace Research
Laurence G. Hanscom Field
Bedford, Massachusetts
III. Contract AF19(604)-8057

UNITERMS

Surface
Radiating
Waves
Slots

Armed Services Technical Information Agency

UNCLASSIFIED

AD Div. 8/2

TRG, Inc., East Boston, Mass.
EFFICIENT FLUSHMOUNTED SURFACE WAVE LAUNCHER
by Mats E. Viggh. Scientific Report November 28, 1962, 86 p. incl. illus. (Rept. No. 151-4) Contract AF19(604)-8057
Unclassified Report

Various methods for launching surface waves are reviewed, and the basic design principles are outlined for different kinds of launchers.

The case of a slot in a dielectric-clad groundplane is analyzed in detail, and experiments supporting the calculated results are reported. A way of combining several slots for good launching efficiency is derived and a five-slot launcher designed after this principle is described. Results from measurements of radiation patterns and efficiency are reported; as well as from measurements of radiation patterns from discontinuities on a surface waveguide excited by this launcher in combination with a cylindrical parabolic reflector.

In particular, a launching efficiency of over 80 percent was achieved with five slots, as compared to about 48 percent with one slot. Radiation patterns due to abrupt changes in dielectric thickness were measured, and compared with theoretical results for a corresponding change in surface reactance. The agreement was good at least within the main lobe.

UNCLASSIFIED

1. Surfaces - Wave Transmission
2. Antennas - Theory
3. Antennas - Performance
I. Mats E. Viggh
II. Electronic Systems Division
Air Force Systems Command
Office of Aerospace Research
Laurence G. Hanscom Field
Bedford, Massachusetts
III. Contract AF19(604)-8057

UNITERMS

Surface
Radiating
Waves
Slots

Armed Services Technical Information Agency

UNCLASSIFIED

AD Div. 8/2

TRG, Inc., East Boston, Mass.
EFFICIENT FLUSHMOUNTED SURFACE WAVE LAUNCHER
by Mats E. Viggh. Scientific Report November 28, 1962, 86 p. incl. illus. (Rept. No. 151-4) Contract AF19(604)-8057
Unclassified Report

Various methods for launching surface waves are reviewed, and the basic design principles are outlined for different kinds of launchers.

The case of a slot in a dielectric-clad groundplane is analyzed in detail, and experiments supporting the calculated results are reported. A way of combining several slots for good launching efficiency is derived and a five-slot launcher designed after this principle is described. Results from measurements of radiation patterns and efficiency are reported; as well as from measurements of radiation patterns from discontinuities on a surface waveguide excited by this launcher in combination with a cylindrical parabolic reflector.

In particular, a launching efficiency of over 80 percent was achieved with five slots, as compared to about 48 percent with one slot. Radiation patterns due to abrupt changes in dielectric thickness were measured, and compared with theoretical results for a corresponding change in surface reactance. The agreement was good at least within the main lobe.

UNCLASSIFIED

1. Surfaces - Wave Transmission
2. Antennas - Theory
3. Antennas - Performance
I. Mats E. Viggh
II. Electronic Systems Division
Air Force Systems Command
Office of Aerospace Research
Laurence G. Hanscom Field
Bedford, Massachusetts
III. Contract AF19(604)-8057

UNITERMS

Surface
Radiating
Waves
Slots

Armed Services Technical Information Agency

UNCLASSIFIED